THE FLOW OF A NEWTONIAN LIQUID ON ROTATING INCLINED SURFACES WITH APPLICATION TO ATOMIZATION

by

DAVID FREDERICK BOOKER

A Doctoral Thesis

Submitted in partial fulfilment of the requirements

for the award of

Doctor of Philosophy of the Loughborough University of Technology

December 1973

Supervisor: R J AKERS, B.Sc., Ph.D.

Department of Chemical Engineering

ACKNOWLEDGEMENTS

I would like to express my sincere gratitude to Dr R J Akers, my supervisor, for his considerable help and guidance during the last three years. To Mr B Scarlett, my thanks for his help, particularly on the theoretical aspects of this thesis. Finally, my thanks to Mr G Boyden for his photographic assistance, Professor D C Freshwater for the research facilities and Loughborough University for the financial assistance which made this research possible.

TABLE OF CONTENTS

INTRODUCTION

Spinning cup atomizers are used industrially to produce an airborne spray. Often the size distribution of the spray is important. The size distribution of the spray depends on the physical dimensions of the cup, the operating conditions and the physical properties of the fluid to be atomized.

A spinning cup atomizer can be considered in the following way. The liquid to be atomized is fed centrally on to the surface of the cup where it begins to thin into a liquid film under the centrifugal action of the rotating cup. As the liquid flows film-wise to the lip of the cup, where atomization occurs, it obtains energy from the cup. Obviously, efficient atomization will occur if the liquid reaches the lip of the cup after it has picked up sufficient energy and if it was evenly distributed on the cup initially.

Chapter One attempts some of the more pertinent problems that were considered to be of interest, for instance the effect maldistribution of the liquid feed on the surface of the cup, has on the resultant drop size distribution. Likewise the experimental difficulties of accurately monitoring the film thickness variations and the drop size are discussed.

The recognition that the film flow ultimately influences the atomisation prompted an interest, both theoretically and experimentally, into the film flow on the cup. Chapter two is concerned with the early experimental work in determining the liquid film thickness as a function of the physical properties of the test liquid and the operating conditions as well as the distribution of the liquid on the surface of the cup. Photographic drop sizing was also tested as a viable drop sizing technique

during this initial experimental period.

The literature has been surveyed in Chapter Tree. Because of the importance of the film flow of the liquid on the cup prior to atomization the film flow literature has been examined in some detail. Initially the film flow of a liquid down an inclined plane was studied before reviewing the film flow of a liquid in a centrifugal field. As there are similarities between the two cases and as the inclined plane application has received a lot of attention it was thought that the techniques used in the inclined plane work might be transferable to the centrifugal case. Apart from a relatively short section on liquid distribution on to rotating discs the remaining part of this chapter is devoted to the atomization of the liquid and the sizing of the droplets so produced.

The design and operation of the experimental equipment and the calibration that was needed is discussed in Chapter Four. Here the optical technique, that of light extinction, which was finally used as the method of determining the liquid film thickness for both the average and continuous film thickness results is discussed. The drop sizing technique is also described in this chapter. The drop sizer used was in fact a charged wire drop sizer. This sizer is capable of handling a large number of droplets in a short time period. Also it can be used at the same time as the optical system described above, an added advantage if both the film thickness and drop size distribution are required concurrently.

The theoretical chapter, Chapter Five, considers the fluid mechanics of the liquid film flow on a spinning cup. Various models are discussed: the Nusselt and Nikolaev models which contain some of the inertial terms in the Navier Stokes equation; the creeping flow solution which ignores

the inertial terms and are essentially the three dimensional solution of the Navier Stokes equation.

The last chapter contains the discussions and conclusions of the film thickness and drop size distribution results. As this thesis is concerned with the liquid film flow on a rotating cup atomizer the discussio are directed towards the differences between the ideal smooth flow and the wavy flow encountered in practice on the cup. The transition from the bimodal to continuous drop size distribution is noted and the effect of volumetric flowrate on this transition is quantified, but only at one set of operating conditions.

CHAPTER ONE

THE STATEMENT OF THE PROBLEM

THE STATEMENT OF THE PROBLEM

Experimental and theoretical work that has been carried out by researchers has indicated that it is possible to separate the film flow régime of a liquid on a spinning cup from the atomization at the lip by carefully choosing the geometry of the cup. This would appear to be the case so long as the liquid is initially evenly distributed on the cup and the waves that may be produced have insufficient inertia to influence the eventual atomization.

Qualitatively it is relatively easy to observe the effect maldistribution of the liquid feed and wave formations have on the atomization (Photograph 5). Inevitably the question arises, what is the quantitative effect of maldistribution and wave formations? With this question in mind the research described in this thesis was carried out. If the industrial usage of rotating disc atomizers was limited to small throughputs the question asked above would become redundant. However, industrially these atomizers are more often used in the sheet régime, that is at high liquid throughputs where the problems of maldistribution and wave formations becomes of interest, especially for low viscosity liquids.

To assess the effect the film thickness distribution has on the drop size distribution it is obviously necessary for these distributions to be determined. In the case of the film thickness distributions continuous monitoring of the film thickness is required if the instantaneous values are to be obtained. As the speed of rotation can be relatively fast the probe used to measure

the film thickness has to have a response time several orders of magnitude faster than the fluctuation or disturbances which occur on the disc. Although the probe may be capable of detecting these high frequency fluctuations the recording of the signal is a problem which has to be faced. Once again fast response times will be necessary if the signal from the probe is not to be distorted.

To quantify the effect that the wave distribution has on the drop size distribution, it is necessary to determine the drop size distribution as the drops are produced, that is adjacent to where the drops are formed. If this was not observed mass transfer, coalescence and drop rupture might affect the distribution obtained. This however imposes a severe practical restriction on the sampling as the drop flux is at its greatest in the region close to the cup. The sampling method must therefore be able to handle a very large number of drops as the frequency of drops passing through a specified area decreases with increase in distance from the lip of the cup.

CHAPTER TWO

THE INITIAL EXPERIMENTAL WORK

2.1 Film Thickness Measurement

2.2 Surface Velocity Measurement

2.3 Photographic Drop Sizing

2.4 Distributor Designs

INTRODUCTION

The experimental techniques described in Chapter Four grew out of the experience gained during the initial experimentation period. Observations from the literature were often tested to ensure the techniques adopted gavé the degree of accuracy required in the easiest possible manner. Some of the methods tried were abandoned after a short while, when such methods indicated difficulties or inaccuracies that could not easily be overcome.

In order to assess a spinning cup atomizer in any one of the three atomization regimes[1] it is necessary to know how much rotational energy has been transferred to the liquid prior to atomization as azimuthal surface film velocities of up to 50% lag have been observed[2]. If lags of this order still exist when the film approaches the lip of the cup the resultant atomization will inevitably be adversely affected.

The film flow of an incompressible liquid on the inside surface of a rotating cup can be fully described by the Navier-Stokes equations. Exact solutions of these equations are normally extremely difficult, therefore approximate solutions are generally found. Classically the experimental investigations into the validity of these solutions have been concerned with the measurement of either the local film thickness, the components of the film surface velocity or both of these.

2.1 Film Thickness Measurement

Devices which measure liquid film thickness can be divided into several groups. These have been summarised in Chapter Three. Suffice it to say the method of finding the film thickness is important as it will dictate which value of the film thickness is found. Therefore serious thought is necessary before adopting any particular technique.

2.1.1 Stationary Probe

The cup used during the early investigations (see Figure 2.1) was made of brass and was therefore thought to be ideally suited to the capacitance probe technique of measuring the liquid film thickness. A brass probe of approximately 8 cm^2 in area was accurately machined to fit the inside surface of the brass cup. The probe was initially fitted flush to the surface of the cup before being displaced slightly from it so that a uniform gap was left between the probe and the cup. The capacitance between the isolated probe and the cup was measured so the air gap could be determined.

The liquid used during this period was mains water and so it was possible to assume that the capacitance measured was a direct function of the air gap (as the dielectric constant of water is nearly two orders of magnitude greater than that of air). The liquid film thickness was therefore found as the difference between the air gap readings in the no-liquid flow and the liquid flow conditions respectively. Measurements of the capacitance were taken directly on an oscilloscope that incorporated a capacitance bridge network. By careful adjustment of the trigger level on the oscilloscope it was possible to record

the capacitance for consecutive revolutions on the storage facility of the oscilloscope. It was necessary to match the values of the capacitance in the flow and no-flow conditions at different positions on the cup due to a slight amount of eccentricity which was detected by the probe.

The air gap between the probe and the cup was deliberately kept small so that the capacitance change, when liquid was present on the cup, was readily detectable. Unfortunately when the air gap was small two unwanted effects were observed. The first of these occurred when the liquid, usually in the form of a wave crest, bridged the gap between the capacitance probe and the cup causing the probe to short circuit. Although the short circuiting was possibly transient in effect, small globules of the liquid had a tendency to sit on the face of the probe even when that face had previously been coated with an anti-wetting agent such as P.T.F.E. Wetting of the capacitance probe was most pronounced during start-up, probably because of the wave front that precedes the formation of a totally wetted surface. The second of these effects concerned the positioning of the probe. A stationary probe affects the air flow which is a feature of all types of rotary atomizers. The change in air flow near the surface of the liquid film might in some extreme cases cause disturbances that result in wave formations. Of these two effects mentioned the first is thought to be the most important as it limits the degree of accuracy obtainable by this method.

FIGURE. 2.1.

BRASS CUP USED DURING THE INITIAL EXPERIMENTATION PERIOD.

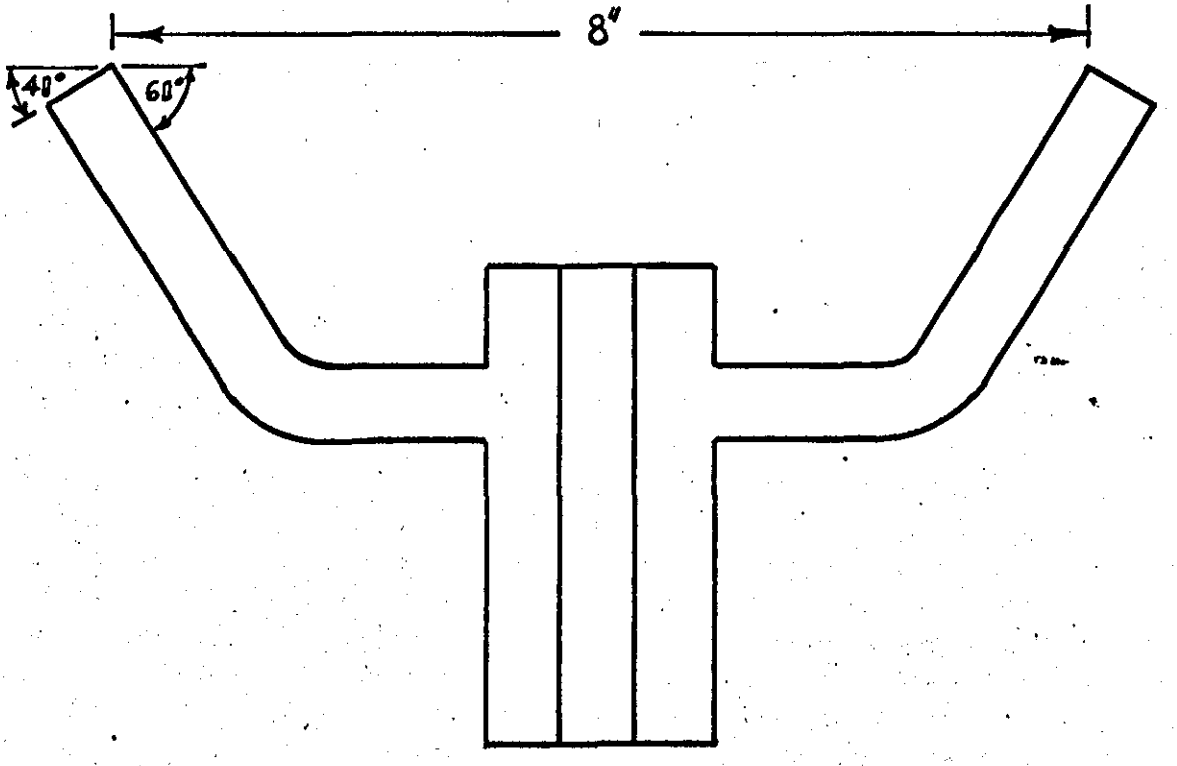

Problems were experienced because of the geometry of the cup. For instance, the probe could only be used at one particular band of radii. If the film thickness at any other radius was required it would have necessitated a probe that had been machined to the dimensions of the cup at that radius. Although this particular problem is by no means insurmountable it was felt that it severely limited the degree of flexibility of this technique. Another of the problems encountered concerned the positioning of the probe at start up. The theoretical equation, used to determine the initial air gap, is only applicable for a parallel plate capacitor. If the probe was not set up exactly 'parallel' to the cup the capacitance recorded would not be the same as the capacitance that would be recorded if the probe was 'parallel'. This can be more clearly seen when expressed mathematically.

The capacitance of a parallel plate capacitor in air is given by:-

$$C = \frac{8.85 \times 10^{-12} \times a}{t} \quad \text{farads} \qquad (2.1.1)$$

where C is the capacitance in farads

a is the area of the capacitor (m^2)

t is the distance between the plates (m)

From equation 2.1.1. it can be readily seen that the greatest change in capacitance with change in air gap will occur when the distance between the plates (t) is small. The following simple model

demonstrates how the capacitance is affected when the plates are not quite parallel.

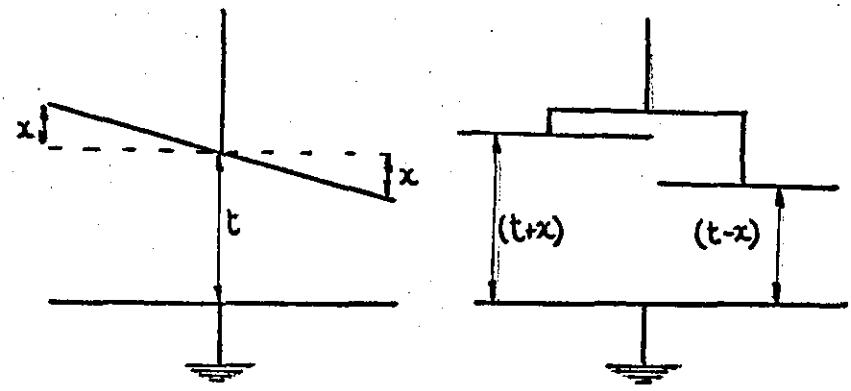

Any capacitor can be expressed as an infinite number of capacitors in parallel,

$$\text{i.e.} \quad C = C_1 + C_2 + C_3 + C_4 \quad +----+ \quad C_n \qquad (2.1.2)$$

We could therefore consider the non-parallel capacitor to be equivalent to, say, two parallel plate capacitors in parallel. It is readily shown that the resultant capacitance is given by:-

$$C \propto \frac{a \times t}{t^2 - x^2} \qquad (2.1.3)$$

Hence the effective distance between the plates is seen to be less than the average distance between the plates. The presence of a uniform layer of water on the cup would modify the equation slightly.

$$C \propto \frac{a \times (t-y)}{(t-y)^2 - x^2} \qquad (2.1.4)$$

Obviously the errors involved depend upon the relative values of

the average air gap at no flow, (t), and the displacement, (x). However it is generally true that if the plates are not precisely parallel the liquid film thickness predicted will be greater than that actually on the cup.

In practice there are two more factors which complicate the interpretation of the results. For true uniform flow the film thickness decreases with increase in the radius of the cup. Therefore, even if the probe was initially set up 'parallel' to the face of the cup, the liquid would form a wedge-shaped layer due to the thinning of the liquid with increase in radius. This would affect the results as described above. Secondly, if waves were present in the liquid layer the recorded capacitance would once more be affected. When there are waves present on the cup the air gap would no longer be constant and so the situation again becomes analogous with the preceding treatment.

The results obtained using the capacitance probe method can be seen in Figure 2.2. There they are compared with the results obtained by other authors[3-6] for both centrifugal and gravitational force fields.

2.1.2 Rotating Probe

A stationary probe only gives information at a static frame of reference, that is, it scans a particular radius as the cup rotates past it. Any possible periodicity in the wave motion that is present on the cup may be lost or distorted

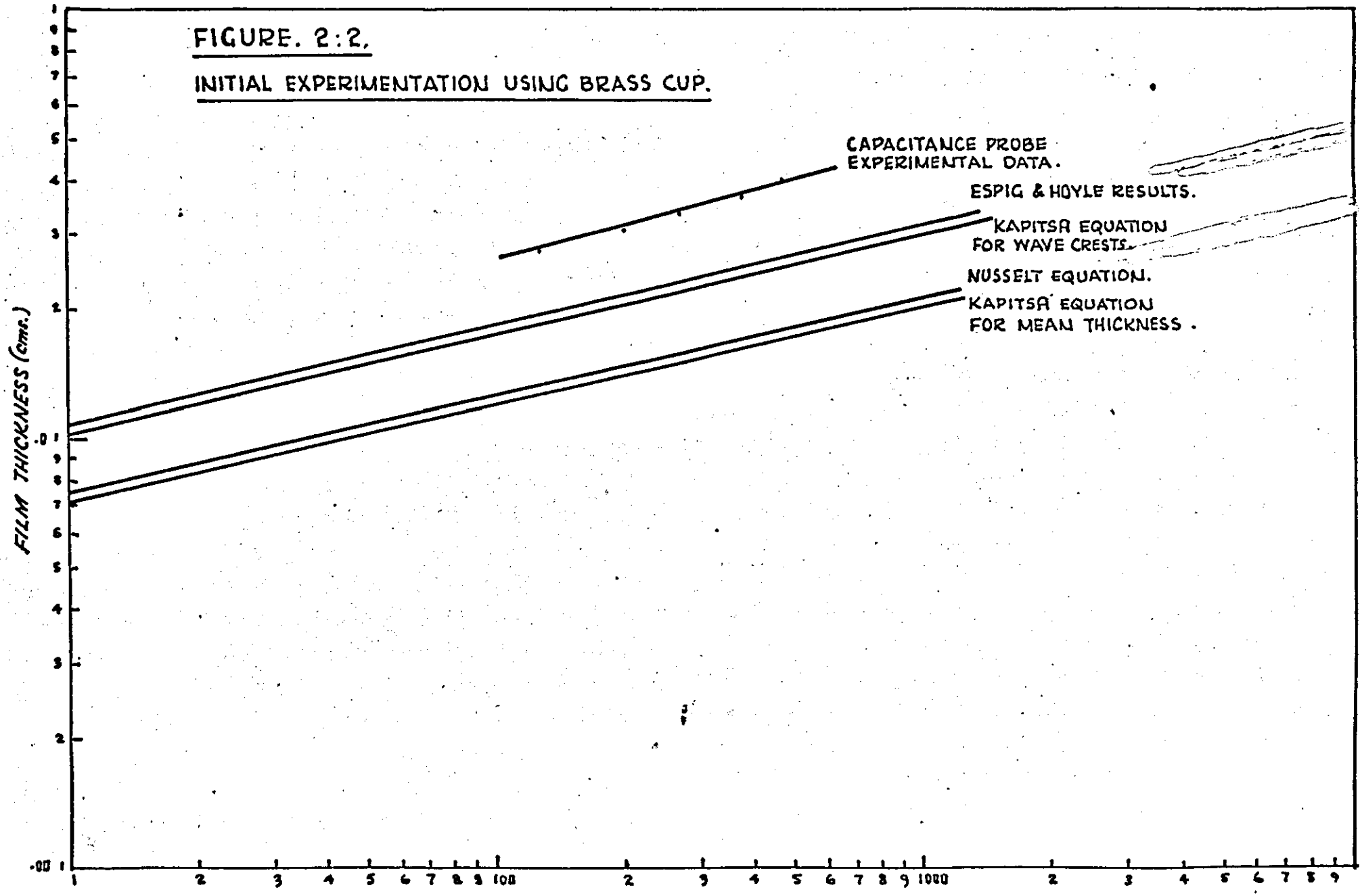
FIGURE. 2:2.
INITIAL EXPERIMENTATION USING BRASS CUP.
CAPACITANCE PROBE EXPERIMENTAL DATA.
ESPIG & HOYLE RESULTS.
KAPITSA EQUATION FOR WAVE CRESTS.
NUSSELT EQUATION.
KAPITSA EQUATION FOR MEAN THICKNESS.
FILM THICKNESS (cms.)

unless the flow at that given point on the cup is continuously monitored. An attempt was made to construct a rotating capacitance probe that could be fixed at any given point adjacent to the cup. No experimental results were forthcoming due to a number of problems, including noise at the rotary contacts and wetting of the capacitance probe with small globules of water.

Two designs of rotary contacts were tried. The first, and the simplest, consisted of two carbon brushes touching the previously cleaned surface of a circular, insulated, brass contact that had been mounted above the liquid distributor. This system proved inadequate due to a high level of noise, which was attributed to the carbon brushes. A second design was tried comprising of a perspex disc that was mounted, as before, above the liquid distributor. A circular reservoir was cut into the disc so that when it was filled with mercury, none was lost when the system rotated. A clean platinum wire was dipped carefully into the mercury well thus completing the rotary contact. Once again noise was recorded at an unacceptable level. Although the noise could possibly have been reduced it was decided to curtail this line of investigation. Apart from the noise problem two other problems not elsewhere mentioned were encountered. The first was due to the ironwork in the apparatus, there being an oscillating force field which was detected as the probe rotated. The second problem concerned the size of the capacitance probe. Due to its area the probe was monitoring an average film thickness and not an instantaneous film thickness at a point. Therefore the

probe was unable to detect the wave motion precisely, whereas information about the wave motion was regarded as important.

A mechanical design fault was also encountered. As the three-phase motor that drove the spinning cup was turned on the value of the capacitance changed due to flexing of the T bar that formed the carrier for the probe. Unfortunately it was not possible to tell whether the arrangement acquired a steady state deflection as the noise level previously mentioned did not allow precise measurements to be taken.

2.2 Surface Velocity Measurements

When a liquid film is accelerated on the inside surface of a spinning cup the unbounded surface, the air/liquid surface, will attain a velocity which is a function of the physical properties of the liquid and the position of the liquid on the cup. Consequently any theory regarding the liquid film flow could be tested using surface velocity measurements. For an orthogonal curvilinear coordinates system the overall velocity can be represented by its component velocities, namely the meridional and azimuthal velocities. In practice it is difficult to measure the components of the surface film velocity at a precise designated point. This being so, the surface velocities were found at a number of random positions on the cup and from this information the surface velocities, at the required position, were interpolated.

The technique used to measure the surface velocities during this investigation was streak photography. Small paper discs, from a punch paper tape machine, were floated on the surface of the liquid as it left the distributor weir lip. Due

to the low mass of these markers it was assumed they quickly reached the same velocity as the liquid surface as it accelerated across the surface of the cup. Continuous lighting was used so that when the camera shutter opened exposure of the film commenced. The shutter time was selected so that the paper discs would travel one or two centimetres during the time the shutter was open. Because of the movement of the discs relative to the camera streak images of the discs were formed on the negative from which an estimate of the velocity of the paper discs was made. The position of the discs on the cup when the shutter opened was naturally uncontrollable and so sufficient information had to be amassed so that a graph of surface velocity against radius could be drawn from which the surface velocity at any point was available.

The extreme ends of the streak images were often difficult to assess. This was because the effective exposure time of the extreme ends of the streak was not the same as the main body of the streak, due to the fact that the marker had a finite diameter. This can be seen more clearly with the aid of the following diagram.

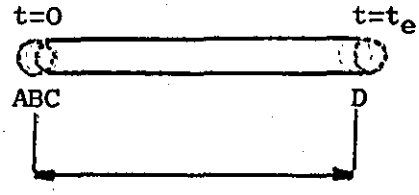

where t_e = exposure time

effective length of streak
as seen on the negative

A,B and C are three points on the negative when the shutter opens, point A will be exposed instantaneously whereas point B will

be exposured for the time it takes the disc to travel from A to B. Likewise point C will be exposed for the time it takes the disc to travel from A to C; this will be the maximum exposure time, assuming the velocity of the marker remains constant. From C to D the exposure at any point will be constant and so the contrast in this band will be greater than the areas at the ends.

The camera used, an Exakta, had a focal plane shutter and so it was necessary to compensate for the focal planing effect i.e. the elongation of the image due to the shutter acting as a slit which traverses the negative whilst the image is moving. As the elongation of the image due to focal planing is a direct function of the speed at which the image moves, it is possible to find an effective exposure at any position on the cup by measuring the length of streak when the bowl rotates at a known speed. A calibration of the effect that focal planing has on the length of streak was obtained by measuring the streaks produced by markers that had been stuck to the inside surface of a dry cup.

The surface velocity results obtained, an example of which can be seen in Figure 2.3, contain an appreciable amount of scatter. This may be interpreted as the product of two effects, firstly, the surface velocity is a function of the waves that are often present when a liquid flows film-wise on a rotating cup and secondly, because of the geometry of the cup, errors could have occurred when the data was extracted from the negatives.

2.3 Photographic Drop Sizing

A series of photographs were taken of the spray in the region close to the lip of the rotating cup. The slides that were made were projected on to a screen from which the droplet diameters were measured using a pair of calipers. These calipers were directly connected to a potentiometer which could easily be adjusted to give a read-out that was directly proportional to the drop size diameter. The readings obtained were stored on punch paper tape via a data logging unit. Only small displacements of the calipers were permitted as the voltage from the potentiometer was proportional to the arc that the calipers described and not the chord which represented the drop diameter. However, by calibrating the output voltage in terms of a chord (i.e. a drop diameter) the resultant errors, with small caliper displacements, are negligible.

In order to obtain a drop size distribution, a large number of drops must be analysed. This meant that numerous photographs were necessary as the number of clearly defined droplets visible on each negative was relatively small. Collection of the drop size data by this method was therefore tedious and lengthy. As the photographs had to be processed before the quality and quantity of the data was known, the precise number of photographs required to give a sufficiently accurate drop size distribution was not predictable. This inability to qualitatively decide whether a drop size distribution appeared satisfactory at the time of the experiment meant that wastage of photographic film and time was inevitable.

FIGURE. 2:3.

SURFACE VELOCITY RESULTS.

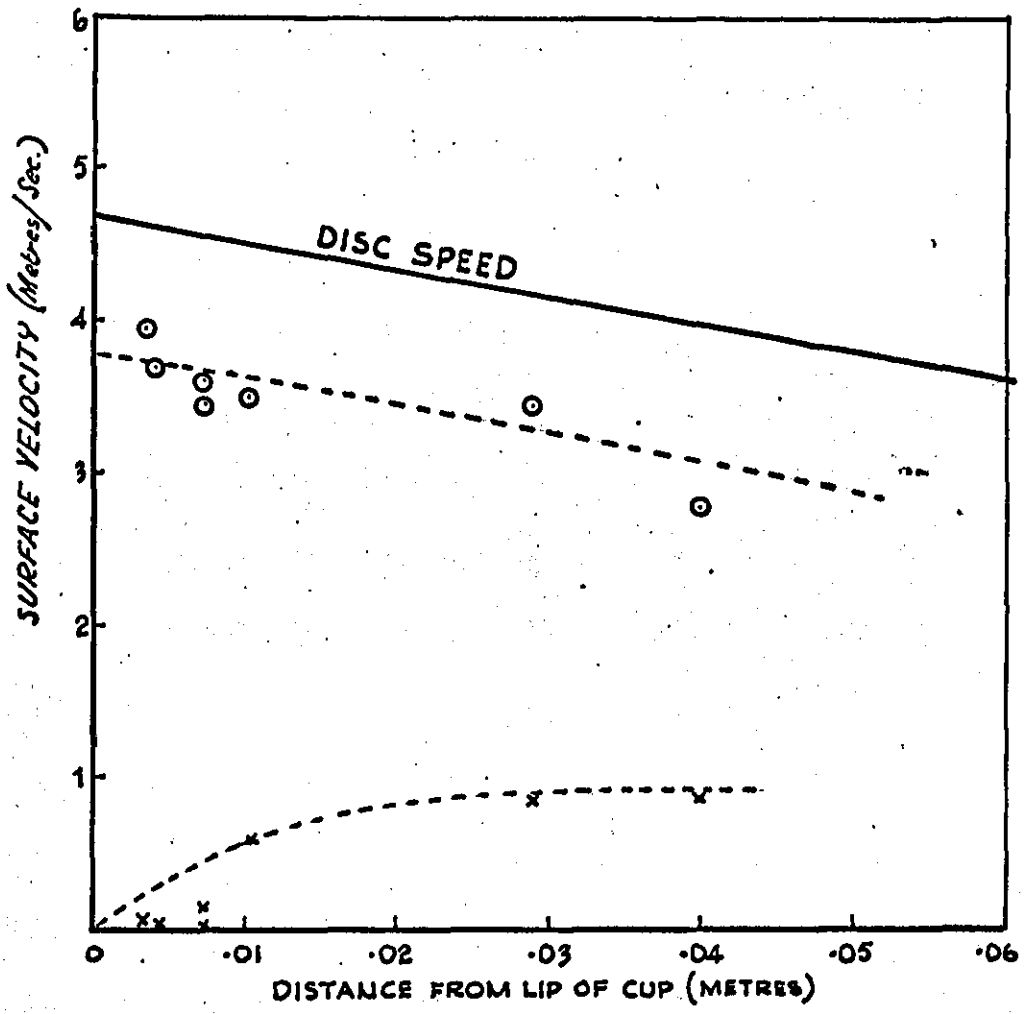

FLOWRATE. 1·05 L/MIN.; SPEED OF ROTATION 6·95 R.P.S.; VISCOSITY = 1 cP.

⊙ AZIMUTHAL VELOCITIES.
× MERIDIONAL VELOCITIES.

If droplets are photographed whilst they are in flight the number in each size range that will be in view will be a function of the velocity, corresponding to that drop size range, assuming that each size range has a unique, distinct, velocity. It is only when all droplets have the same velocity that no correction factor is needed to compensate for the spatial distribution of the droplets.

When a photographic technique is used to measure the drop size distribution of a spray it is therefore necessary to determine the velocity distribution as mentioned above. The velocity distribution is highly dependent on the speed at which the disc rotates and so it would have to be determined at each of the operating conditions used. It can be seen that although at first sight the photographic technique of drop sizing appears simple the method is in fact quite lengthy and open to experimental error.

2.4 Distributor Designs

The distributor used during this early work was rather crude (see Figure 2.4.A). It consisted of a piece of copper tube that had been fashioned into a circular manifold. Numerous holes had been drilled into the manifold thus allowing the feed to be spread equally around the centre of the spinning cup. The feed issued, as a fine jet from these holes, onto the surface of the cup causing the production of a series of helical waves. The main value of this distributor was its compactness as it did not obscure the field of view when the surface velocity photographs were taken. None the less it was decided to redesign the distributor system.

The second design, see Figure 2.4.B, was constructed mainly of wood so that it would float on the surface of the feed to be distributed thus allowing a constantly variable clearance of precisely the right value. In this way it was hoped that the distributor would adjust itself to the flow conditions and as a consequence produce disturbance-free liquid distribution. This distributor was allowed to rotate freely for it was not clamped in any way. Unfortunately it had a tendency of producing secondary disturbances, as droplets which originated on the outside edge of the distributor, impacted on the inside surface of the cup. This distributor also tended to pitch slightly causing uneven liquid distribution.

The third type of distributor tested, see Figure 2.4.C, was constructed entirely in perspex. This distributor was designed to force the liquid feed into a small trough or reservoir from which the liquid would spill out onto the surface of the cup. The distributor rotated at the same speed as the cup thus minimising the viscous shearing of the liquid as it passed between the base of the cup and the distributor lip. During the testing of this distributor small air bubbles were observed emerging from the reservoir. These air bubbles were probably formed inside the distributor when the incoming feed was rotated by the four webs that positioned the distributor on to the central shaft. For this distributor to work efficiently (i.e. no air bubble formation) the distributor had to be flooded which meant that its effective working range was limited.

FIGURE. 2:4.

A. CIRCULAR MANIFOLD TYPE DISTRIBUTOR.

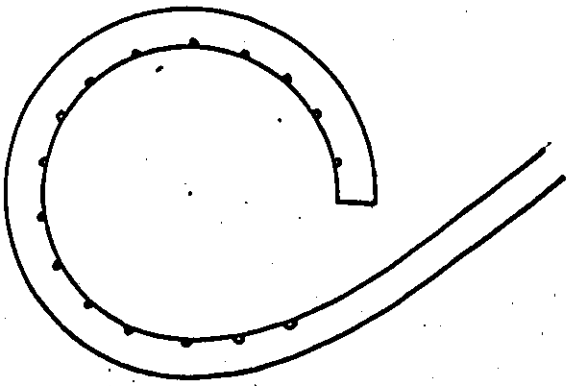

B. WOODEN FLOAT TYPE DISTRIBUTOR.

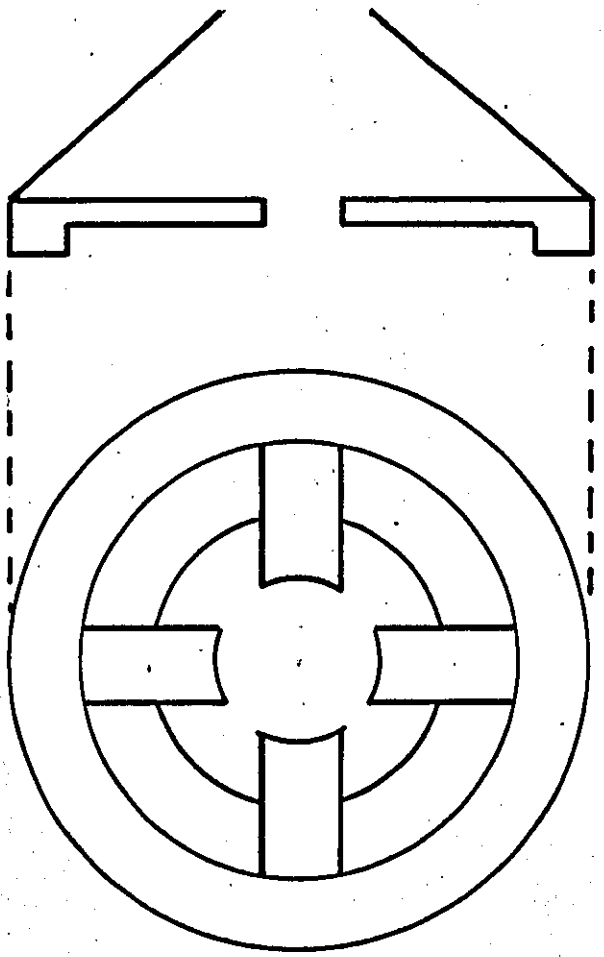

FIGURE. 2:4c.

PERSPEX DISTRIBUTOR.

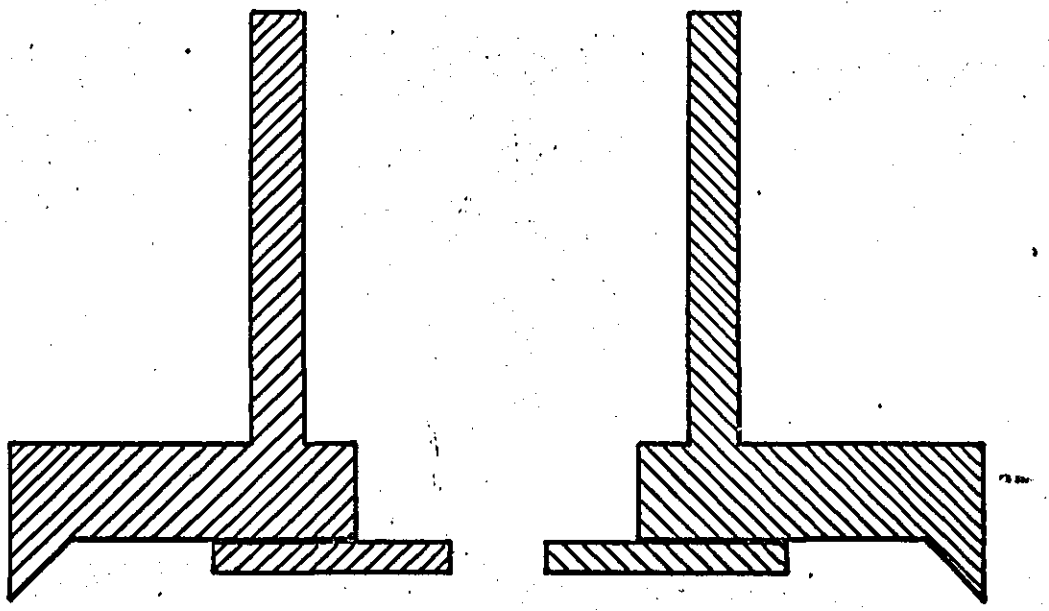

CHAPTER THREE

THE LITERATURE SURVEY

3.1 Film Flow Review

3.2 Film Flow in Centrifugal Fields

3.3 Film Thickness Measurement

3.4 Liquid Film Distribution

3.5 The Operating Equations for Liquid Atomization

3.6 The Mode of Atomization From a Rotating Cup Atomizer

3.7 The Mechanism of Capillary Atomization

3.8 The Sizing of Droplets

INTRODUCTION

In the chemical industry film flow plays an important part in many of the unit operations. There are several evaporators which use the principle of a thin film for enhanced mass transfer. These include falling film evaporators, climbing film evaporators, wiped film evaporators and boilers of the Hickman-Badger type. Consequently much interest has been shown in the film flow of a liquid down vertical pipes and inclined planes. Most of the experimental techniques used for measuring the film thickness on rotating surfaces were developed originally for inclined plane work. And so it is instructive to briefly follow the developments of film flow on an inclined plane before studying the specialised case of rotating surfaces.

Once film flow is established on a rotating cup the liquid will discharge itself at the periphery in one of three ways depending on the operating conditions : as discrete droplets (direct drop régime); as ligaments (ligament régime); and as a continuous sheet (sheet régime). The atomization which occurs is complex and although it does not always behave exactly as Rayleigh's theory predicts, it is advantageous to study capillary jet instability in order to obtain a grounding in the theory underlying atomization.

3.1 Film Flow Review

3.1.1 Laminar flow

The incompressible flow of a Newtonian fluid can be fully described by the equation of motion and the continuity equation. In general orthogonal curvilinear coordinates these can be written[7] as follows; using the Gibbs notation:

$$\frac{\partial \underline{v}}{\partial t} + \underline{v} \cdot \nabla \underline{v} = -\frac{1}{\rho} \nabla p + \nu \nabla^2 \underline{v} \qquad 3.1.1$$

$$\nabla \cdot \underline{v} = 0 \qquad 3.1.2$$

The body forces have been ignored and so they have been omitted from Equation 3.1.1.

3.1.2 Smooth two dimensional film flow under gravity

In rectangular curvilinear orthogonal coordinates the equation of motion can be reduced to the following equations if the flow is steady and if the non linear inertial terms are ignored.

$$\frac{\partial^2 u}{\partial y^2} + \frac{g}{\nu} \sin \theta = 0 \qquad 3.1.3$$

Here, the viscous forces have been balanced with the body forces.

$$\frac{d\Omega}{dy} = \rho g \cos \theta \qquad 3.1.4$$

$$\frac{d\Omega}{dz} = 0 \qquad 3.1.5$$

Film flow only occurs in the x direction and the film thickness is measured in the y direction. θ is the angle the horizontal plane subtends with the inclined plane. These equations are attributed to Hopf[8] and Nusselt[6].

The boundary conditions needed to solve the above equations are :

1, no slip at the liquid solid interface ie u=0 at y=0

2, no interfacial drag at the liquid air interface

ie $\frac{\partial u}{\partial y} = 0$ at $y = \delta_{max}$

On integrating, Equation 3.1.3 becomes:

$$u = \frac{g}{\nu} \sin\theta \left(\delta y - \frac{y^2}{2}\right) \qquad 3.1.6$$

This gives a semi-parabolic velocity profile with a surface velocity equal to

$$u_s = \frac{g\delta^2}{2\nu} \sin\theta \qquad 3.1.7$$

and a mean velocity of

$$u_m = \frac{g\delta^2}{3\nu} \sin\theta \qquad 3.1.8$$

from which it is possible to obtain the film thickness.

$$\delta = \left(\frac{3\nu^2}{4g \sin\theta}\right)^{1/3} N_{RE}^{1/3} . \qquad 3.1.9$$

where $N_{RE} = \frac{4Q}{\pi D \nu}$ (based on the hydraulic diameter) 3.1.10

and Q is the volumetric flowrate.

Wave Formation under two dimensional smooth flow conditions

Numerous experimenters have observed interfacial disturbances in the laminar region when studying film flow down vertical surfaces. The same disturbances have been noted for liquids on inclined planes. However, as the inclined plane approaches the horizontal position the onset of wavy disturbances is progressively suppressed until eventually onset does not occur until the flow is turbulent.

Most theoretical treatments [5,9,10] on the inception of wavy flow are similar, namely the addition of a small perturbation into the Navier-Stokes equations. This yields

equations of the Orr-Somerfield type whose solutions are approximations and usually very complicated. Different treatments give different Reynolds' numbers at which wave inception should occur, but usually the value of N_{RE} for onset varies from 0 to 12.

For wavy laminar film flow Levich[11] has shown the Navier-Stokes equation may be written in the form

$$\frac{\partial u}{\partial t} + u\frac{\partial u}{\partial x} + v\frac{\partial u}{\partial y} = \frac{-1}{\rho}\cdot\frac{\partial P}{\partial x} + \frac{\gamma\partial^2 u}{\partial y^2} - \frac{\partial \Omega}{\partial x} \qquad 3.1.11$$

assuming gravitational flow only the body force term $-\frac{\partial \Omega}{\partial x}$ being equivalent to the component of the gravitational force constant g. By using the normal boundary conditions and assuming that the velocity profiles are semi-parabolic, namely

$$u = \frac{3\bar{u}}{\delta}\left(y - \frac{y^2}{2\delta}\right) \qquad 3.1.12$$

the following equation was developed

$$\frac{\partial \bar{u}}{\partial t} + \frac{9}{10}\bar{u}\frac{\partial \bar{u}}{\partial x} = \frac{\sigma}{\rho}\frac{\partial^3 \delta}{\partial x^3} - \frac{3\gamma\bar{u}}{\delta^2} + g\sin\theta \qquad 3.1.13$$

the continuity equation being

$$\frac{\partial \delta}{\partial t} = \frac{-\partial(\bar{u}\delta)}{\partial x} \qquad 3.1.14$$

By assuming

$$\delta = \bar{\delta}(1 + \phi) \qquad 3.1.15$$

where ϕ is the free surface deformation function.

Equation 3.1.15 becomes

$$\frac{\sigma\bar{\delta}}{\rho}\frac{\partial^3 \phi}{\partial x^3} + (c-\bar{u})\left(\frac{c-9\bar{u}}{10}\right)\frac{\partial \phi}{\partial x} - \frac{3\gamma}{(\bar{\delta})^2}(c-3\bar{u})\phi + g\sin\theta - \frac{3\gamma\bar{u}}{(\bar{\delta})^2} = 0 \qquad 3.1.16$$

The first approximation to this when $\phi = c = 0$ is

$$\bar{u} = \frac{(\bar{\delta})^2 g \sin\theta}{3\nu} \qquad 3.1.17$$

This shows that the mean velocity is not affected by the wave formations.

More recently the film flow of a liquid down an inclined plane has been studied by a number of workers [12-16]. Experimentally, one of these[16] has determined the increase in surface area as well as the variation in film thickness over a larger area of the plane.

3.2 Film Flow in Centrifugal Fields

In comparison with the amount of work that has been published on the inclined plane type of application very little has been published on the film flow of a liquid on a rotating cup or disc. So far most of these treatments have considered the smooth two dimensional laminar flow case only.

One popular method of describing the film flow in a centrifugal field has been to modify the Nusselt equation by substituting the composite acceleration in place of the acceleration due to gravity. This method was chosen by Espig[17], Espig and Hoyle[3] and by Beardall[18]. The resulting modified equation can be written as follows :-

$$\delta\left(\frac{W^2 r \sin\theta - g\cos\theta}{\nu^2}\right)^{1/3} = \left(\frac{3}{4} N_{RE}\right)^{1/3} \qquad 3.2.1$$

where the Reynolds number (N_{RE}) is defined as in section 3.1.1 as

$$N_{RE} = \frac{4Q}{\pi D \nu} \qquad 3.1.1$$

Theoretical treatments by Hinze and Milborn[1] on a horizontally mounted rotating cup, and Emslie et al[19] on a flat disc, when rearranged and modified, to take the differences in geometry into account, produce solutions which are identical to the modified Nusselt equation.

A more recent solution of the Navier-Stokes equation for the film flow of an incompressible Newtonian liquid on a rotating conical disc was presented by Nikolaev et al[20]. Using an orthogonal set of conical coordinates, see Figure 3.1, they produced the following series of dimensionless equations:

$$f_1 = C_1 \text{ Cosh } \beta.\cos\beta + C_2 \text{ Cosh } \beta.\sin\beta + C_3 \text{ Sinh } \beta.\cos\beta + C_4 \text{ Sinh } \beta.\sin.\beta \qquad 3.2.2$$

$$f_\phi = C_1 \text{ Sinh } \beta.\sin\beta - C_2 \text{ Sinh } \beta.\cos\beta + C_3 \text{ Cosh } \beta.\sin\beta - C_4 \text{ Cosh } \beta.\cos\beta - \frac{\cos\alpha}{2R}\beta + C_5 \qquad 3.2.3$$

where f_1 and f_ϕ are the dimensionless velocities in the meridional and azimuthal directions respectively; C_1, C_2, C_3, C_4 and C_5 are functions of L the dimensionless length in the '1' direction.

Equations 3.2.3. and 3.2.4. were found from the solution of two linearised partial differential equations, these being;

$$\frac{\partial^4 f_1}{\partial \beta^4} + 4 f_1 = 0 \qquad 3.2.4$$

$$\frac{\partial^3 f_1}{\partial \beta^3} + 2\frac{\partial f_\phi}{\partial \beta} + \frac{\cos\alpha}{R} = 0 \qquad 3.2.5.$$

FIG. 3.1.

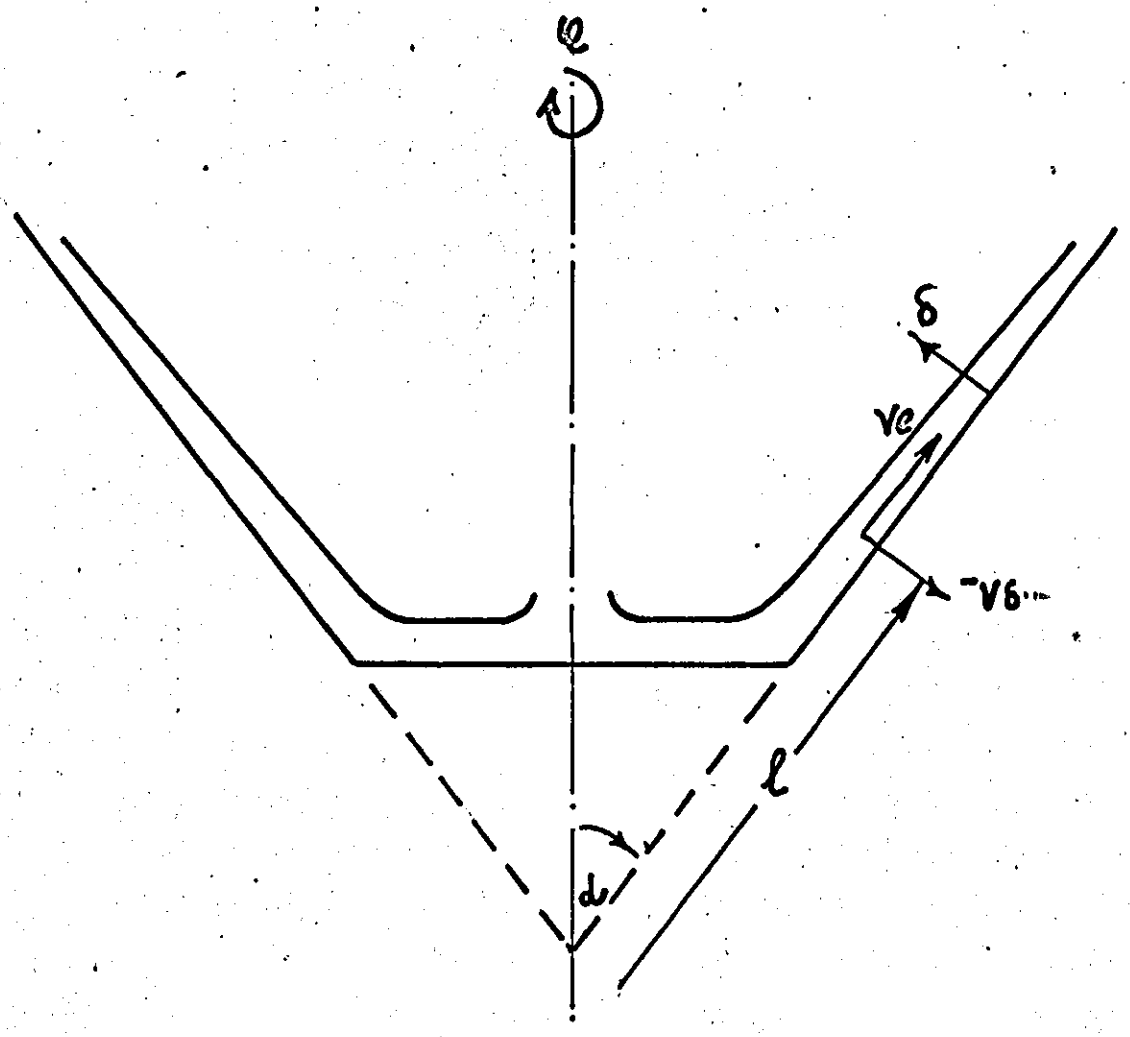

CONICAL COORDINATE SYSTEM (ℓ, δ, φ.)

In Nikolaev's notation the dimensionless variables are defined as:

$$f_l = \frac{V_l}{\sqrt{\frac{w\,\nu}{\sin\alpha}}}.R \qquad f_\phi = \frac{V_\phi}{\sqrt{\frac{w\,\nu}{\sin\alpha}}}.R \qquad f_\delta = \frac{V_\delta}{\sqrt{\frac{w\,\nu}{\sin\alpha}}}.R$$

$$\beta = \frac{\delta}{\sqrt{\frac{\nu}{w\sin\alpha}}} \qquad L = \frac{l}{\sqrt{\frac{\nu}{w\sin\alpha}}} \qquad R = \frac{r}{\sqrt{\frac{\nu}{w\sin\alpha}}}$$

3.2.6

The conical coordinate system used can be seen in Figure 3.1.

Bruin[21], followed the work of Nikolaev et al but used a spherical coordinate system and reduced the Navier-Stokes equations to their linear form. With the use of simplifying assumptions and dimensionless groups Bruin developed four manageable equations. He employed what he called his Ω criterion, in the further simplication of these equations. The Ω criterion is essentially a ratio of the tangential velocity to the average radial velocity and as such is an indication of the type of flow on a cup. When Ω, is so large that its square is much greater than itself (ie $\Omega^2 >> \Omega$) the equations when solved give a solution of the Hinze and Milborn type. In Bruin's notation this is given as :-

$$\delta^+ = \left(\frac{3\,Q_o{}^+}{1 - \frac{\cot\alpha}{Fr}}\right)^{1/3} \qquad 3.2.7$$

where $\delta^+ = \left(\frac{w}{\nu}\right)^{1/2}\delta$; $Q_o{}^+ = \frac{Q_o}{2\pi\sin^2\alpha r^2(w\nu)}{}^{1/2}$ $Fr = \frac{w^2 r\sin\alpha}{g}$

3.2.(8,9,10)

r is measured from the apex of the cone and α is the half cone angle.

$$U = \frac{V_r}{wr\sin\alpha} - \left(1 - \frac{\cot\alpha}{Fr}\right)\left(\delta^+\delta - \frac{1}{2}\delta^2\right) \qquad 3.2.11$$

$$V = \frac{V_\theta}{(w,\nu)}1/_2 = \left(3\sin\alpha - 2\frac{\cos\alpha}{Fr}\right)\left(\frac{1}{2}\delta^+\delta^2 - \frac{1}{6}\delta^3\right) \qquad 3.2.12$$

$$W = \frac{V'\phi}{wr\sin\alpha} = -\frac{1}{3}\left(1 - \frac{\cot\alpha}{Fr}\right)\left(\delta^+\delta^3 - \frac{1}{4}\delta^4 + 2(\delta^+)^3\delta\right) \qquad 3.2.13$$

$$P = \frac{\rho - \rho_0}{\rho(w,\nu)^{\frac{1}{2}}\, r\sin\alpha} = \left(\cot\alpha + \frac{1}{Fr}\right)\left((\delta^+ - \delta)\right) \qquad 3.2.14$$

Bruin then considered the case where $\alpha > 1$. Once again the linear case was chosen which resulted in the following two simultaneous equations;

$$-1 + 2W = -\frac{\cot\beta}{Fr} + U_{66} \qquad 3.2.15$$

$$-2U = W_{66} \qquad 3.2.16$$

These were solved using the complex function $\Psi = U - iW$, the solution being;

$$\Psi = -1/2\, i\, F(z)[\tanh(\delta^+\sqrt{(2i)})\sinh(\delta\sqrt{(2i)}) + 1 - \cosh(\delta\sqrt{(2i)})] \qquad 3.2.17$$

where $F(z) = 1 - \frac{\cot\alpha}{Fr}$ 3.2.18

Taking the real and imaginary parts, the final solutions for U and W were :

$$U = -1/2\, F(z)\ [-\sinh\delta\sin\delta + E_r] \qquad 3.2.19$$

$$W = 1/2\, F(z)\ [1 + E_i - \cosh\delta\cos\delta\ ] \qquad 3.2.20$$

where:

$$E_r = \frac{\sin 2\delta^+ \sinh\delta \cos\delta + \sinh 2\delta^+ \cosh\delta \sin\delta}{\cosh 2\delta^+ + \cos 2\delta^+} \quad 3.2.21$$

$$E_i = \frac{\sinh 2\delta^+ \sinh\delta \cos\delta - \sin 2\delta^+ \cosh\delta \sin\delta}{\cosh 2\delta^+ + \cos 2\delta^+} \quad 3.2.22$$

One interesting variation of the solution for the film flow on a rotating disc is attributable to Hege[22]. He developed a relationship which enabled him to predict the operating conditions necessary for what he called the optimum atomization in the ligament régime (see section 3.6). This relationship provided an identity between the volumetric flowrate and the speed of rotation and so permitted him to substitute the operating conditions in place of the volumetric flowrate. This resulted in the following equation:

$$\frac{\delta_r}{r} = \left(\frac{3}{Re.We}\right)^{1/3} \left(\frac{Fr}{2\pi}\right)^{1/12} \quad 3.2.23$$

where

$$Re = \frac{r^2 w}{\nu} \quad 3.2.24$$

$$We = \frac{r^3 w^2 \rho}{\sigma} \quad 3.2.25$$

$$Fr = \frac{r w^2}{g} \quad 3.2.26$$

It follows from the initial assumptions that equation 3.2.23 will only predict the film thickness, at radius r, for the case when the flowrate is at the optimum atomization value.

An experimental investigation was carried out by Voinov and Khapilova[23] on the film flow of a fluid on the inside surface of a rotating cone. The film thicknesses they measured were in the

range of 0.491 mm to 1.85 mm which are in fact quite substantial when it is realised that the cones they used were relatively large ($\sim$220 mm diameter). Their results tended to be greater than their theoretical prediction at the inlet and at the lip their results were less than their predicted values.

The work of Emslie et al[19] previously mentioned was mainly concerned with the possibility of using a centrifugal spin off technique so as to coat colour television screens with a uniform thickness of phosphor particles. As such they were interested in the rate of change in film thickness with respect to time. By assuming a series of initial contours they were able to predict the level of uniformity of the final liquid from the characteristic curves they constructed. However, as they were not interested in the steady flow of a liquid on a disc or cup their work shall not be discussed further.

3.3 Experimental Techniques Used to Measure Liquid Film Thicknesses

The experimental techniques used to measure liquid film thicknesses have, in the main, been developed for the inclined plane type of application. Consequently some of the techniques are hardly suitable for a rapidly rotating system where the film thicknesses are generally very thin. However, it is interesting to trace the development of film thickness measurement as it indicates the level which the theoretical analysis has reached. These techniques have been quite adequately reviewed by Beardall[18]; however, as they are of considerable interest a short account of the various methods will be given.

3.3.1 Probe and dial gauge

The use of a probe and dial gauge to measure film thicknesses has proved very popular[8,24-30]. Initially this technique consisted of lowering a probe until it just touched the surface of the film. By knowing the dial gauge value of the inclined plane an assessment of the maximum film thickness which would correspond to the maximum wave crest height was made. Direct observation of the film was needed to judge when the probe touched the film.

A slight modification of this technique was introduced to overcome the difficulties in deciding when the probe touched the liquid film. This modification was essentially an electrical circuit incorporating a light bulb so that an optical indication of when the probe was touching the film was given.

This technique was first adopted for spinning discs by Espig[17] and later by Espig and Hoyle[3] and then by Voinov and Khapilova[23]. The first two of these used the modified method in an attempt to correlate film thickness results using a modified form of Nusselts Theory.

3.3.2 Photographic methods

Previously this method has only been used on the inclined plane type of application, where generally the liquid profile has been photographed. Two main criticisms have been levelled at this technique; firstly, due to orthogonality, the wave crests tend to obscure the troughs in the three-dimensional wave region, and secondly surface tension effects at the sides of the inclined plane influence the recorded film thicknesses.

It is possible that this technique could be used for the case where the film flow is on the outside surface of a rotating "male" cone. Once again the results obtained would be biased due to the wave crests obscuring the troughs as in the above case.

Recently a photographic technique has been developed[15] to measure the interfacial area of a liquid film in a three dimensional wavy flow. The experimental work, due to Clegg[16], was based essentially on a light extinction technique where the intensity of light passing through the film was dependent on the dye concentration and the film thickness and hence followed Beer's Law[31]. In this technique the photograph was used as an instantaneous record of the surface features of the falling film over a large area.

This technique could be adopted for the film flow on a rotating disc when orthogonality problems are not important (cf. cups and other geometries). This would enable a substantial section of a disc to be analysed and hence from relatively few plates large amounts of experimental data could be gathered quickly and accurately.

3.3.3 Electrical capacitance methods

The electrical capacitance method is capable of high accuracy and has been used successfully by a number of experimenters[32-34] for the inclined plane type of application. Essentially the air gap between the accurately machined capacitance probe and the liquid surface is continually monitored by means of a capacitance bridge arrangement. If the dimensions of the probe are correctly designed it is possible to use this type of probe to measure wave profiles. However the probe must be smaller than

the wavelengths under investigation, and must only be used in the periodic flow regime if instantaneous results are required.

In the case of a rotating disc the film thickness monitored by this method would not normally be the instantaneous film thickness as the wave profiles are not generally two dimensional nor are the wavelengths large. Difficulties would occur if the instantaneous film thickness was required using this technique as the probe would have to be very small. Consequently to get measurable capacitance values the air gap would have to be extremely small, in which case wetting of the probe and cup eccentricities would become significant.

3.3.4 Electrical resistance

The electrical resistance technique measures the film thickness indirectly by continuously monitoring the resistance between two probes set in the walls of an inclined plane. High accuracy may be obtained using this method when the film thickness is required in the two dimensional wavy region. However, anomolous results are obtained when this technique is used in the random or three dimensional wave region. This technique is unsuitable for measuring the film thicknesses on rotating cups and bowls and it is also doubtful whether it is suitable for vaned discs due in part to the associated problem of electrical 'noise' at the rotary contacts which would be needed.

3.3.5 Light Extinction

The light extinction method has been used by Clegg[16] (see 3.3.2) to measure the local film thickness and the interfacial surface area for the flow of liquids down an inclined plane. The principle of light extinction can be expressed mathematically by

means of the Lambert-Beer Law [31]. This states that the intensity of light passing through a liquid is a function of: the incident angle; the dye concentration; the film thickness and finally the incident light intensity.

Experimentally a light beam is passed through the liquid film and the exeunt intensity is monitored continuously using an optical light cell. Often it is necessary to add a dye to the liquid under test, this can affect the physical properties (e.g. surface tension) and so this technique may only be used when the change in properties is unimportant.

Reflection and refraction are two optical properties which must be considered where there are interfaces present in an optics experiment. These have been considered in an investigation by Hewitt and Lovegrove [35]. The nature of the interface is also of importance as the exeunt light intensity is sensitive to the interface e.g. solid/air or liquid/air interfaces.

By using a narrow beam and a large detector (so as to 'catch' any refracted light due to wave fronts) this technique is ideally suited to the continuous monitoring of the instantaneous film thickness.

3.3.6 Radio-active tracer

Rapid and accurate average film thickness results can be achieved using the radio-active tracer method. Jackson [36] used this method in an inclined plane type of application using Yttrium 90 as the radio-active source.

Although in essence this method is extremely reliable care must of course be exercised, as is the case with all radio-active materials.

3.3.7 β-backscatter device

This technique, used by Beardall[18] in determining averaged liquid film thicknesses on the outside surface of a rotating 'male' cone, can be considered to be a more sophisticated application of the radio-active technique. The device consists of a central radio-active source which is surrounded by a protected detector. Emitted radiation is partially absorbed by the film and so the detected backscattered radiation can be directly calibrated in terms of film thicknesses.

This device has been used extensively in the paint industry where it is used to measure the paint film thickness. Experience has shown that this technique is capable of a high degree of accuracy.

3.3.8 The correlation of film thickness results

The most generally accepted method of expressing film thickness results, whether it be for inclined planes, vertical tubes or rotating discs, seems to be by utilising what is known as the Nusselt film thickness parameter.

The modification of the Nusselt parameter which is attributable to Espig and Hoyle[3] replaced the gravitational component, $g \cos \Theta$, by the centrifugal component, $W^2 r \sin \alpha$. More generally the modified Nusselt equation, for a rotating cup, should be :

$$\left(\frac{3}{4} N_{RE} \right)^{1/3} = \delta \left(\frac{W^2 r \sin\alpha \pm g \cos\alpha}{\nu^2} \right)^{1/3} = N_T^* \qquad 3.2.1$$

where N_T^* is known as the modified Nusselt film thickness parameter.

More recently the theories of Nikolaev et al[20] and Bruin[21] provided another method of correlating smooth, laminar two dimensional film flow data. In both cases they developed

the following relationship :

(using Bruin's notation) $$I_o(\delta^+) = \frac{\sinh 2\delta^+ - \sin 2\delta^+}{\cosh 2\delta^+ + \cos 2\delta^+} \qquad 3.3.1$$

where $I_o(\delta^+)$ can be found experimentally from the equation:

$$I_o(\delta^+) = \frac{4Q_o^+}{F(z)} \qquad 3.3.2$$

where Q_o^+ is defined by equation 3.2.9 and F(z) by equation 3.2.18.

Nikolaev produced a relationship between an experimentally determinable group and the hyperbolic/trigonometric group in equation 3.3.1 by solving the differential equation which contained the pressure differential term. The solution, in its simplified form, was expressed as follows:

$$\frac{\text{Sinh } 2\beta_o - \sin 2\beta_o}{\cosh 2\beta_o + \cos 2\beta_o} = \Psi_1 = \frac{2Q\sqrt{\frac{w \sin^3\alpha}{\nu}} \Big/ (\pi R^2 \nu) - \frac{\cos\alpha}{R}}{1 - \frac{g \sin\alpha}{\sqrt{w^3 \nu}\, R \tan\alpha} + \frac{\sigma}{\rho\sqrt{\frac{w\nu^3}{\sin\alpha}}\, RL^2 \tan\alpha}} \qquad 3.3.3$$

Thus the left hand side of the above equation can be found for any value of β_o and the theory tested by plotting the right hand side and comparing the results obtained.

Bruin's equivalent to equation 3.3.3 does not contain two of the terms. The first is $-\cos\alpha/R$ which is generally small compared with the volumetric flowrate. The second term which is absent in Bruin's equivalent is the surface tension term which forms part of the denominator in equation 3.3.3. When a liquid with a large surface tension is used (e.g. water), the value of this term can become significant if the radius is reasonably

small. It is this term which can affect the value of Ψ_1 such that it can become significantly different from $I_o(\delta^+)$, Bruin's equivalent.

Nikolaev illustrated the preceding relationship by plotting β_o against Ψ_1. (See Figure 3.2). Their experimental data when plotted fitted their relationship closely, however in the range they choose the difference between a Nusselt type plot and their theory is negligible. Some other experimental evidence was used[2] but only a couple of points extended into the region where the two theories differ.

In the development of equations 3.3.3 several terms were omitted by Nikolaev. Of these only one becomes important and then only when β_o (or δ^+) is less than or equal to 0.3. The full term is:

$$\frac{\cos\alpha}{R}\left(\frac{2\,Ch\,\beta_o\cos\beta_o}{Sh2\beta_o-\sin 2\beta_o}\right)$$

When β_o is small the hyperbolic, trigonometric function becomes significant,

i.e.

β_o	$\frac{Ch\beta_o\cos\beta_o}{Sh2\beta_o-\sin 2\beta_o}$
.1	400
.2	47.2
.3	13.9

For a low viscosity liquid such as water, $\cos\alpha/R$ is usually high e.g. $\cos\alpha/R > 500$ (say), thus for $\beta_o > .3$ this terms becomes insignificant.

3.4 The Distribution of a Liquid on to a Spinning Disc

It is clearly obvious that the researchers investigating inclined plane work were conscious of the need for good initial liquid distribution. Carefully levelled weirs were used to prevent

FIG.3.2.: THE COMPARISON OF THE NIKOLAEV AND NUSSELT RELATIONSHIPS. (SEE SECTION 3.3.8.)

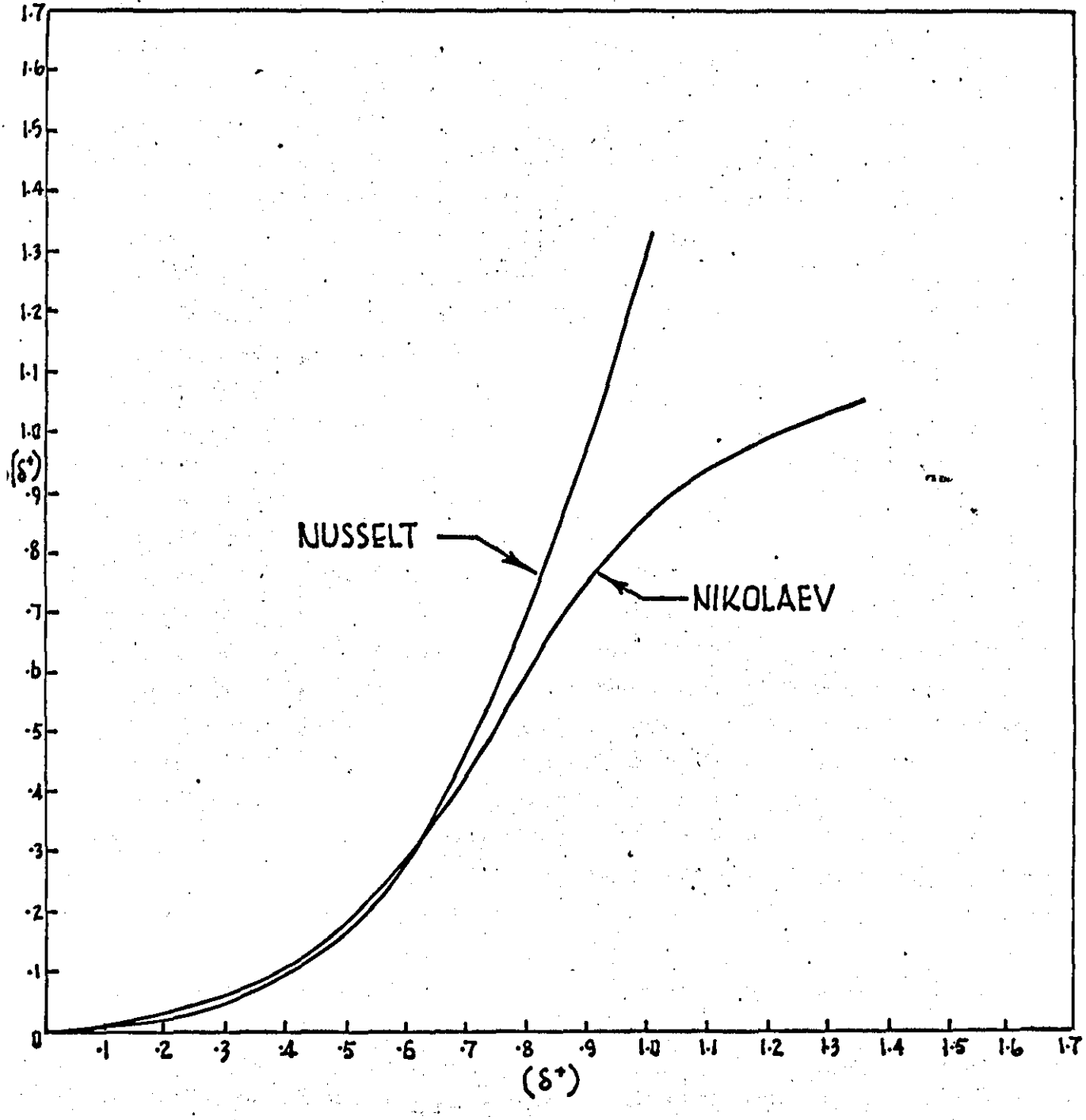

initial disturbances propagating from the weir. Unfortunately the same precautions have not always been taken with spinning cups and bowls. Hinze and Milborn[1] show schematically that in their experiments the feed was discharged straight from the delivery tube to the side wall. They quote that to achieve a uniform film thickness it is necessary that:

1. the centrifugal acceleration must be very great with respect to the gravitational acceleration ($w^2r > 10g$),
2. the rotation completely free from vibrations,
3. a uniform supply of liquid,
4. the liquid to be supplied to the cup wall where the wall is only slightly conical, preferably cylindrical,
5. the wall surface must be perfectly smooth.

Fraser et al[37] emphasised that prior to 1963 most workers considered that slight disturbances caused by the initial distribution of the liquid would smooth themselves out under the centrifugal acceleration. This, they point out, is only true if the liquid can be spread out on an infinite cup at low flowrates (i.e. thin films) without breaking down into rivulets. A series of different distributors were designed and tested for 2-inch diameter cups. These cups were 5 inches long with a 5^{o} taper ending in a 30^{o} taper at the lip (see Figure 3.3).

The liquids they employed to test the various distributors varied in viscosity from 5 to 165 cS whilst the surface tension variations (29-35 dynes/cm) and the density variations (0.81-0.83gm/cm) were relatively small. The authors found that all the distributors were capable of producing a uniform sheet from the cup's lip but the various operating limits were different. Generally, rotating

FIG. 3.3.

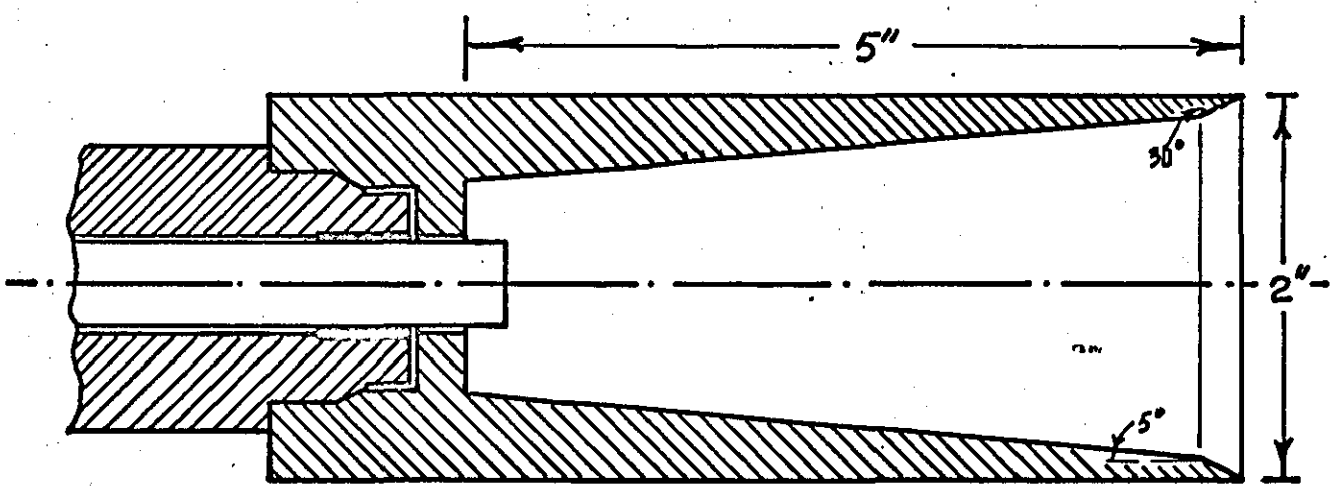

SPINNING CUP USED BY FRAZER ET AL (37)

distributors were found to be more successful than the stationary ones and those incorporating an internal reservoir were the most successful of all.

For cups employing an internal reservoir and weir the depth of the reservoir becomes of interest. Philips[38] has shown that an annular mass of liquid when rotating in a horizontal cylinder inhibits wave formations as long as the Reynolds number is kept small. As this work was done under zero axial flow conditions, in order to approximate to Philips' conditions, a compromise on the depth is necessary. It must be small enough for the Reynolds number $\left(\frac{b^2w}{\nu}\right)$ to be low yet deep enough so as not to seriously violate the zero axial velocity condition.

Espig and Hoyle[3] used a rotating distributor that fed the liquid on to a flat rotating disc. The distributor was mounted directly above the disc on to the central drive shaft and was capable of vertical movement such that the gap between the distributor and the disc could be varied. The authors observed the occurrence of helical waves at their highest flowrates. These waves were presumably generated from the distributor and were capable of being suppressed by the addition of a detergent.

In an article which is mainly concerned with aspects of atomization Hege[22] shows a sketch of the three different types of spinning discs that he investigated. It is interesting to note that the flat disc used has a central well or reservoir, however from the sketch there must be some doubt as to how effective his reservoir would actually be.

Beardall[18] was interested in the coarse classification of slurries from the inclined external surface of male discs. He centre fed his slurries into a rotating distributor in much the same way as Espig and Hoyle. Wave formations were often observed and photographic evidence was supplied. Unfortunately the type of distributor used by Beardall seems to be sensitive to the volumetric flowrate and the rate of rotation. The peripheral gap through which the liquid flows is fairly critical as air can be entrained causing bubbles to appear on the film surface. Secondly, at even moderate rates of rotation water has a tendency to 'climb' the outside edge of the distributor and discharge itself as discrete droplets. These droplets on impaction with the liquid film produce secondary disturbances.

An investigation was carried out by Voinov and Khapilova[23] into the flow of a thin fluid layer on the surface of a rotating cone. They distributed their fluid axisymmetrically by using a deflector plate that had been shaped to follow the contours of their rotating cone near its apex. The deflector plate was bolted onto the cone and so rotated with it, thus helping to accelerate the fluid up to the angular velocity of the cone. During their investigation the flowrates used were high (350ccs/sec and 500ccs/sec) whilst the speed of rotation was relatively modest (600 rpm and 900 rpm). Presumably these operating conditions would suit this type of distributor although from the experimental evidence presented disturbances were possibly present in the fluid on the inside surface on the cone.

Boshoff[39] was interested in the possibility of increasing the throughput of a spinning disc atomizer by increasing the disc's diameter without sacrificing the near 'monosized' characteristics of the direct-drop regime of atomization. He used a flat disc of $14\frac{1}{4}$ inches diameter which had a 90° edge. No mention of the liquid feed arrangement was made other than the liquid was discharged on to the centre of the disc although in his conclusions he states "it is essential to feed the liquid accurately to the centre of the disc". It is not easy to tell whether the mode of liquid distribution on to his discs affected his results. Certainly his correlation coefficient was not very constant, nor was it in agreement with the result of Walton and Prewett[40]. However in the communications that followed the presentation of his paper, Dr Muraszew observed that Boshoff's sampling technique was probably the cause of the erroneous results obtained.

3.5 The Operating Equations for Liquid Atomization

Before any equation can be used it is necessary to determine the limits of its usefulness. In this particular case the type of atomizer initially used must be determined as well as the mode of droplet formation employed. A short characterisation of the different types of atomizers is therefore useful. This can be seen most clearly by referring to Figure 3.4.

FIG. 3.4.

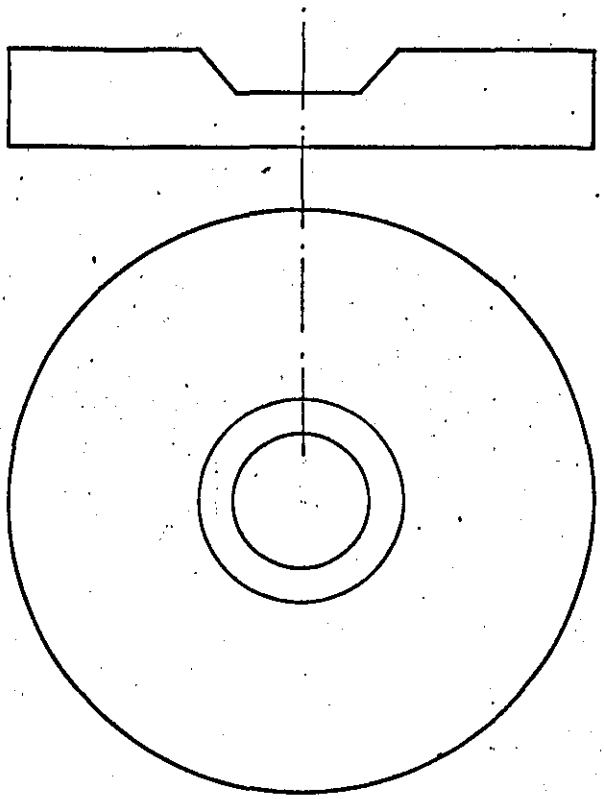

TYPE. A. FLAT DISC WITH RESERVOIR.

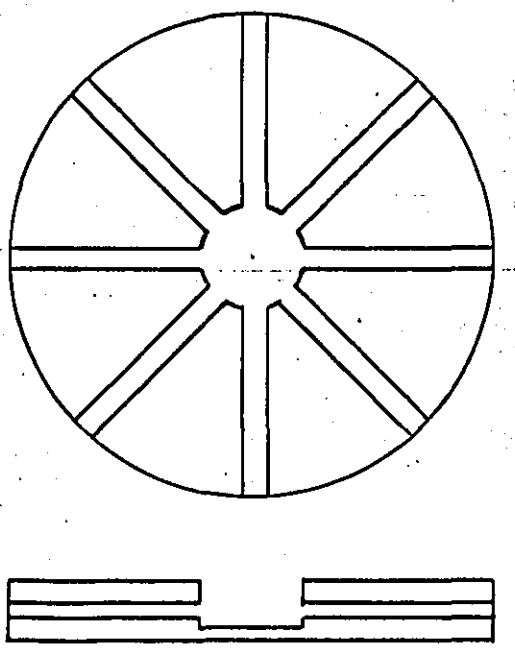

TYPE. B. SPOKED DISC WITH INTERNAL RESERVOIR.

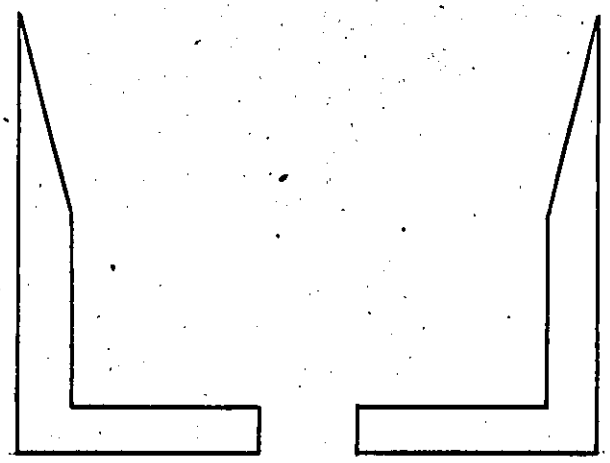

TYPE. C. CUP.

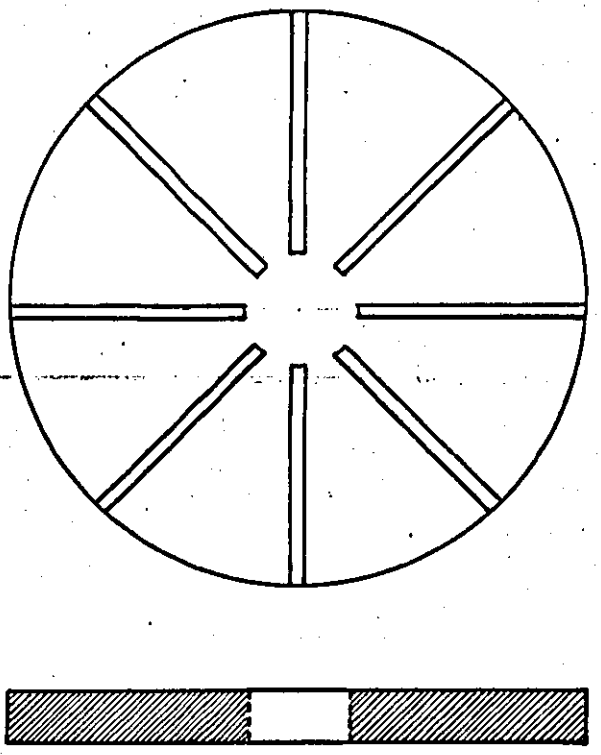

TYPE. D. VANED DISC.

Although these four designs do not cover all the discs used in practice they are representative of the most commonly used rotating atomizers.

Atomization from the peripheral lip of a rotating disc has only been a subject of interest to experimenters[40-44] over the last 50 years. One of the earliest workers was Bär[42] who studied the atomization from two designs of rotating disc (Types A and B). When surface forces predominated and there was individual droplet formation at the low feed rates employed, Bär found the following equation held:

$$d_{max} = \frac{0.525}{n}\left(\frac{\sigma}{D\rho}\right)^{0.5} \qquad 3.5.1$$

For the case of friction and impact controlling atomization the operating equation was found to be:

$$d_{max} = \frac{0.102\,\delta}{n^2 r^2 \rho_c} \qquad 3.5.2$$

Walton and Prewett[40] developed an equation for the atomization of a liquid on a flat rotating disc (Type A). They found that at relatively low flowrates a uniform main drop size could be achieved but they also observed the occurrence of satellite drops of considerably smaller diameter. They postulated that:

$$d_{max} = \frac{0.428}{n}\left(\frac{\sigma}{r\rho}\right)^{0.5} \qquad 3.5.3$$

However, at high speeds of rotation the constant has been found to be 0.495 (i.e. in the aerosol range) and at lower rates of rotation where the droplets are larger ($\sim$1mm) the constant is approximately 0.36.

For large discs at small flowrates or high viscosities to eliminate slippage - the following equation held:

$$d = 6.855\ D \left(\frac{\mu_L}{\rho_L \sigma D}\right)^{0.041} \left(\frac{w^2 D^3 \rho_L}{\sigma}\right)^{-0.522} \qquad 3.5.4$$

Maraszew[43] presented the same formula as Walton and Prewett for small discs at high speeds but this was not substantiated with data. At more ordinary operating conditions, lower speeds and greater flowrates, Maraszew suggested a modification to Triebnigg's formula.[45]

$$d_{max} = \frac{4\sigma}{\Psi V^2 \rho_a} \qquad 3.5.5.$$

Ψ = air resistance coeff.
V = velocity ft/min

If $V = 2\sqrt{2}\pi nr$ then the above equation is comparable with Bär's second equation.

Two operating equations were developed by Ryley[46] for flat rotating discs (Type A) of 2, 3 and 5cms. diameter. The rotational speeds varied from 19,000-70,000 revs/min and the flowrates from 0.121 to 0.771 gm/sec. From Figure 3.5 it can be seen that this work was mainly carried out in the ligament regime. The general correlation of droplet sizes was quoted using the Sauter mean diameter criteria.

$$\frac{d_{sv}}{r} = 3.81 \times 10^{-5} \left(\frac{T}{\mu}\right)^{1.48} \left(\frac{T}{\rho n r^2}\right)^{1.41} \left(\frac{\sigma \rho_L}{T^2}\right)^{1.35} \qquad 3.5.6.$$

Whilst the maximum droplet size equation was given as :

$$\frac{d_m}{r} = 7.41 \times 10^{-5} \left(\frac{T}{\mu}\right)^{1.48} \left(\frac{T}{\rho n r^2}\right)^{1.41} \left(\frac{\sigma \rho_L}{T^2}\right)^{1.35} \qquad 3.5.7.$$

where T is the mass flowrate at the lip of the disc gm/(cm-sec), and L is the wetted periphery.

In order to express quantitatively the extent of the dispersion in the spray Ryley used the Rosin-Rammler[47] equation i.e.

$$R = \exp\left[- (d/d_1)^q \right] \qquad 3.5.8$$

The distribution constant q denotes the uniformity of the spray, thus if q is maximised the size distribution will be at its most peaky. For each test conducted a value of q was obtained from a Rosin-Rammler plot. These were then correlated giving the following expression.

$$q = 7.9 \times 10^{-3}\ n^{0.53}\ T^{-0.29} \qquad 3.5.9$$

Ryley points out that this correlation is somewhat tenuous as the experimental data, from which it is derived, contains considerable scatter. However, this empirical equation is useful as it enables an operator to choose a spinning disc so that the desired degree of uniformity in the spray may be achieved.

Using vaned discs (Type D), Friedman et al[48] developed the following equations by means of dimensional analysis.

$$\frac{d_{sv}}{r} = 0.4 \left(\frac{T}{\rho n r^2}\right)^{0.6} \left(\frac{\mu}{T}\right)^{0.2} \left(\frac{\rho \sigma_L}{T^2}\right)^{0.1} \qquad 3.5.10$$

and

$$\frac{d_{max}}{r} = 1.2 \left(\frac{T}{\rho n r^2}\right)^{0.6} \left(\frac{\mu}{T}\right)^{0.2} \left(\frac{\rho \sigma_L}{T2}\right)^{0.1} \qquad 3.5.11$$

In their judgement these equations are quoted to $\pm$ 30% or better. It is interesting to note, as Ryley did, that the ratio d_{max}/d_{sv} for Friedman's work is 3 whilst for Ryley's work the value is 2. Both Friedman et al and Ryley used coated slides (magnesium oxide coatings) during their investigations. Ryley however corrected his results in accordance with the work of May[49]. May showed that for droplets over 200 μm the crater produced on impact with the magnesium

oxide coating was larger than that expected. It was reasoned that droplets over 200 μm are structurally weaker and hence deform on impaction.

Baryshev et al[50] investigated the atomization of liquids from rotating discs with a co-current gas stream interaction. Experimentally they covered a range from 500-3000 rpm on discs from 5-20 cms diameter. The liquid flowrates varied from 2.5 - 90 ccs/sec whilst the gas velocity varied from 0.5 - 14.5 m/sec. Their results were correlated into a dimensionless equation of the form:

$$\frac{d}{D} = K\left(\frac{Q_L \rho_L}{D \mu_L}\right)^a \left(\frac{v_g D \rho_g}{\mu_g}\right)^b \left(\frac{D^2 w \rho_g}{\mu_g}\right)^c \left(\frac{\sigma_L}{D^3 w^2 \rho_L}\right)^d \qquad 3.5.12$$

the indices were found to be a = 0.10; b = -0.10; c = -0.35; d = 0.05 and the constant, K = 1.10 where d is the arithmetic mean drop size.

The experimental results obtained by Baryshev have been plotted on a log/log graph and found to give a reasonably linear plot. Drop sizing was achieved by using the familiar oil bath technique and the usual corrections for the change in shape of the drops in the bath due to surface tension and gravity forces were made. No indication was made of the droplet size uniformity, i.e. the size distribution, and as only 200 to 300 droplets were sized it is doubtful if an accurate size distribution could be found with this amount of data. Dunsky et al[51] were interested in the relative quantities and sizes of satellite drops formed from a spinning disc. Their work was conducted in the direct drop regime (flowrates from 0.03 to 1.7 cm^3/sec; angular velocity from 31.4 to 660 rads/sec; radius from 1 to 11 cms; density from 0.89 to 1 gm/cm^3 and surface tension from 29 to 73 gms/sec^2). They concluded that the percentage relative weight of satellite droplets (E) could

be expressed mathematically as $E = E(w, \nu, R, Q, \sigma, \rho)$ from which they developed the following relationship;

$$E = 86 \frac{w^{0.48} \nu^{0.12}}{R^{0.30}} \left(\frac{\rho Q}{\sigma}\right)^{0.62} \leq 100\% \qquad 3.5.13$$

An equation was also developed giving the size of satellite droplet on the mass median basis:

$$d_{SAT.M} = \frac{1.1}{w} \left(\frac{\sigma}{R\rho}\right)^{1/2} \qquad 3.5.14$$

The experimental data given in support of equation 3.5.13 shows considerable scatter; however, this equation does show the trends most clearly.

The factors affecting the drop size distribution of a spray from a spinning disc were investigated by Reusova and Lykov[52]. Several experimental graphs were presented showing the dependence of Sauter diameter, and the two Rosin-Rammler coefficients with change in viscosity, surface tension and rate of disc rotation. These were analysed to give a series of operating equations which can be used to predict the homogeneity of a given product.

Straus[53] investigated the direct drop régime and observed that the mode of atomization was similar to the formation of a droplet from a capillary tip except that there is satellite drop formation on a spinning disc. He conducted numerous qualitative experiments and found that in fact the atomization more closely resembled the capillary tip than the Rayleigh instability mechanism. Straus also concluded that the lip geometry had a significant effect on the drop size whereas Walton and Prewett[40] had earlier concluded the lip geometry did not influence the atomization.

The "capillary tip" theory of Straus was quantitatively supported by Dunskii and Nikitin[54]. They found the equation governing the capillary tip mechanism can be written as:

$$r_d\,(2g\rho_L/\sigma) = \text{const} = 2.0 \qquad 3.5.15$$

where r_d is the droplet radius (the constant, for Rayleigh instability, would be 2.3[55]). Dunskii and Nikitin found that the range of the constant varied from 1.87 to 2.14 with an arithmetic mean of 2.0 thus substantiating the earlier work of Walton and Prewett and of Straus.

3.6 The Mode of Atomization from a Rotating Cup Atomizer

Once the liquid film reaches the periphery of the cup the liquid must discharge, assuming that the operation is at steady-state. The manner in which the liquid discharges has been summarised by Hinze and Milborn[1]. They also studied the transition from State II to State III, namely the transition from the ligament régime to the sheet régime. Fraser et al[56] substantiated the work of Hinze and Milborn when they investigated the transition from the sheet régime to the ligament régime.

According to Hinze and Milborn the three régimes of liquid discharge may be defined as follows:

State I "At a very small supply rate a liquid torus is formed around the edge. The diameter of this torus is determined mainly by equilbrium conditions between centrifugal and surface-tension forces. Because of disturbances the torus will be varicosely deformed. Incidentally, drops will be formed singly at one or more bulges of the torus by the action of centrifugal forces; these drops are flung off from the edge...." This they describe as "disintegration by direct drop formation".

State II "At an increased rate of supply, the state of formation of drops singly at the bulges of the torus may transit into the formation of complete thin jets or ligaments. The number of these ligaments increases with increasing rate of supply up to a maximum value, after which the number remains constant, irrespective of the rate of supply. Apparently, in this state the ligaments grow in thickness with increasing rate of supply. The ligaments themselves are unstable for disturbances and break up into drops at some distance from the edge of the cup." This they called "disintegration by ligament formation".

State III "Still further increasing the rate of supply, a condition is reached where the number of ligaments can increase no more, nor can they grow in thickness. The ligaments are unable to consume all the liquid supplied to the cup. The result is that, roughly speaking, the torus will be flung off the edge and a film will be formed extending to a certain distance from the edge where it breaks up in an irregular way into ligaments and clots of liquid..." This they called "disintegration by film formation".

Hinze and Milborn developed the following equation to express the number of ligaments on a rotating disc as a function of the operating variables.

$$Z = 0.215\left(\frac{\rho_w \omega^2 D^3}{\sigma}\right)^{5/12}\left(\frac{\rho \sigma D}{\mu^2}\right)^{1/6} \qquad 3.6.1$$

They assumed that transition from the ligament to the sheet regime would occur if,

$$Q > \text{constant} \times Z\, \delta^2_{l(max)} U_l \qquad 3.6.2$$

i.e. transition would occur when the ligaments were unable to discharge all of the inflowing liquid. They found that the

following operating equation fitted their experimental evidence quite closely:

$$\frac{\rho Q^2}{\sigma D^3}\left(\frac{\rho_w^2 D^3}{\sigma}\right)^{0.60}\left(\frac{\mu^2}{\rho\sigma D}\right)^{0.167} = 1.77 \qquad 3.6.3$$

This they plotted on log/log graph paper (see Figure 3.5). The experimental agreement seems to be very good even though the authors accept some scatter in these results.

A more thorough mathematical treatment was made by Fraser et al[56] when they considered the transition from the sheet régime to the ligament régime. Firstly they assumed the liquid was inviscid and so they were able to write down the following balance:

$$\rho_L Q V_c = 4\pi\gamma\left(\frac{d_L}{2} + a\right) \qquad 3.6.4$$

where V_c is the contraction velocity and 'a' is the sheet extent. Viscous forces were then allowed for by using a simple function of the Reynolds number.

Thus

$$V_c = K_o \frac{4\pi\gamma}{\rho_L Q}\left(\frac{d_L}{2} + a\right)\left[\frac{Q}{\nu(d_L+2a)}\right]^b \qquad 3.6.5$$

For transition to occur the authors argue that the contraction velocity V_c must exceed the radial velocity component and in such cases the sheet extent, "a", tends to zero. After various substitutions they arrived at their operating equation -

$$\left(\rho_L \frac{n^2 d_L^3}{\gamma}\right)\left(\frac{Q}{n d_L^3}\right)^{4/3}\left(\frac{\nu d_L}{Q}\right)^{(b-1/3)} > 14.4\, K_o \qquad 3.6.6$$

With the use of the experimental data of Hinze and Milborn, Fraser found the final form of their equation to be:

FIG. 3.5.

CHART OF THE THREE RÉGIMES OF DROP FORMATION.

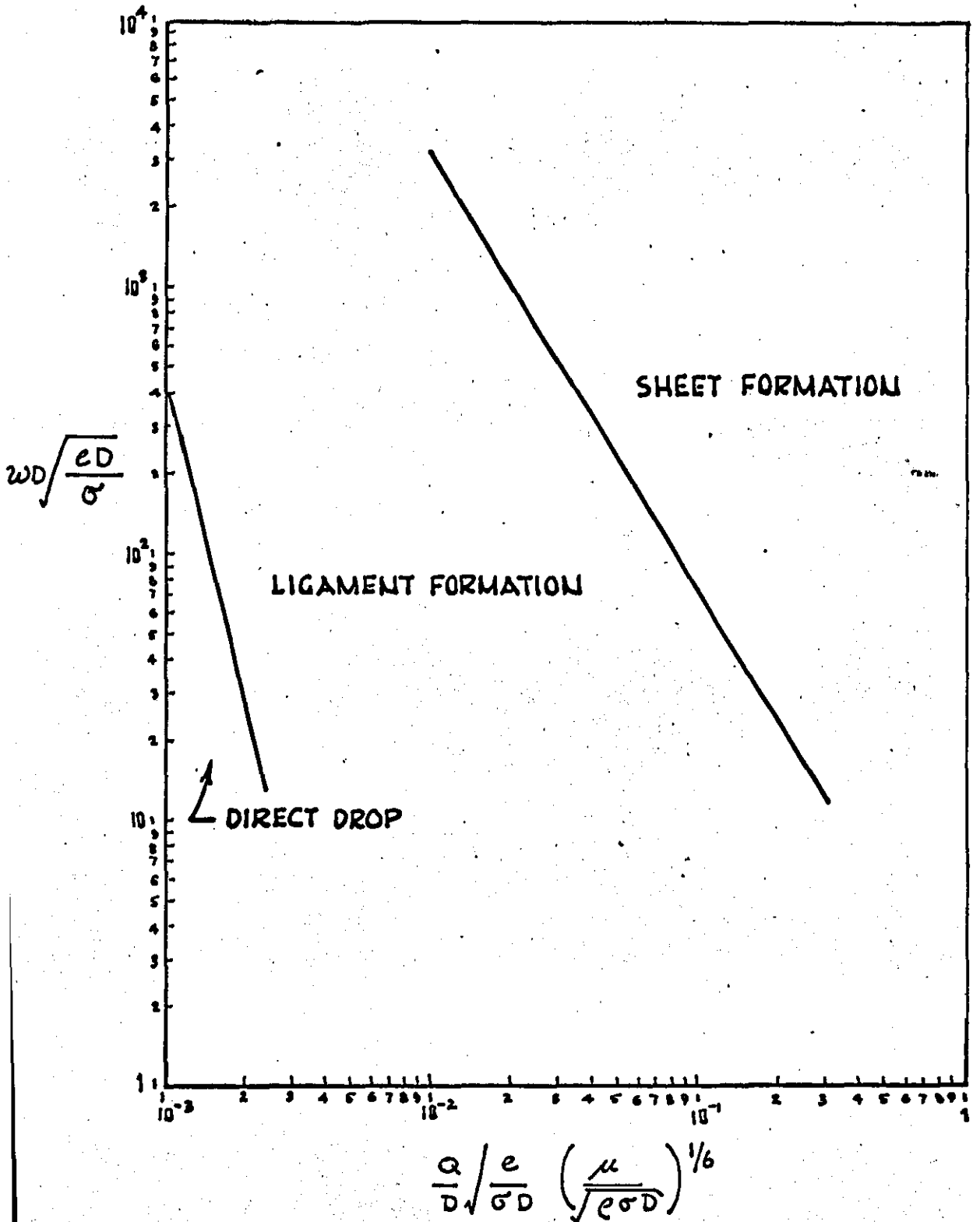

$$\left(\frac{\rho_L n^2 d_L^3}{\gamma}\right)\left(\frac{Q}{n d_L^3}\right)^{4/3}\left(\frac{\nu d_L}{Q}\right)^{0.19} > 0.363 \qquad 3.6.7$$

This the authors point out agrees quite closely with the semi-empirical equation that Hinze and Milborn developed.

A series of photographs showing the effect of increasing volumetric flowrate on atomization were presented by Hege[22]. These photographs illustrated how the ligament régime is sensitive to volumetric flowrate, indeed Hege proposed that there is an optimum volumetric flowrate at set operating conditions, at which the atomization is in its most uniform state. A chart was constructed, see Figure 3.6, which indicated the optimum conditions necessary to achieve the stablest atomization in the ligament régime. This chart is a plot of two dimensionless groups on log/log paper, the dimensionless groups being :

$$Fr = \frac{r w^2}{g} \qquad 3.6.8$$

$$\frac{l}{z} = \frac{r w \gamma}{(\dot{v}^+)\rho g} \qquad 3.6.9$$

where $\dot{v}^+$ = volumetric flowrate for the optimum atomization conditions.

These two groups do not contain any viscous force terms and therefore it is not possible to compare this chart with the Hinze and Milborn chart.

Hinze and Milborn considered the spacing between ligaments on a rotating cup. A disturbance of the form

$$\zeta = \zeta^+ e^{\beta t} \cos(kx) \cos(S\theta) \qquad 3.6.10$$

was chosen. The pressure balance at the outermost part of the torus was then set up, assuming equilbrium.

$$\text{ie} \quad -\text{number} \quad \delta_t \rho \frac{\partial^2 y}{\partial t^2} + \frac{1}{2}\rho w^2 D y + \gamma \left(\frac{4}{\delta_t^2} + \frac{4}{\delta_t^2}\frac{\partial^2}{\partial \theta^2} + \frac{\partial^2}{\partial x^2}\right) y = 0 \qquad 3.6.11$$

INTERNAL PRESSURE NEEDED TO ACCELERATE THE LIQUID — IMPACT PRESSURE — EXCESS PRESSURE DUE TO SURFACE TENSION

$$\text{ie -number} \quad \delta_t \rho \beta^2 + \frac{1}{2}\rho w^2 D + \frac{4\gamma}{\delta_t^2}\left(1 - S^2 - \frac{k^2 \delta_t^2}{4}\right) = 0 \qquad 3.6.12$$

From the form of the disturbance it can be seen that the disturbance can only grow out into a ligament if the exponential indice β is positive. Eisenklam[57] considered the same problem but approached it from a slightly different angle. Using the instability theory of G I Taylor[58] he concluded that the growth rate, β^2, could be equated in the following way:

$$\beta^2 = \left[\begin{pmatrix}\text{acceleration}\\ \text{towards the}\\ \text{denser fluid}\end{pmatrix} - \frac{k^2 \gamma}{\rho}\right] k \tanh kh \qquad 3.6.13$$

At equilibrium the inwards acceleration is given by $W^2 D/2$.

Thus the neutral wave number would be:

$$k_c = \left[\frac{W^2 D}{2} \cdot \frac{\rho}{\gamma}\right]^{1/2} \qquad 3.6.14$$

By maximising the growth rate the wave number of the most unstable disturbance is found. Eisenklam used as an example the case where $h \geq 2/k$ and $h \leq 0.4/k$

when $h \geq 2/k$ $\quad k_m = \frac{k_c}{\sqrt{3}}$ i e $\lambda_m = \frac{\pi}{w}\sqrt{\frac{24\gamma}{D\rho}}$ $\qquad 3.6.15$

and $h \leq 0.4/k$ $\quad k_m = \frac{k_c}{\sqrt{2}} \qquad \lambda_m = \frac{\pi}{w}\sqrt{\frac{16\gamma}{D\rho}}$ $\qquad 3.6.16$

FIG. 3.6: HEGE'S CHART.

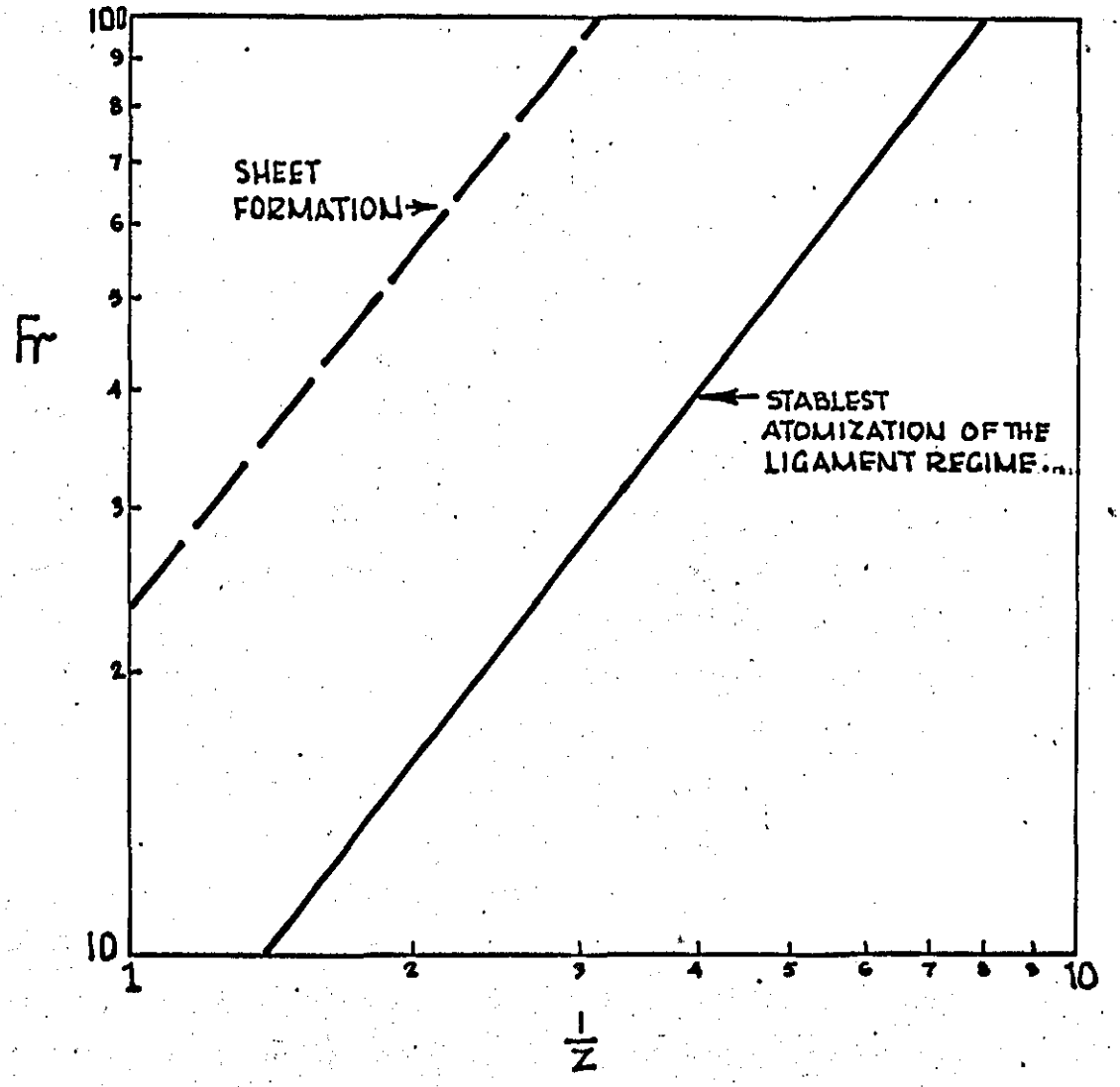

From the single piece of photographic evidence presented the agreement between the predicted and measured spacing of the ligaments appears excellent, when the spacing is predicted assuming $h \geq 2/k$.

3.7.1 The Mechanisms of Atomization

The break up of a capillary jet has been characterised by Ohnesorge[59]. Using the experimental data of Haelein[60], he constructed what is now known as the Ohnesorge chart. This chart, Figure 3.7, is a log/log plot of Z number against jet Reynolds number, the Z number in this case is a ratio of the Weber number and the Reynolds number. Four different régimes were classified; these were:

1. Slow dripping from an orifice, no jet formation
2. The Rayleigh mechanism of capillary instability
3. The break down of a liquid sheet due to sinuous disturbances.
4. Complete atomization of a jet.

Zones I, II and III on the Ohnesorge chart correspond to the 2,3 and 4 régimes indicated above.

Marshall[61], proposed that the three régimes of atomization observed by Hinze and Milborn could be considered equivalent to the first three régimes attributable to Ohnesorge. That is, the direct drop régime is equivalent to section one, the ligament régime is equivalent to section two and finally the sheet régime is equivalent to the third section.

FIG. 3.7. OHNESORGE CHART.

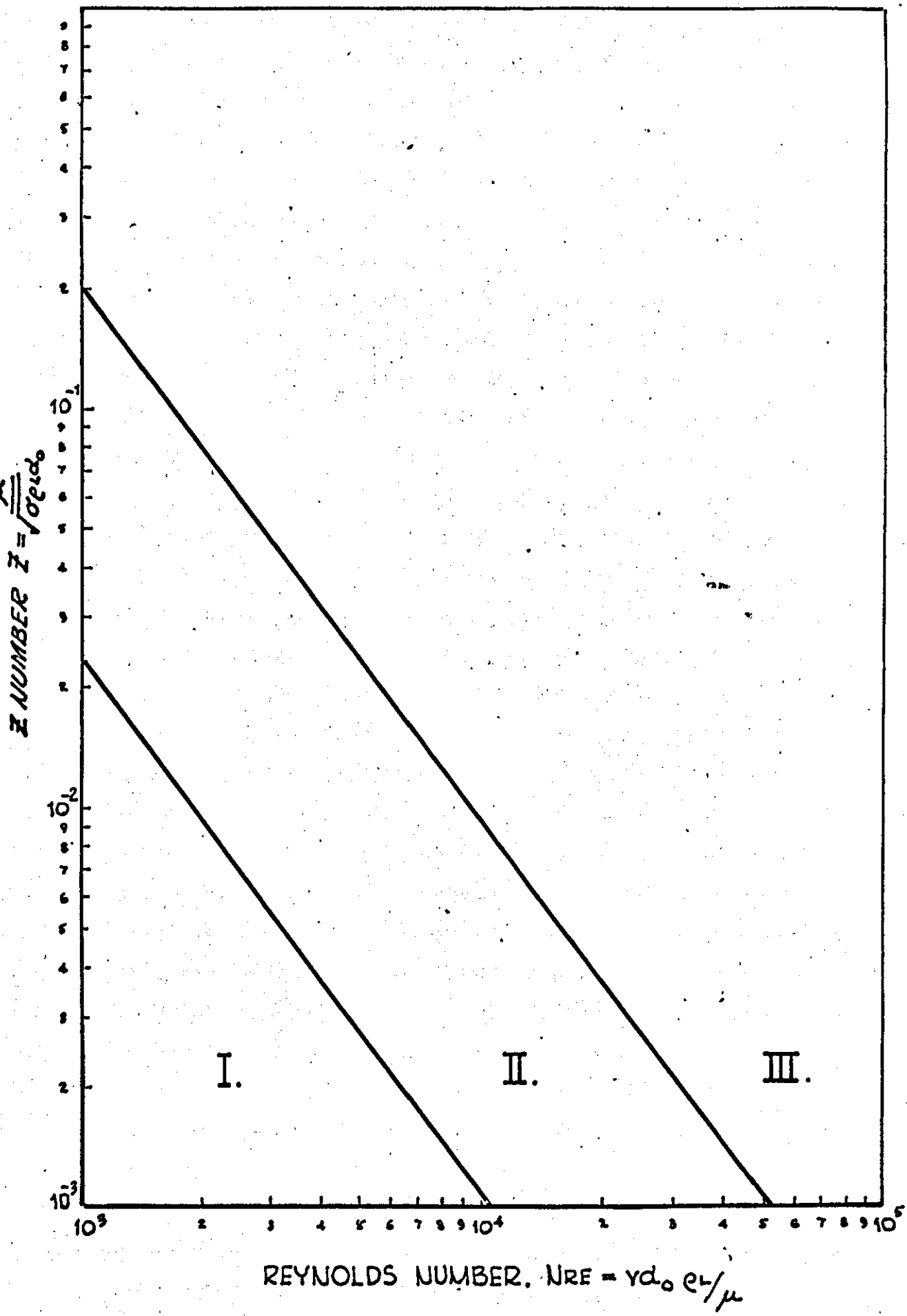

3.7.2 The Break-up of Capillary Jets

The early classical study of the instability of capillary jets was made by Rayleigh[62]. This work assumed that jet break up would occur when the amplitude of a disturbance grew to a value of one half of the undisturbed jet diameter. Rayleigh produced a linear theory, which assumed irrotational flow but did not take into account viscous forces.

The amplitude of the disturbance, at any time t, was defined by the following equation;

$$\epsilon = \epsilon_o e^{qt} \qquad \text{where } \epsilon \text{ is the amplitude, } q \text{ is the growth rate} \qquad 3.7.1$$

From Rayleigh's analysis q, the growth rate, was found to be:

$$q = \sqrt{\frac{\sigma}{\rho_L R_o^3}} \left(\frac{2\pi R_o}{\lambda} \frac{I_1 (2\pi R_o/\lambda)}{I_o (2\pi R_o/\lambda)} \right) (1 - (2\pi R_o/\lambda)^2)^{1/2} \qquad 3.7.2$$

$$= \sqrt{\frac{\sigma}{\rho_L R_o^3}} \; f\left(\frac{2R_o}{\lambda}\right)$$

where I_o I_1 are Bessel functions of zero and 1st order.

From this the maximum growth rate was found to correspond to a wave number of $k = 0.697$ $(k = 2\pi R_o/\lambda)$.

The instability of a capillary jet was shown by Plateau[63] to be dependent on the surface tension, an infinite cylinder of liquid being unstable because of the surface tension forces. From his work he showed that if a surface was deformed slightly then the deformation would be unstable if the product, kR, was less than unity and stable if it was greater than unity. This work led Plateau to conclude that a cylindrical jet would break up into pieces of length $2\pi R$. Later Rayleigh proved that the jet would not in fact break up into lengths of $2\pi R$.

Capillary instability of a jet where the viscous forces are not controlling the break up[64] is governed by the equation:

$$p_o + \delta p = T\left(\frac{1}{R_1} + \frac{1}{R_2}\right) \qquad 3.7.3$$

where $$\frac{1}{R_1} + \frac{1}{R_2} \equiv \frac{1}{R + \epsilon e^{i(kz + m\phi)}} + \epsilon\left(k^2 + \frac{m^2}{R^2}\right)_e \, i(kz+m\phi) \qquad 3.7.4$$

Where viscous forces are controlling the equation is modified slightly,

$$\text{i e} \quad \left(p + \delta p - 2\nu\rho \frac{\partial u_w}{\delta_w}\right)_R = T\left(\frac{1}{R_1} + \frac{1}{R_2}\right) \qquad 3.7.5$$

which results in the final form of the equation:

$$2x^2(x^2+y^2)\frac{I_1(x)}{I_0(x)}\left[1 - \frac{2xy}{x^2+y^2}\frac{I_1(x)}{I_1(y)}\frac{I_1'(y)}{I_1'(x)}\right] - (x^4-y^4) = J\frac{xI_1(x)}{I_0(x)}(1-x^2) \qquad 3.7.6$$

here $$J = \frac{TR}{\rho\nu^2} \qquad 3.7.7$$

More recently the instability of jets has been studied by Chandrasekhar[64], Yuen[65], Goedde and Yuen[66], Donnelly and Glaberson[67] and by Rutland and Jameson[68]. Yuen calculated the higher order terms of the surface deformation and found that non-sinusoidal surface deformation was a non-linear effect. Donnelly and Glaberson had earlier concluded that Rayleigh's assumptions that the break up was not affected and the non-sinusoidal surface deformations were due to higher harmonics. Rutland and Jameson based their study on the work of Yuen and observed the presence of secondary waves, which Yuen's theory predicted, but Yuen discounted, as he regarded this prediction to be caused by a breakdown in his theory.

Rutland and Jameson[68,69] corrected two of Yuen's coefficients (b_{22} and C_{22}) whilst Yuen showed there was a further unpublished error in coefficient d_{31}. It appears likely[70] that there is an error in coefficient C_{33};however the effect of this coefficient is thought to be relatively unimportant in predicting the wave profiles.

3.8 Sizing of Droplets

The method of drop size analysis used in an investigation affects the results that are obtained. For instance, if a spray was photographed and an analysis was made of the negatives, the resultant drop size distribution would probably be quite different from the analysis of droplets captured in, say, an oil bath sampling device. Because of this it is important to decide at what stage the analysis must be performed, e.g. immediately after atomization has occurred, that is in the atomizing region, or after the spray has travelled a fixed distance. For liquids which are appreciably volatile, the problem of sizing becomes acute. It has been reported[71] that a 100μ drop of water at room temperature and 90% relative humidity when issued from an atomizer, will have reduced, by evaporation, to 90μ after 1 ft and will have disappeared altogether after $6^{3}/_{4}$ ft. This highlights some potential hazards in drop sizing but it does not deal with all the problems.

Fraser and Eisenklam[72] state "The method of sampling must also be considered since the drop size on a particular surface will be quite different from that of the drops in flight". For that reason alone the location of the sampling device must be recorded as sampling can often be a function of the location, as in the case of fan nozzles where droplets produced at the extremes of

the 'fan' are often coarser than those from the middle.

There are a number of commonly used sampling devices. These can be categorised into two main groups, those that retain an image of the spray and those that do not. In the first group one can list the slide coating techniques[39,46,48,49] and the oil bath method[50,72-75]. Also to be included in this group are the techniques of photographing the spray in flight[76-78] and that of sizing the solidified droplets of waxes[79-82], metals[83-85] or final product from a spray drying tower[86]. The sizing techniques most commonly used for solidified products are sieving and microscope counting. All of these techniques have practical drawbacks e.g. the coating techniques provide a soft layer of either magnesium oxide or soot into which the droplets impact and create craters. The diameters of these craters are not always the same as the drops which produce them[87], especially for larger droplets. Indeed May[49] showed that for drops over 200 μm the crater produced in a magnesium oxide coating was larger than that expected. In these cases correction factors have to be applied to get the true size distribution. The oil bath technique has associated problems. Firstly the sample often has to be photographed within minutes of it being collected otherwise significant changes in size might be observed. Secondly the droplets deform in the oil due to surface tension effects. This relationship is well known[72] so correction is relatively straightforward. Photographs give rapid accurate information of the frequency of droplets in the field of view, however double flash photographs, or cine film, would be necessary to assess the velocity profile of the various drop sizes as their spatial distribution is a function of droplet velocity[78]. Another

technique that has been used[88,89] records an image of a stain produced when a droplet which contains a dye is absorbed on chromatographic paper. This technique is especially suitable to larger droplets, (>100 μm). Calibration is quick and relatively easy when a microburette is employed. Like the coated slide and oil bath methods this technique is sensitive to spray concentrations, the right exposure time having to be found by trial and error. The disadvantage of using the solidified product is that it is only applicable to waxes, metals and similar feeds. The solidified product also contract on cooling and so the actual drop size would have to be calculated from thermal expansion data. However, even this is not the precise picture as solid droplets have been observed to rupture due to the outer surface forming a crust whilst the centre is still molten.

The second group of sampling devices consists of: a gravimetric technique[90]; a light extinction technique and a electrically charged wire device. The gravimetric technique as used in a commercial unit relies on the spray sedimenting on to a sensitive balance. As droplets impinge on the balance the mass is continuously monitored, thus the weight fraction is found. This method must be suspect as it assumes that the spray does not preferentially impact on the wall of the sedimentation column and that it is not originally spatially distributed into the column.

Fraser et al[44] used the photometric technique of Sauter[91] which allows a rapid drop size to be recorded but unfortunately does not give the drop size distribution.

The method employs a rectangular beam of light which is shone through the spray cloud (Figure 3.8). The light absorbed by N droplets of mean drop size d_s is given by:

$$A = \frac{N \pi d_s^2}{4\ bc} \qquad 3.8.1$$

where b c is the area of the rectangular beam. These droplets will occupy a given volume e,

$$\text{where } e = \frac{N \pi d_s^3}{6} \qquad 3.8.2$$

$$= \frac{b}{V d_s} Q_L \qquad 3.8.3$$

where Q_L is the volumetric flowrate through plane c and V_{d_s} is the velocity of the mean drop size.

Sauter reasoned that as the concentration of droplets increased the probability of an eclipse also increased. From a statistical analysis he showed the actual light (A) that should be absorbed by N droplets is related to the measured value (A') by;

$$A = \ln\ (1 - A'/100) \qquad 3.8.4$$

Combining these equations, 3.8.1, 3.8.3 and 3.8.4, gives:

$$d_s = 1.5\ \frac{Q_L}{V d_s \ln\ (1-A'/100)} \qquad 3.8.5$$

This procedure was modified by Fraser et al[44] by altering the value of Q_L for their geometry, as Sauter's work investigated a confined spray from a twin fluid, venturi type atomizer. They quote that the light absorption as measured on a galvanometer via two photo-multipliers (one acting as a control) was accurate to within $\pm$ 1/2 per cent.

FIG. 3.8.

DROP SIZING USING A PHOTOMETRIC TECHNIQUE AS USED BY FRASER.

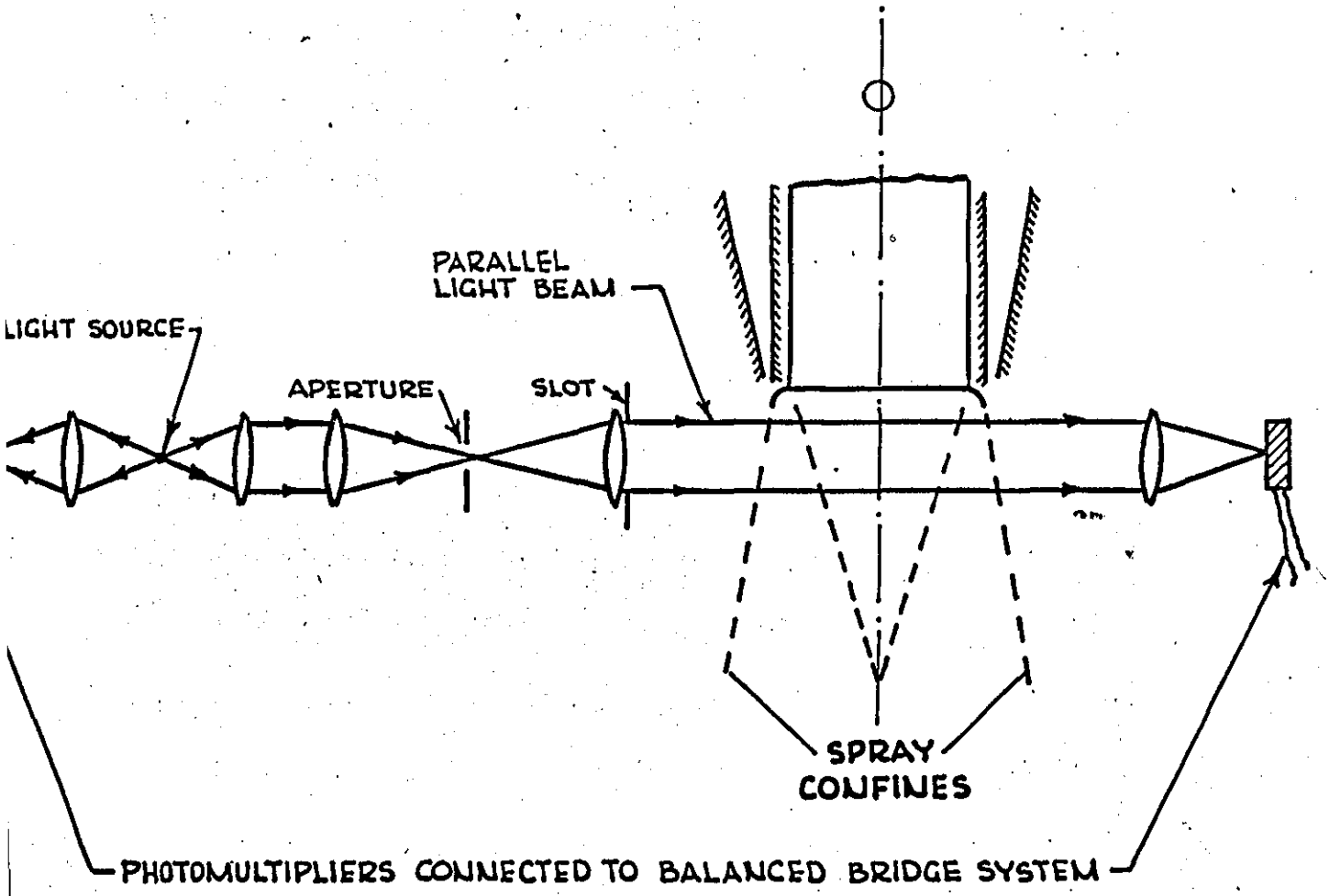

The charged wire device[92] provides a rapid method of analysis for droplets, especially applicable to aqueous sprays due to the short rise-times in charging the droplets.

When a droplet impinges on to a charged wire it acquires part of that charge. However, the charge acquired is not constant over all the surface of the drop. Indeed at the point of contact the charge density can be shown to be zero. The size of the drop will determine the height and duration of a pulse. Hence by recording the pulses over a sufficiently long period the distribution can be found.

A series of correction factors are required. This is so, as the size of drop that touches the wire influences the effective catchment area. (See diagram below.)

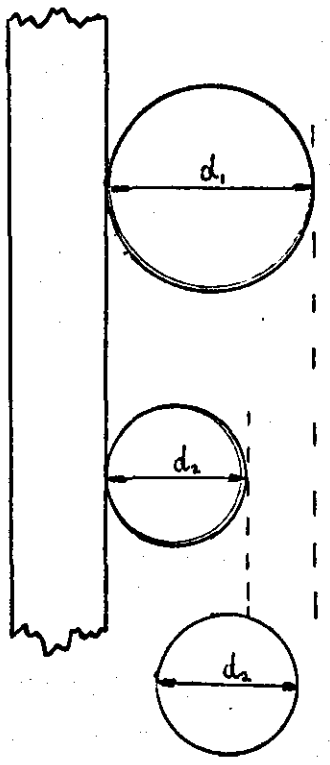

The equipment has first to be calibrated in the environment in which it is to be used. This is to ensure that no environmental electrostatics bias the results obtained. Gardiner[92] suggests two methods for calibration: for droplets up to 300 μm a vibrating pin was suggested and for droplets over 300 μm a vibrating hypodermic needle[93].

Steen and Chatterjee[94] used the charged wire technique to size droplets in the size range 1500 μm to 5000 μm. They used liquids of varying electrical conductivity and expressed their results in the form of a log/log plot of pulse height (Channel Number) against drop diameter. Although there appears to be some scatter in their experimental results the trends are most clearly evident. They discuss the relationship between the size of the pulse height and drop producing it. Theoretically it appears that the pulse height will be proportional to the drop size when the drop size is small compared with the charged wire, and is proportional to the square of the drop diameter when the drop is large compared with the wire. This was worked out on the basis that in the first case the system was equivalent to a sphere obtaining charge from a point source and in the second case it was equivalent to the two flat plate capacitor system. One interesting conclusion they draw is the effective catchment area may in fact be larger than that predicted by the collision theory, especially when the charge density is large. However, due to the complexity of assessing this factor only mention was made of this probability.

CHAPTER FOUR

THE EXPERIMENTAL EQUIPMENT AND ITS CALIBRATION

4.1 Introduction

4.2 The Rotary System

4.3 The Liquid Supply

4.4 The Optical System used for Film Thickness Measurements

4.5 The Charged Wire Drop Sizer

4.6 Ancillary Equipment

4.1 Introduction

It was clear, from a review of the literature, that there are a number of design points that must be observed if a liquid is to be atomized efficiently by a spinning cup. The literature cites the case for vibrationless rotation, for even liquid distribution and a steady feed supply. The initial experimental work confirmed the need for the correct liquid distributor design in order to minimize the propagation of spurious disturbances, as these could otherwise affect the film flow of the liquid and its eventual atomization at the periphery of the cup.

To give ease of access to the spinning cup, the equipment was designed in such a way that each section could be removed leaving the rotary system on its own. Such tasks as cleaning the cup in use and adjusting the front silvered mirror which formed part of the optical system were consequently made easier.

The equipment can be seen in Photographs 1 and 2.

4.2 The Rotary System

The rotary system employed was essentially the same as that used by Beardall[18]. This consisted of a three phase, 0.5 HP electric motor which provided the drive, via a vee belt, to the central spindle assembly on to which the cups were secured. The spindle assembly had preloaded bearings to help overcome the possibility of any lateral displacements which could result in oscillations being transferred to the liquid. The whole assembly was bolted very securely on to a cement and brick plinth, which was built on a vibrationless concrete pad mounted in the floor.

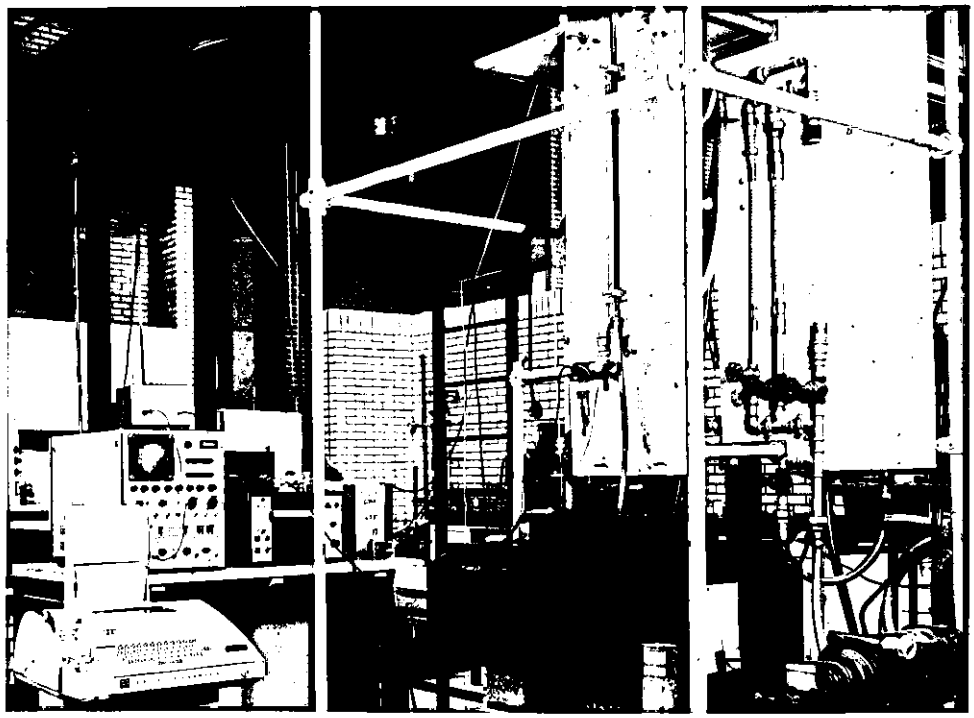

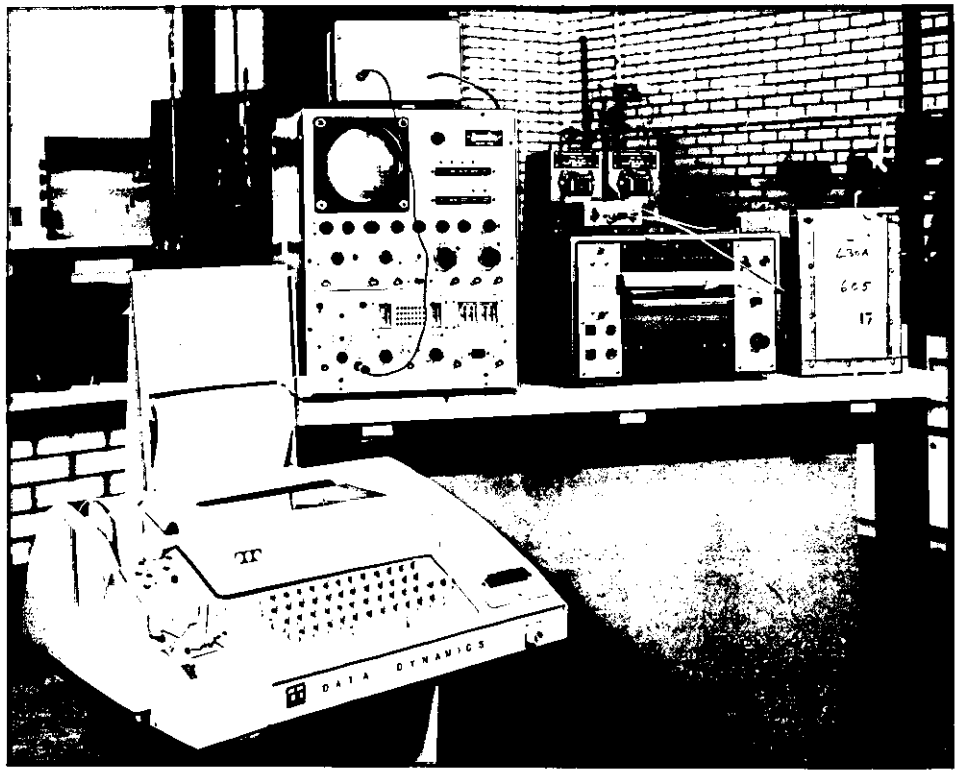

PHOTOGRAPH 1

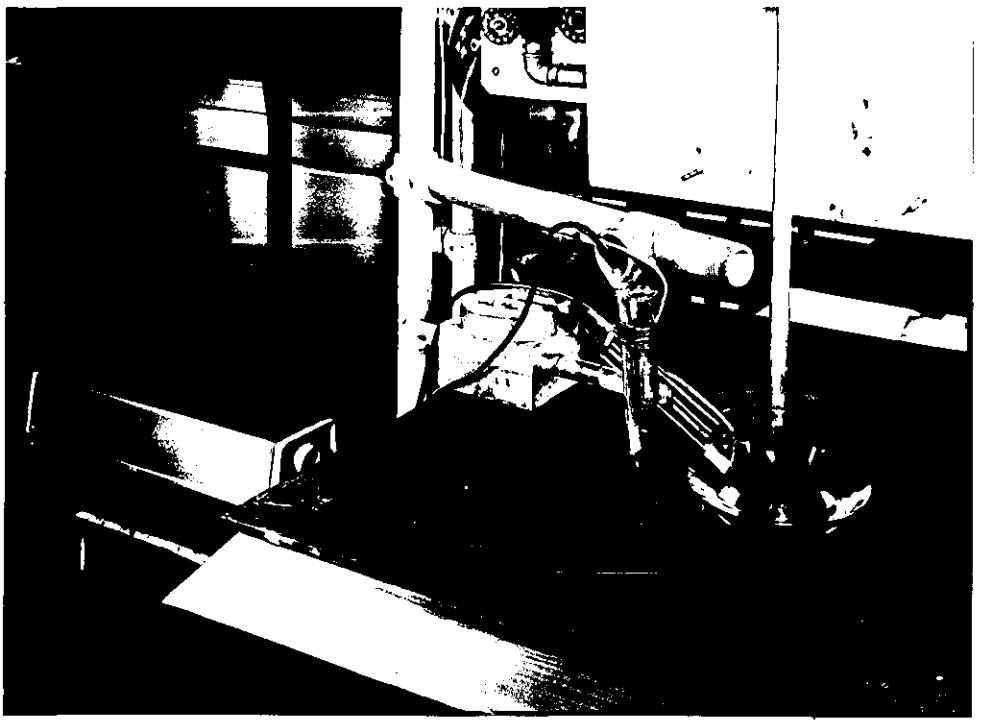

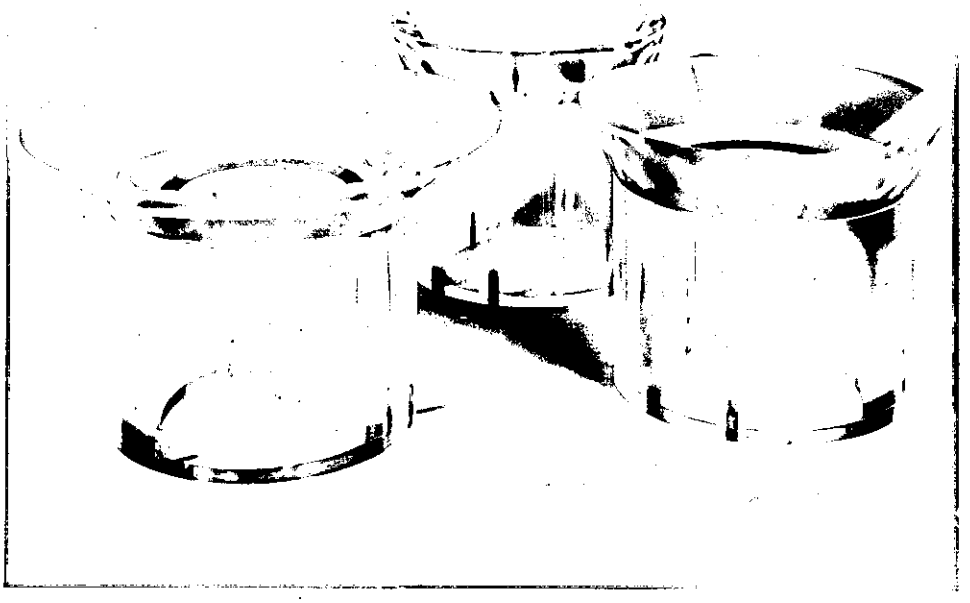

PHOTOGRAPH 2

FIG. 4.1.

SCHEMATIC REPRESENTATION OF THE LIQUID SUPPLY.

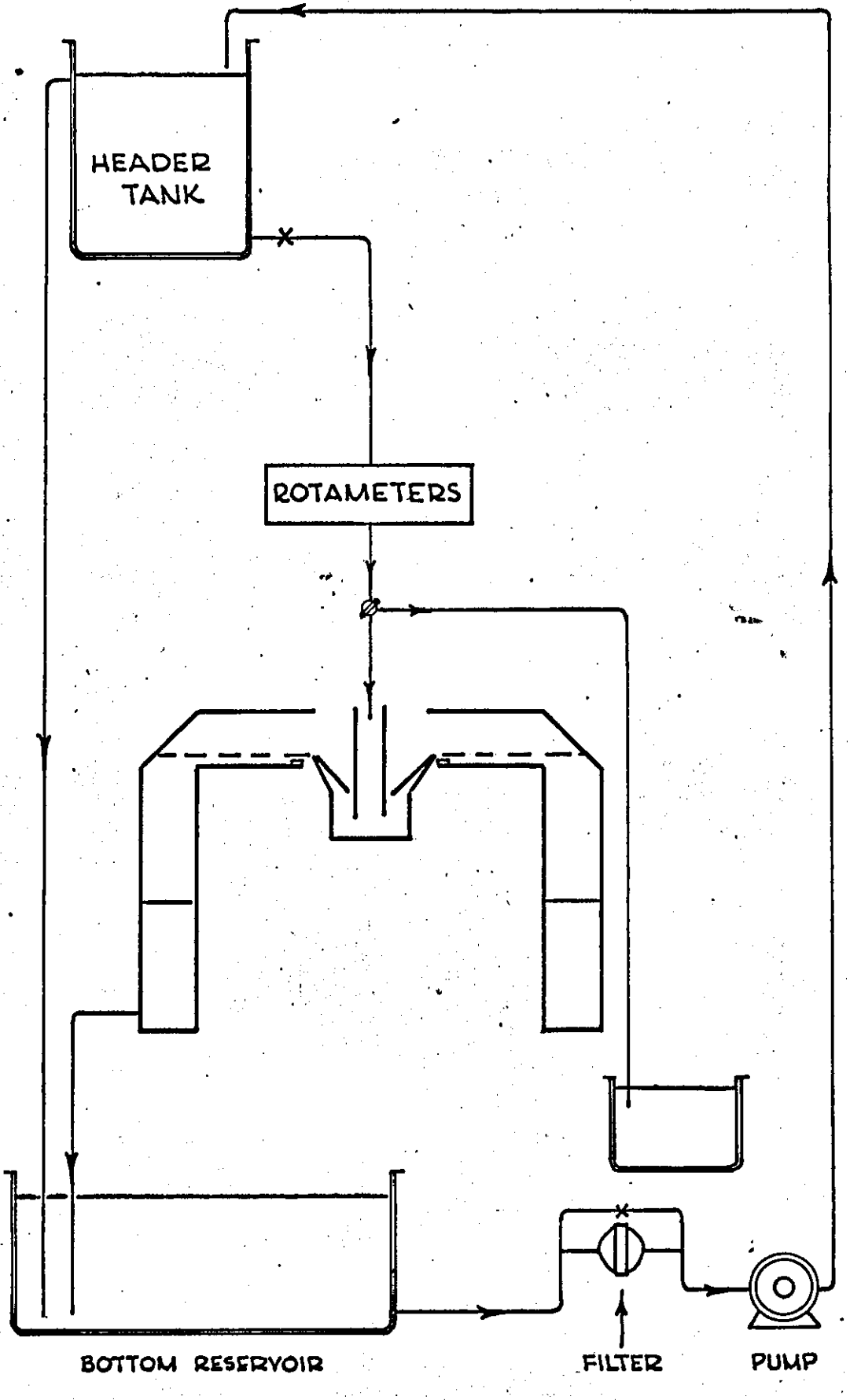

The perspex cups used throughout the investigation were designed to incorporate an internal reservoir and weir. These cups were fully interchangeable and so only one integral base and distributor was needed. A photograph of the three cups, the integral base and distributor can be seen in Photograph 2.

The liquid under test was fed vertically from above into the feed tube of the integral base and distributor where it was found that the liquid formed a dynamically stable head. Some rotational energy was transferred to the liquid (whilst it was in this section) by means of viscous drag on the tube wall and the nut and spindle arrangement. Liquid passed from the feed tube into the internal reservoir through small radial holes that had been drilled into the feed tube assembly. By virtue of the distributor rotating at a constant angular velocity, the liquid, as it passed through the drilled holes, reached the same speed of rotation as the cup. As this liquid was discharged under the surface of the liquid in the reservoir, entrance disturbances due to impaction were minimised.

A uniform supply of liquid into the reservoir is essential if the discharge at the weir on to the conical surface of the cup is to be steady. This uniform supply was achieved as the dynamically stable head previously mentioned acted not unlike a capacitor in that it smoothed out minor fluctuations in the feed supply. No indications of disturbances which propagated inside the reservoir were observed. Indeed under the conditions where these would be most manifest the discharge at the weir was at its smoothest. Because of the low speeds of rotation used during this

experimental work aerodynamic forces inside the reservoir section were not regarded as important, especially as there was only a relatively small air gap between the liquid in the reservoir and the central feed tube.

4.3 The Liquid Supply

In order to maintain a uniform supply of liquid, of constant optical density, a closed circuit liquid supply system was adopted (Figure 4.1). This consisted of the following arrangement. A header tank delivered water via a rotameter bank to the feed tube of the spinning cup. After atomization the liquid drained into the bottom reservoir tank from the spray collector. From there it was pumped back into the header tank after being filtered through a glass sinter filter. Excess liquid drained directly back into the bottom reservoir from the header tank.

The header tank produced a pressure head of about 10 ft of water to the rotameter bank. The tank was made of stainless steel so there were no corrosion problems. This was important as suspended matter would certainly have interfered with the optical techniques used to measure the film thickness of the liquid on the conical cup surface.

Flowrates were measured during the initial experimentation period with the aid of the rotameter bank. Unfortunately these could not be used once a light extinction technique was chosen to measure liquid film thicknesses as it was impossible to see the rotameter floats through the dye solution at all but the smallest flowrates. Because of this, flowrates were measured by collecting the liquid over a known time period, after which it was weighed directly.

FIG. 4.2.

SCHEMATIC REPRESENTATION OF THE OPTICAL SYSTEM.

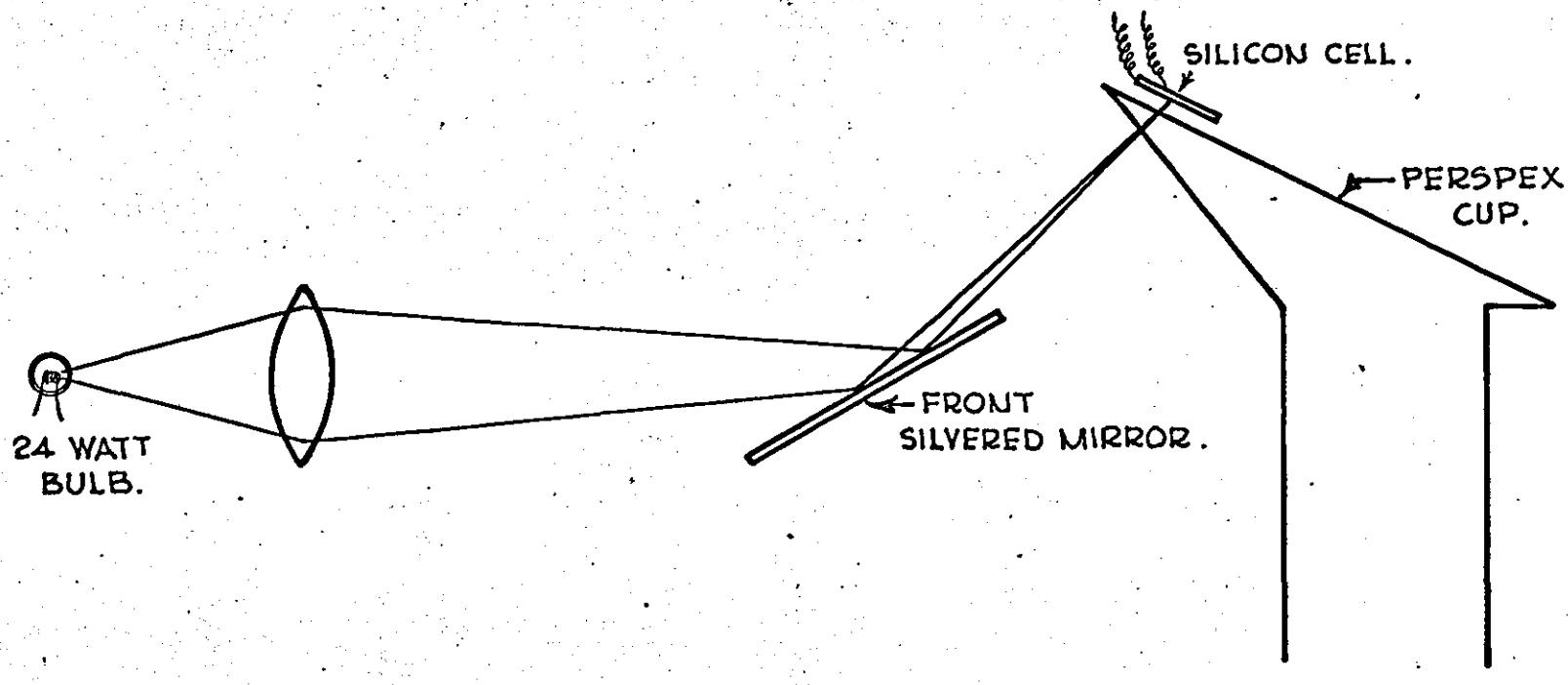

Once atomization had occurred at the periphery of the cup the resultant spray had to be collected so that the dye solution could be returned to the bottom reservoir. To minimise mist formation, due to the impaction of high velocity droplets, the droplets were made to impinge obliquely upon the surfaces of the spray collector. Because of the small volume inside the spray collector it was hoped that the relative humidity would be very high and hence evaporation from the droplets would be minimised, once steady state was achieved.

4.4 The Optical System used for Film Thickness Measurements

A diagram of the optical system used to obtain the time averaged film thickness results can be seen on (Figure 4.2). A 24 volt, 24 watt light bulb, connected to a Farnell L30B stabilised power supply, was used as a light source. This power supply was guaranteed not to change the output by more than 0.02% so long as the mains supply did not change by more than 10%. Some 10 min were necessary before the light supplied to the photo-voltaic cell became steady, this was due to the inevitable heating of the bulb and its surroundings, and thus was the time taken for the system to reach thermal equilibrium.

Light from the filament passed through a convex lens before it was deflected by a front silvered mirror that was mounted under the perspex spray collector. The front silvered mirror was fully adjustable and so the angle through which the beam was deflected and hence the radius at which the beam passed through the conical surface of the perspex cup was controllable. Monitoring the intensity of the beam as it left the surface of the cup was

FIG. 4.3.

THE PERSPEX CUPS USED DURING THE EXPERIMENTAL WORK.

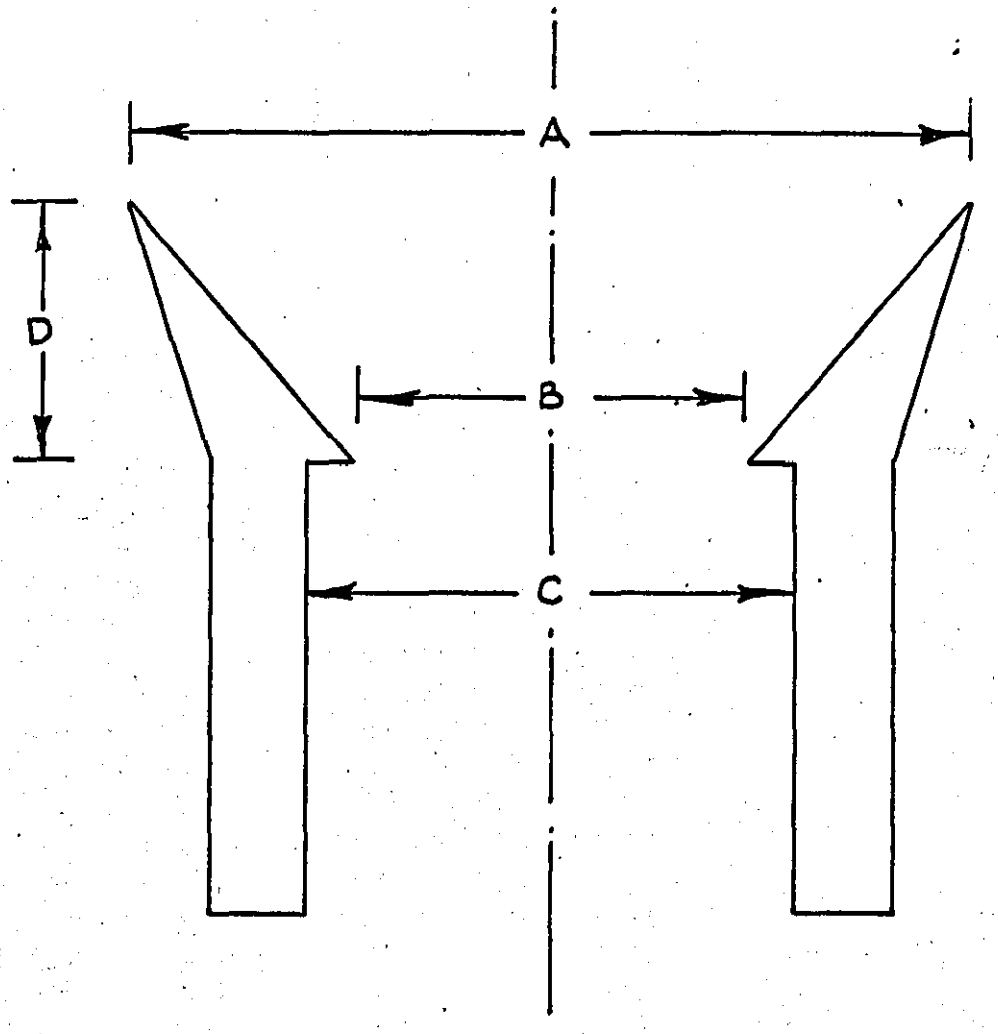

CUP	A	B	C	D	
1	4·420	2·316	2·762	0·986	INCHES
2	5·820	2·288	2·762	0·961	"
3	6·200	2·288	2·762	0·993	"

achieved using a Ferranti photo-voltaic solar cell. The response of this cell was made linear by short circuiting it with a 2kΩ resistance.

When light passes through a substance, the angle at which it will leave that substance is a function of the incident angle and the refractive index, ie Snell's Law must be obeyed. When a light extinction technique is used to measure film thicknesses on spinning discs, the light beam will only pass straight through (ie at a normal to the surface of the disc) if the flow is completely steady. Once irregularities occur on the liquid surface, the exeunt light beam will be refracted, and so the area over which the beam can be detected must be large in order that all the light is continuously monitored. It was specifically for this reason that the Ferranti light cell was chosen. Furthermore the response of this cell is known to be independent of the position at which the beam strikes the surface of the cell.

Calibration of the optical system proved difficult. In some initial experiments a laser with a known peak wavelength was used. Consequently it was relatively easy to match this wavelength on a spectrophotometer and calibrate, using the null point technique, with a sample taken from the bottom reservoir. (A Lambert-Beer Law relationship had previously been confirmed during an accurate calibration test.) Without any liquid on the cup the laser's light output was observed to be cyclic in nature. In fact it was later found that the ambient light was causing this cyclic effect. However at the time it was decided to abandon the laser as a light source and adopt the light bulb and lens system described above.

Once the 24 watt light bulb had been adopted the spectrophotometer could no longer be used as the calibrating instrument because the bulb emitted "white light", that is, it emitted a continuous spectrum over the visible range. Thus no distinct wavelength could be matched on the grid of the spectrophotometer. To overcome this problem, calibration was carried out on the inclined faces of the cups using a 1 mm spectrophotometric cell.

A sample of the liquid was taken from the bottom reservoir after the pump which transferred liquid from the bottom reservoir to the header tank had been operating for some time. This precaution was taken to eliminate the possibility of taking a sample that was not representative of the bulk of the liquid. Accurately weighed amounts of this sample were then taken and diluted with known amounts of water. These diluted samples were thoroughly shaken to ensure complete mixing.

A clean 1 mm spectrophotometric cell was filled with clear water by means of a Pasteur pipette. In this way no water managed to contaminate the outside surface of the cell. Care was taken throughout not to touch the outer surfaces of the cell as this would have affected the calibration. The cell was then placed on the previously cleaned inclined conical surface of the spinning cup in use so that the light beam shone through it on to the centre of the rectangular face of the silicon solar cell. Because of the intensity of the ambient light the surroundings had to be blacked out. This was achieved by placing a matt black wooden cover on top of the spray collector, see Photograph 1.

A reading, in millivolts, was taken from the digital volt meter which formed part of the data logging unit used during the experimental runs. This voltage was directly proportional to the 100% transmission light intensity and as such it was used to represent 100% light transmission. The diluted samples were each, in turn, transferred to the cup in the spectrophotometric cell and tested. The digital volt meter reading was taken for each sample and transformed into a transmission reading. The usual plot of logarithmic transmission against concentration yielded a straight line which passed through the origin. As the absolute concentration was not known the dilution of the original sample was used in place of the concentration. . The accuracy in calibrating using this technique was understandably less satisfactory than that usually achieved by a spectrophotometer, however with care sufficient accuracy was obtained to assume the Lambert-Beer Law held under the operating conditions.

The amount of light that passes through an interface is governed by the nature of the interface. During the calibration the surface of the cup was kept perfectly dry and so the interface was perspex/air. Obviously with the spectrophotometric cell present there were additonal interfaces, air/glass, glass/water, water/glass and finally glass/air. Each of these interfaces permits a certain fraction of the light through and therefore the 100% transmission voltage recorded during the calibration was a function of these interfaces. The inference of this is important, namely that the voltages recorded, for the case where there is no liquid on the cup and where there is an infinitely thin layer of liquid, will not be the same as the interface in these two cases is

different. This technique was chosen to measure the local film thickness and so the important voltage reading was the one where there was an infinitely thin layer of liquid left on the cup. Experimentally this was found by recording the voltage continuously and cutting the liquid supply off. The liquid film thinned until surface tension forces broke the film up into a series of rivulets. Correspondingly the voltage increased until rivulet formation occurred after which the voltage decreased. Hence the maximum voltage represented most nearly, the condition of an infinitely thin liquid layer present on the cup.

The ratio of the voltage when there was a liquid film and when there was an infinitely thin film present was taken as the transmission under the operating conditions. Hence the film thickness was calculated with the aid of the calibration graph.

A similar approach was adopted in the calibration for the continuous film thickness experimental runs. A sample was taken from the bottom reservoir and samples of this were diluted accurately as previously stated. These diluted samples were transferred to the spectrophotometric cell, as before, and the readings were taken as traces on a Ultra-Violet Oscillograph. The signal from the silicon light cell was amplified with an integrated circuit amplifier (741) so that a specific galvanometer could be used. This galvanometer was chosen as it was sufficiently damped and therefore would not have the characteristics of a ballistic galvanometer. Hence the trace would more accurately represent the profile of the liquid on the cup.

Two major related problems were encountered during this part of the experimental work. The width of the chart was not wide enough for the complete 0-100% transmission to be recorded. This meant that the calibration could not be checked as the 100% transmission value was not known. Likewise the 100% transmission reading was not known for the case, where the cell was absent and an infinitely thin liquid layer present. However this was overcome by taking digital volt meter readings and extrapolating these on to the chart scale.

The light bulb and lens system proved inadequate as the filament's image monitored by the silicon light cell was too large. A laser was tried and found to be perfectly acceptable. Because of the characteristics of a continuous laser beam it was not necessary to focus the beam with the aid of a lens system.

By using a Vanguard X-Y reader the experimental data was extracted from the UV charts. The instrument was zeroed and the scale adjusted so that convenient readings were obtainable. As the Vanguard has a step length control, this feature was used so that film thicknesses recorded would not be biased due to the operator. The instantaneous voltage corresponding to an instantaneous film thickness was therefore taken every 2.5 mm. This reading was stored by a teletype.

4.5 The Charged Wire Drop Sizer

The charged wire drop sizer used during the experimental investigation was essentially the same as that used by Gardiner[92]. The high voltage, c. 1000 volts, was achieved by placing ten 90 volt dry cell batteries in series. As the current demand was so slight

this system was considered to be satisfactory, and so more sophisticated power supplies were not needed.

The wire used was a length of single core copper coaxial wire of 0.813 mm diameter. The sheathing was removed from the last $1\frac{1}{2}$" of the wire thus exposing this section. This length was deliberately kept short for two reasons. Firstly only a short sampling length was required as the spray produced from the spinning disc was almost perfectly horizontal in the sampling zone close to the disc. Secondly an unprotected length of wire acts as an aerial and so picks up spurious 'noise' which would show up as a pulse and thus could be counted as a drop striking the charged wire.

The signal was amplified a nominal ten times using an epsilon amplifier before being fed into a Laben 100 channel pulse height analyser. Because of the presence of unwanted 'noise' - probably due to thrystor control circuits - an anticoincidence device was constructed. This device sensed the pulses which were on the mains and produced a standard voltage of known pulse shape. These pulses, when fed into the anticoincidence input on the pulse height analyser, produced a 'dead time' so that no signal during that time would be counted and analysed, hence minimising the error due to noise.

Calibration of the charge wire drop sizer was accomplished in two ways. For the top end of the scale $\sim$2500 to 3000μm a hypodermic needle was filled with a sample of the liquid from the bottom reservoir. By keeping the level of the sample in the hypodermic constant it was possible to produce a stream of mono-sized free-falling droplets. The charged wire was

angled such that this stream of droplets struck the wire. Thus it was relatively easy to collect a known number of droplets and to weigh them, thereby finding their diameter, and observing which channel number these droplets were placed in. By changing the initial height of the liquid in the hypodermic syringe it was possible to change the diameter of the droplets slightly so a number of calibration points could be found. However this was not found to be necessary experimentally as the change in diameter per unit change in channel number is small at this end of the scale.

Advantage was taken of the ability of a spinning disc to produce a clearly defined narrow distribution of droplets in the so-called[1] Direct-Drop Régime. This régime has been documented by Walton and Prewett[40] and an operating equation has been experimentally verified. This equation was used to predict the diameter of the main droplets produced under the operating condition, whilst the channel number corresponding to the main drop was observed experimentally from the pulse height analyser. By altering the rate of rotation a number of main peaks were identified and the resulting straight line through these points passed through the point found by experiment in the top end of the size range. It was therefore concluded that this was evidence enough to accept these calibration charts as accurate.

Care was taken throughout the calibration and ensuing experimentation not to alter the electrostatic environment. Indeed it was found necessary to earth the liquid inside the hypodermic syringe so as to obtain a narrow size distribution. As a consequence of this the liquid discharged into the rotating

distributor was also earthed even though it was probably adequately earthed via the bearings of the shaft on which the cup rotated.

The pulse height analyser was set up in the following way:- rise time of 10μ secs; voltage of 1 volt for the 100 channels. The analyser was set on automatic cycle for a measured sampling time of 300 secs and a dead time of 90 secs. The amount of noise was always measured before the run so as to check that the results obtained were not significantly affected by the general noise level.

4.6 The Ancillary Equipment

Density Determination

The density of the dye solution was found using a specific gravity bottle. The results obtained were found to be consistent and within the range of accuracy required for the investigation.

Surface Tension Determination

The surface tension of the liquid was found using a Du Noüy Tensiometer. Before the instrument was used it was calibrated as recommended in the manufacturer's handbook.

Experimental results were obtained using the ring method, the accuracy of this method has been quoted to within 0.1 dyne/cm. However the method is slightly operator-sensitive and a correction factor should be introduced[95] to allow for the meniscus that forms around the ring.

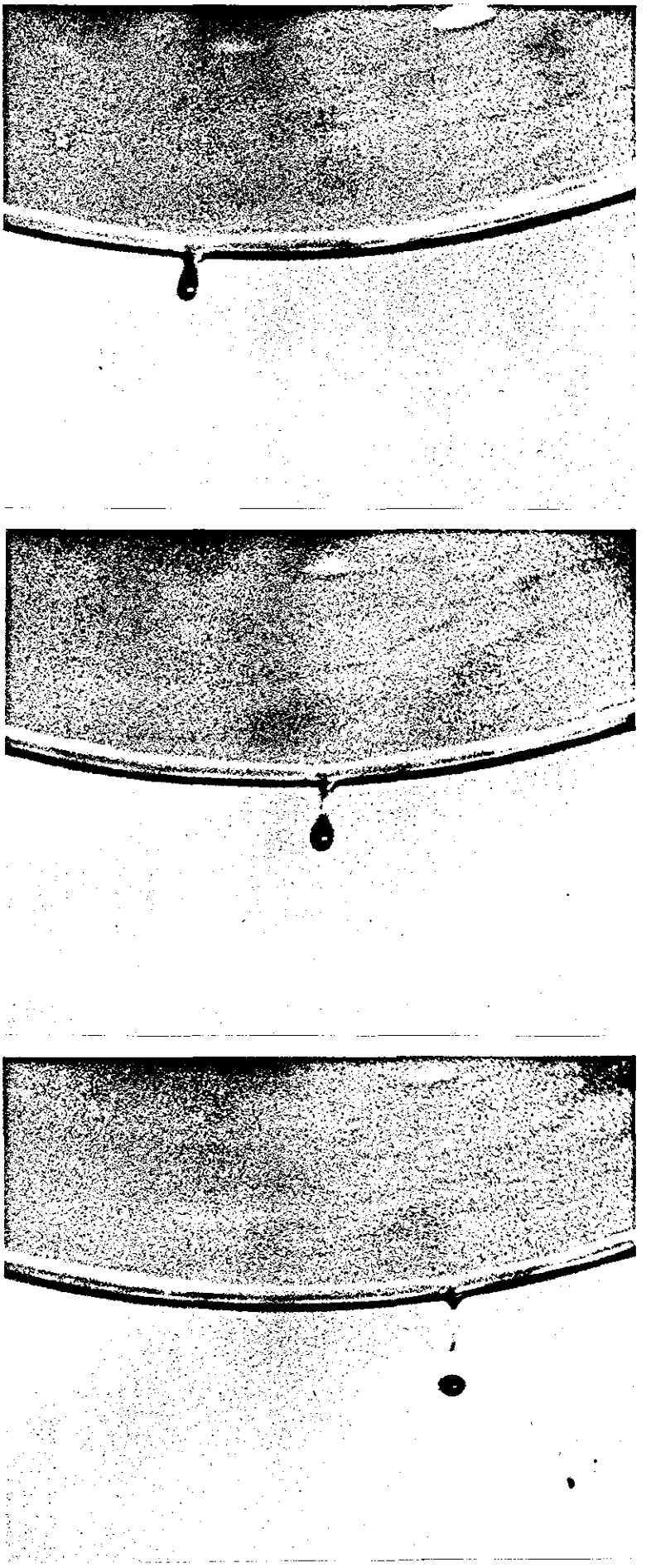

PHOTOGRAPH 3

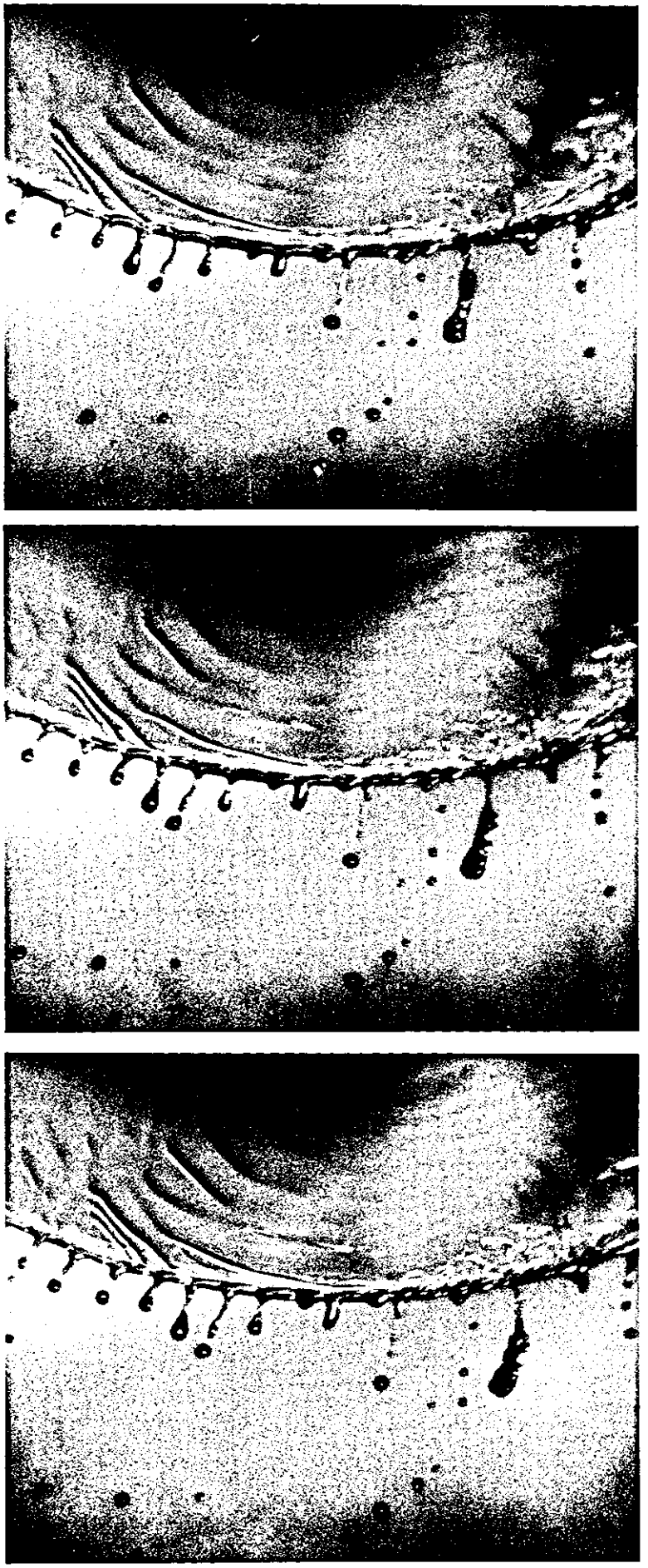

PHOTOGRAPH 4

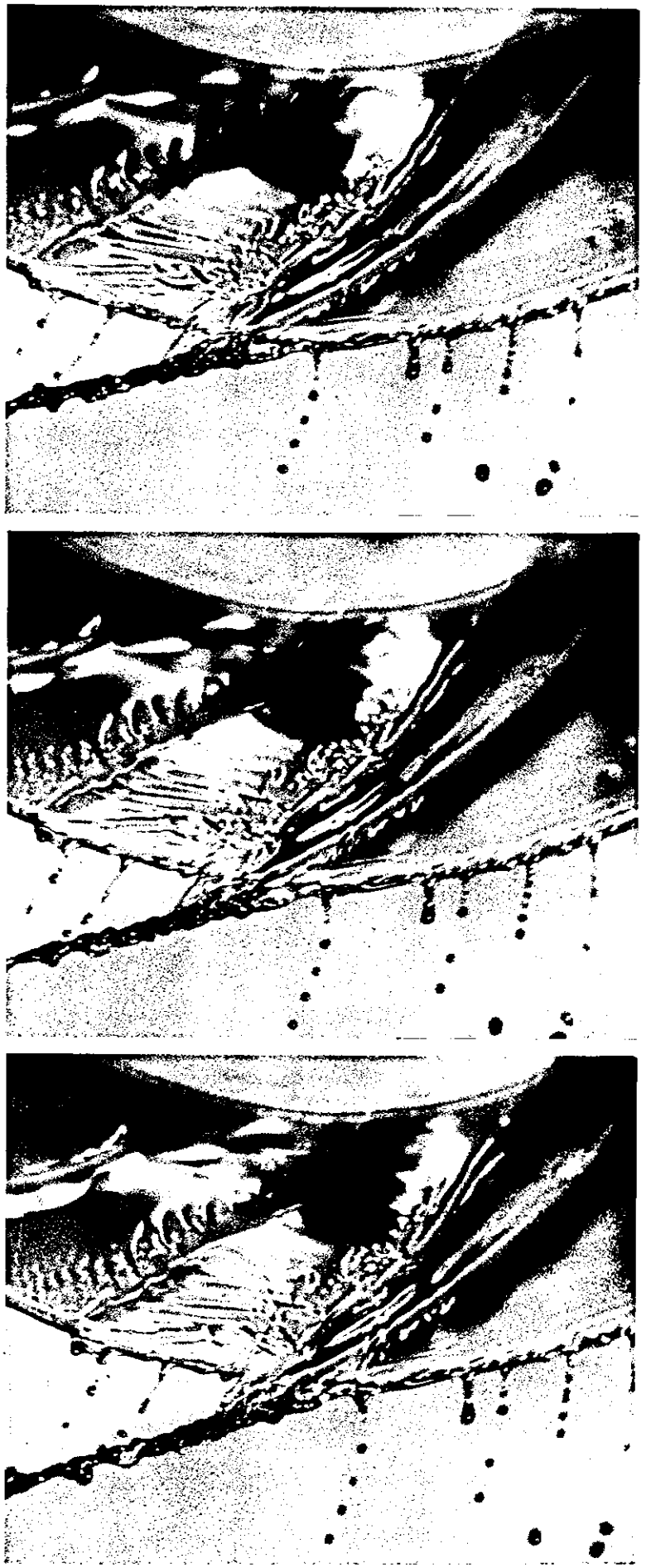

PHOTOGRAPH 5

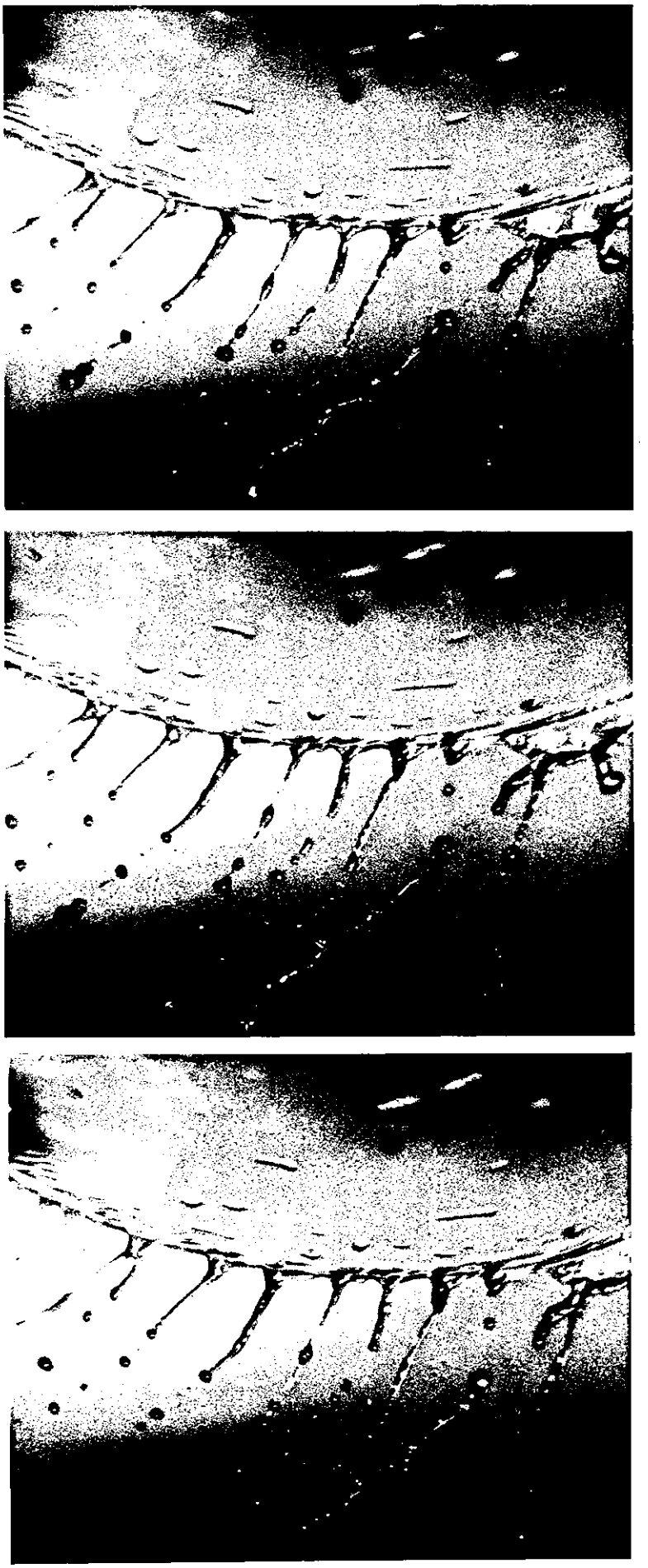

PHOTOGRAPH 6

CHAPTER FIVE

THE THEORY OF LIQUID FILM FLOW ON A ROTATING INCLINED SURFACE

5.1 Introduction

The film flow of a liquid on a rotating conical surface can be fully described by the equation of motion and the continuity equation. Due to the complexity of these equations some simplifying assumptions must be made before any worthwhile analytical solution can be found.

The assumptions made throughout this work are: the liquid flowrate is steady; the liquid is incompressible and Newtonian; the whole operation is carried out isothermally and isobarically, hence the viscosity and density are constant, finally the flow is smooth, that is there are no waves present.

At very low Reynolds numbers (i.e Re < 1.) the film flow on the disc would correspond to creeping flow. Under such conditions the film flow has been found[17], as expected, to obey the modified Nusselt theory. Once the Reynolds number becomes significant (i.e. Re $\geq$ 1) the inertial terms in the equation of motion begin to take effect and so deviation from the creeping flow equation might be expected.

Due to the apparent symmetry that exists in the film flow on a conical disc it would appear that the flow is axisymmetrical. However even in the creeping flow case the flow cannot be considered to be axisymmetrical with respect to the rotating disc as the conditions which are necessary for axisymmetrical flow[7] are:

$$\frac{\partial \underline{V}}{\partial \phi} = 0 \qquad 5.1.1$$

and

$$\underline{i}_\phi \cdot \underline{V} = 0 \qquad 5.1.2$$

That is, the velocity vector is independent of the azimuthal angle and that the azimuthal velocity component is everywhere zero. (see Appendix 5.1)

The flow, with respect to the disc, may be considered to act in two directions, that is in the meridional direction and across the thickness of the film. In this case the flow in the meridional direction will be by far the most significant. Due to the magnitude of the meridional velocity it is possible to consider this case as a unidirectional flow problem. Alternatively this case may be solved with the aid of the stream function technique.

Once slippage occurs in the azimuthal direction, that is once there is an azimuthal velocity gradient, the flow on the disc becomes more complicated. Under this condition the flow is three dimensional with the azimuthal and meridional velocities being predominant, as such, the flow could be considered to be essentially two dimensional. Superficially it would seem that this problem could be solved using a stream function type of solution. However, solving this two dimensional case is not possible by the stream function technique as the flow has a degree of symmetry about the axis of rotation which prohibits the meridional velocity being represented by the first derivative of the stream function with respect to the azimuthal angle. This may be shown mathematically as follows :-

$$\underline{V} = h_2 \underline{i}_2 \times \nabla \Psi = \underline{i}_1 h_2 h_3 \frac{\partial \Psi}{\partial q_3} + \underline{i}_2 0 - \underline{i}_3 h_1 h_2 \frac{\partial \Psi}{\partial q_1} \qquad 5.1.3$$

where equation 5.1.3 satisfies the continuity equation.

It can readily be seen that the meridional component will be zero because of the symmetry in the azimuthal direction (in the above notation this will correspond to the $\underline{i}_1$ component). The

second component of velocity (the $\underline{i}_2$ component) is zero as we are taking the two dimensional case (i e the velocity across the thickness of the film is negligible).

5.2 The Equations of Motion

The film flow of a liquid on a rotating conical disc can be fully described by the equation of motion and the continuity equation. Using Gibbs notation for an incompressible, Newtonian liquid these have been summarised as follows :-

$$\rho\left(\frac{\partial \underline{V}}{\partial t} + \underline{V}\cdot\nabla\,\underline{V}\right) - \mu\nabla^2\,\underline{V} = -\nabla p \qquad 3.1.1$$

$$\nabla\cdot\underline{V} = 0 \qquad 3.1.2$$

It should be noted that in equation 3.1.1 the body force terms have been omitted. Using the following vector identities (7) equation 3.1.1 can be modified;

$$\underline{V}\cdot\nabla\,\underline{V} = {}^1/_2\nabla V^2 - \underline{V} \times (\nabla \times \underline{V}) \qquad 5.2.1$$

$$\nabla^2\,\underline{V} = \nabla\cdot(\nabla\cdot\underline{V}) - \nabla \times (\nabla \times \underline{V}) \qquad 5.2.2$$

The result, after taking the curl of the modified form of equation 3.1.1 will be :

$$\frac{\partial}{\partial t}(\nabla \times \underline{V}) - \nabla \times \underline{V} \times (\nabla \times \underline{V}) + \nu\nabla \times \nabla \times \nabla \times \underline{V} = 0 \qquad 5.2.3$$

If the flow was axisymmetrical equation 5.2.3 could be expressed in terms of a stream function as follows :-

$$\underline{i}_\phi h_\phi \frac{\partial}{\partial t}(E^2\psi) - \nabla \times (h_\phi^2 E^2\psi \nabla\psi) - \underline{i}_\phi h_\phi \nu E^4\,\psi = 0 \qquad 5.2.4$$

When the inertial terms are omitted and the flow is steady we obtain the well known equation :

$$E^4\,\psi = 0 \qquad 5.2.5$$

where the operator E^2 is represented by:

$$E^2 = \frac{h_1 h_2}{h_3}\left[\frac{\partial}{\partial q_1}\left(\frac{h_3 h_1}{h_2}\frac{\partial}{\partial q_1}\right)+\frac{\partial}{\partial q_2}\left(\frac{h_3 h_2}{h_1}\frac{\partial}{\partial q_2}\right)\right] \qquad 5.2.6$$

Here the solution of equation 5.2.5 will represent creeping flow under axisymmetrical flow conditions.

As there is a high degree of axial symmetry, that is, the scalar velocity in the azimuthal direction is a constant at constant radius and position in the fluid, then a similar type of approach as used above can be adopted to represent the three dimensional case. At steady state conditions, equation 5.2.3 can be considered to comprise of two parts, namely the viscous and inertial terms. Because of the above mentioned symmetry the volumetric flowrate can be assumed to act principally in the meridional direction and across the thickness of the film. This enables a stream function to be used (Appendix 5-2) even though the flow is not axisymmetrical. The viscous term in equation 5.2.3 can then be written as follows :-

$$\nu\,\nabla x\nabla x\nabla x\,\underline{V} = h_1 h_2 h_3\left\{-\underline{i}_1\frac{1}{h_1}\frac{\partial}{\partial\theta}\left(E^2\left(\frac{V\phi}{h_3}\right)\right)+\underline{i}_2\frac{1}{h_2}\frac{\partial}{\partial r}\left(E^2\left(\frac{V\phi}{h_3}\right)\right)\right.$$
$$\left.-\underline{i}_3\frac{1}{h_1 h_2}E^4(\psi)\right\} \qquad 5.2.7$$

Whilst the inertial term is given by :

$$\nabla x\underline{V}x(\nabla x\underline{V}) = h_1 h_2 h_3\left\{-\underline{i}_1\frac{1}{h_1}\left(\frac{\partial}{\partial\theta}\left(V_r h_1\frac{\partial}{\partial r}\left(\frac{V\phi}{h_3}\right)+V\theta h_2\frac{\partial}{\partial\theta}\left(\frac{V\phi}{h_3}\right)\right)\right)\right.$$
$$+\underline{i}_2\frac{1}{h_2}\left(\frac{\partial}{\partial\theta}\left(V_r h_1\frac{\partial}{\partial r}\left(\frac{V\phi}{h_3}\right)+V\theta h_2\frac{\partial}{\partial\theta}\left(\frac{V\phi}{h_3}\right)\right)\right)$$
$$+\underline{i}_3\frac{1}{h_3}\left[\frac{\partial}{\partial r}\left(V\phi h_3\frac{\partial}{\partial\theta}\left(\frac{V\phi}{h_3}\right)-V_r\frac{h_3}{h_2}E^2\psi\right)\right.$$
$$\left.\left.-\frac{\partial}{\partial\theta}\left(V\theta\frac{h_3}{h_1}E^2\psi+V\phi h_3\frac{\partial}{\partial r}\left(\frac{V\phi}{h_3}\right)\right)\right]\right\} \qquad 5.2.8$$

Once again, the creeping flow solution will be exactly as before, that is the solution of equation 5.2.5 However once the inertial terms are taken into account the equations to be solved are non-linear and therefore difficult.

5.3 The Nusselt Model

This model was originally formulated for the film flow of a liquid down an inclined plane. It is essentially a simple model in that only pure creeping flow is considered, that is the non-linear inertial terms were neglected.

If we assume that the plane down which the liquid is flowing is infinitely wide, so that wall effects can be neglected, and the plane is vertical, then the system is more easily represented using a rectangular coordinate system. By assuming steady viscous flow, i.e. no waves present, and that the pressure gradient across the film is negligible, then the equation of motion including the body forces can be represented as follows :

$$\mu \nabla \times \nabla \times \underline{V} = \nabla \phi = \underline{g} \qquad 5.3.1$$

Here the gravity vector $\underline{g}$ has been represented by the divergence of the scalar, ϕ[96]. In the z direction (the vertical direction) we will have ;

$$\frac{\partial^2 U_z}{\partial y^2} = -\frac{g}{\mu} \qquad 5.3.2$$

hence

$$U_z = \frac{g}{\mu}\left(y\delta_{max} - \frac{y^2}{2}\right) \qquad 5.3.3$$

Equation 5.3.3 predicts a semi-parabolic velocity profile where velocity is zero at the surface of the plane (at y = 0) and is a maximum at the liquid/air interface (at $y = \delta_{max}$).

It follows that the volumetric flowrate is given by:

$$Q = \int_0^{\delta_{max}} U_z \, dy$$

$$= \left(\frac{g}{\nu}\right) \frac{\delta_{max}^3}{3} \qquad 5.3.4$$

Hence the Nusselt relationship

$$\delta \left(\frac{g}{\nu^2}\right)^{1/3} = \left(\frac{3}{4} N_{RE}\right)^{1/3} \qquad 5.3.5$$

where once again the Reynolds number is based upon the hydraulic radius.

For the case where a liquid is flowing film-wise on a rotating disc a Nusselt type solution can be found. For a flat disc cylindrical coordinates are most convenient. Here the Z direction is along the axis of revolution.

From the modified form of equation 3.1.1 we have

$$\nu \nabla x \nabla x \underline{V} + \tfrac{1}{2} \nabla (\underline{V}.\underline{V}) - \underline{V} x \nabla x \underline{V} = 0 \qquad 5.3.6$$

where the body forces have once again been omitted.

The Z component gives us :

$$\frac{\partial^2 U_r}{\partial z^2} = \frac{-w^2 r}{\nu} \qquad 5.3.7$$

from which we get

$$U_r = \frac{w^2 r}{\nu} \left[z\delta - \frac{z^2}{2} \right] \qquad 5.3.8$$

For the case where the film flow is on a rotating conical surface a similar solution is obtained, namely :

$$U_r = a - \frac{w^2 r^3}{\nu}\left[\frac{t^2}{2} + \frac{t^4}{6} + \frac{t^6}{9} + \frac{t^8}{12} + \frac{t^{10}}{15} + \ldots\ldots\right] - \frac{gr^2}{\nu}\left[\frac{t^3}{6} + \frac{t^5}{10} + \frac{t^7}{14} + \frac{t^9}{18} + \ldots\ldots\right] - b\left[t + \frac{t^3}{3} + \frac{t^5}{5} + \frac{t^7}{7} + \frac{t^9}{9} + \ldots\right] \quad 5.3.9$$

where the constants a and b and the variable t are defined in Appendix 5-3, in which a full derivation is also given. For this solution a spherical coordinate system was chosen. It should be noted that this solution is the general solution for the case where Θ is greater than zero and less than 180°. Equation 5.3.8 is therefore a limited solution of equation 5.3.9 as indicated in Appendix 5-3.

5.4 The Nikolaev Model

Nikolaev and his co-workers attempted to solve the equation of motion for an incompressible viscous fluid by linearizing these equations using the familiar dimensionless analysis techniques. The orthogonal curvilinear coordinate system they used was the conical one. This system can prove to be awkward as it becomes difficult to separate the variables. Nikolaev decided to overcome this problem by ignoring a term which he considered insignificant. However there must be some doubt as to the validity of this assumption as the terms which remain when this term is included are not always insignificant.

In conical coordinates the metrical coefficients are found to be (with reference to Figure 3.1)

$$h_l = 1. \quad ; \quad h_\delta = 1. ; h_\phi = \frac{1.}{l \sin\alpha - \delta\cos\alpha}$$

The assumption that Nikolaev made was the $\delta \cos\alpha$ part could be ignored as it was much smaller than $l \sin\alpha$. Although this is true, metrical coefficients are differentiated and so according to Nikolaev $\frac{\partial h_\phi}{\partial \delta}$ would not exist whereas it is in fact :

$$\frac{\partial h_\phi}{\partial \delta} = - \frac{\cos\alpha}{(l \sin\alpha - \delta\cos\alpha)^2}$$

Each time that h_ϕ is differentiated with respect to δ the film thickness, another term would be lost irrespective of the importance of that term.

The effect of ignoring the $\delta \cos\alpha$ part of the metrical coefficient in the azimuthal direction is apparent when the full equation is compared with equation 3.2.4. Whereas equation 3.2.4 contains the fourth derivative only, the full equation contains all the lower derivatives as well as a term in f_l the dimensionless velocity. Without detailed information about the mode of flow it is impossible to decide which derivative is the controlling term, if indeed any one in particular is controlling. For that reason the solution found by Nikolaev must be regarded with suspicion.

5.5 Solution of the Creeping Flow Equation

At low Reynolds numbers the inertial effects, which make the equation of motion non-linear, are insignificant. The solution of the equation of motion under this condition will therefore be the solution of the creeping flow equation.

$$\text{i.e.} \quad E^4(\psi) = 0 \qquad 5.2.5$$

The symmetry in the azimuthal direction indicates that the stream function (ψ) is not a function of the azimuthal angle. Hence the stream function may be defined as :-

$$\psi = R(r).f(\theta) \qquad 5.5.1$$

This of course assumes that the variables are separable.

If an infinite cone is considered, rotating at constant angular velocity w, with a constant volumetric flowrate Q, then as the radius becomes very large the film thickness would become very small, hence the meridional velocity component would tend towards zero. This suggests that the stream function is inversely proportional to some power of the radius. Let us therefore assume that the stream function may be defined as follows :-

$$\psi = r^{-n}.f(\theta) \qquad 5.5.2$$

where n is a positive constant.

For a spherical coordinate system we have:

$$E^2(\psi) = r^{-(n+2)}\left[n(n+1) + \cot\theta \frac{\partial f}{\partial \theta} + \frac{\partial^2 f}{\partial \theta^2} \right] \qquad 5.5.3$$

$$= r^{-(n+2)}F$$

$$\text{where} \quad F = \left[n(n+1) + \cot\theta \frac{\partial f}{\partial \theta} + \frac{\partial^2 f}{\partial \theta 2} \right] \qquad 5.5.4$$

thus it follows that :

$$E^4(\psi) = 0$$

$$= r^{-(n+4)}\left[(n+2)(n+3) + \cot\theta \frac{\partial F}{\partial \theta} + \frac{\partial^2 F}{\partial \theta^2} \right] \qquad 5.5.5$$

the solution for $f(\theta)$ being :

$$f(\theta) = D + E\left(t + \tfrac{1}{3}t^3 + \tfrac{1}{5}t^5 + \tfrac{1}{7}t^7 + \ldots\ldots\right) \qquad 5.5.6$$

where D, E and t are functions of Θ

$$t = \cos\Theta \qquad 5.5.7$$

$$D = \left[n(n+1) - a\right]\left[\frac{t^2}{2} + \frac{t^4}{12} + \frac{t^6}{30} + \frac{t^8}{56} + \ldots\right] + b\left[\frac{t^3}{3} + \frac{2}{15}t^5 + \frac{23}{315}t^7 + \frac{44}{945}t^9 + \ldots\right] + (n+2)(n+3)\left[\frac{t^4}{8} + \frac{5}{72}t^6 + \frac{7}{160}t^8 + \ldots\right] + d \qquad 5.5.8$$

$$E = a\,t - (n+2)(n+3)\left[\frac{t^3}{6} + \frac{t^5}{20} + \frac{t^7}{42} + \frac{t^9}{72} + \ldots\right] - b\left[\frac{t^2}{2} + \frac{t^4}{12} + \frac{t^6}{30} + \frac{t^8}{56} + \ldots\right] - n(n+1)t - e \qquad 5.5.9$$

where a, b, d, e and n are constants that depend on the assigned boundary conditions.

The boundary conditions used in the solution of equations 5.3.2, 5.3.7 and 5.3.9 can be used here, for both the r and Θ directions. That is :

$\frac{\partial U_r}{\partial \Theta} = \frac{\partial U_\Theta}{\partial \Theta} = 0$ at $\delta = \delta_{max}$, the film thickness

and $U_r = U_\Theta = 0$ at $\delta = 0$, the solid liquid interface.

The last condition needed to solve for these constants can be expressed in terms of the volumetric flowrate :

$$Q = 2\pi(\Psi_\delta - \Psi_o) \qquad 5.5.10$$

where Ψ_δ and Ψ_o are the values of the stream function at the air/liquid and liquid/solid interfaces respectively.

If the curl operator acts on equation 5.2.7 the following equation is true in the creeping flow case:

$$E^4 \left(\frac{U_\phi}{h_3}\right) = 0$$

A similar reasoning as used in the case of the E operator acting on the stream function may be used here. As the film decreases in thickness with increase in radius we would suspect the amount of tangential slippage to decrease. Also as the radius r approaches infinity the azimuthal velocity would approach infinity as well. Hence we would expect the function (U_ϕ/h_3) to be proportional to some function of the radius.

e.g. $$\frac{U_\phi}{h_3} = \sin^2\theta\, R(r)$$

If a solution of this form is suggested it is found that :

$$U_\phi = W r \sin\theta$$

This is the condition of no slip in the azimuthal direction.

5.6 Potential Flow

The potential flow equation in its invariant form can be expressed as :

$$\nabla^2\phi = 0 \qquad 5.6.1$$

In terms of the metrical coefficients this becomes :

$$\frac{\partial}{\partial q_1}\left(\frac{h_1}{h_2h_3}\frac{\partial\phi}{\partial q_1}\right) + \frac{\partial}{\partial q_2}\left(\frac{h_2}{h_3h_1}\frac{\partial\phi}{\partial q_2}\right) + \frac{\partial}{\partial q_3}\left(\frac{h_3}{h_1h_2}\frac{\partial\phi}{\partial q_3}\right) = 0 \qquad 5.6.2$$

Thus the potential flow equation can be seen to represent the continuity equation where the velocity vector $\underline{V}$ has been replaced by the gradient of a scalar, grad ϕ.

This equation is the same as Laplace's equation, solutions of which are well known[97]. In spherical coordinates the general solution of Laplace's equation is :

$$\phi = \begin{pmatrix} r^n \\ r^{-n-1} \end{pmatrix} P_n^m (\cos\theta) \begin{pmatrix} \sin \\ \cos \end{pmatrix} m\psi \qquad 5.6.3$$

where the function $P_n^m (\cos\theta)$ is described by a modification to Rodrigue's formula, namely :-

$$P_n^m (\mu) = \frac{1}{2^n . n!} (1-\mu^2)^{m/2} \frac{d^{m+n} (\mu^2-1)^n}{d\mu^{m+n}} \qquad 5.6.4$$

In the particular problem at hand the velocities in the r and θ directions, that is the meridional direction and across the thickness of the film, are invariant with change in azimuthal angle. For these conditions to be satisfied the constant m must be zero, leaving a general solution of the form:

$$\phi = \begin{pmatrix} r^n \\ r^{-n-1} \end{pmatrix} P_n^o (\cos\theta) \qquad 5.6.5$$

The solution of this equation excludes a solution for the azimuthal velocity component.

As in the case of the solution of the creeping flow equation, equation 5.2.5, the meridional velocity is expected to decrease with increasing radius. To satisfy this condition the solution will be of the form:

$$\phi = r^{-n-1} \frac{1}{2^n n!} 2n\mu (\mu^2-1)^{n-1} \qquad 5.6.6$$

where $\mu = \cos\theta$ 5.6.7

the components of velocity in the r and Θ directions, see Figure 5.1, being ;

$$U_r = h_r \frac{\partial \phi}{\partial r} = -(n+1)\, r^{-(n+2)} \frac{1}{2^{n-1}(n-1)!}\, \mu(\mu^2-1)^{n-1} \qquad 5.6.8$$

$$U_\Theta = h_\Theta \frac{\partial \phi}{\partial \Theta} = r^{-(n+2)} \frac{1}{2^{n-2}(n-2)!} \cdot \mu^2 (\mu^2-1)^{n-2} \qquad 5.6.9$$

As the constant n is a positive integer it is immediately evident that n must be an even number when Θ is in the range $0 < \Theta < \pi/2$. Such conditions make the value of U_r always positive and U_Θ always positive which is exactly what is expected.

To find the particular solutions to equations 5.6.8 and 5.6.9 the prescribed boundary conditions have to be met. These equations cannot be solved using the boundary conditions used to solve the creeping flow equations. One common method by which these equations are solved is to equate the velocities to either their respective maximum or average velocity at a known finite point and then to assume a velocity at infinity. However in this case this technique is not fruitful as neither the average velocity nor the surface velocity can be defined accurately. If this solution is solved in conjunction with the creeping flow equation, that is by adjusting the conditions until there is continuity across the boundary (the imaginary boundary between creeping flow and potential flow) the general solution so formed should be capable of being extended to higher Reynolds numbers. This type of solution would seem to be more easily soluble using the facilities of a computer as not only have the velocities to match at the boundary but also the gradients have to match as well.

FIG.5.1. THE SPHERICAL COORDINATE SYSTEM.

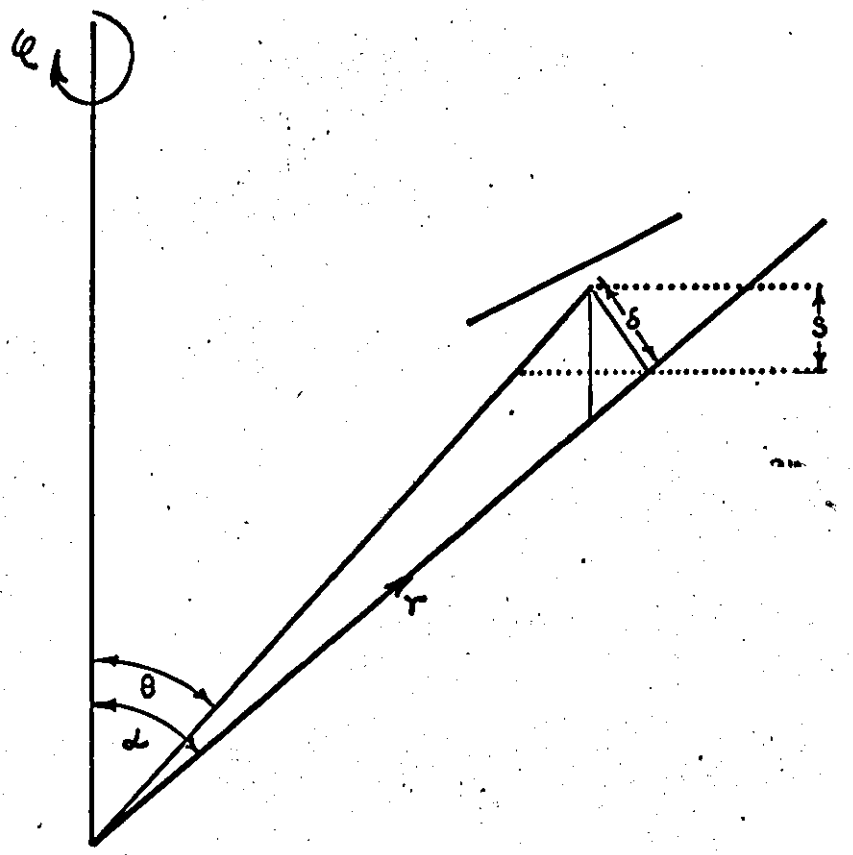

FOR THIN FILMS:

$$S = r(\cos\theta - \cos\alpha)$$

$$\therefore \delta = r\left(\frac{\cos\theta - \cos\alpha}{\sin\alpha}\right)$$

5.7 Numerical Methods

The three dimensional solution of the Navier-Stokes equations has been solved by von Karman[98] and later by Cochran[99] for the case where liquid is entrained by a rotating disc, the axis of which is perpendicular to the disc's surface. The solution depends on the fluid being of "infinite" thickness above the disc and as such this solution does not fully correspond to a thin film of liquid being spun off a rotating disc. However this is only a boundary condition problem, thus the general form of the equations must be true no matter what the film thickness is in practice. For the steady flow of an incompressible fluid the equations of motion and continuity may be written as[11] :

$$F^2 - G^2 + F'H = F'' \qquad 5.7.1$$

$$2FG + G'H = G'' \qquad 5.7.2$$

$$H H' = P' + H'' \qquad 5.7.3$$

$$2F + H' = 0 \qquad 5.7.4$$

where the cylindrical form of these equations has been used and

$$V_r = wr\, F(I) \quad V_\phi = wr\, G(I) \quad V_y = \sqrt{\nu w}\, H(I)$$

$$I = \left(\frac{w}{\nu}\right)^{1/2} \delta \qquad 5.7.5$$

and the boundary conditions were defined as,

$$F = 0 \quad G = 1 \quad H = 0 \quad \text{at } I = 0 \qquad 5.7.6$$

$$F \longrightarrow 0 \quad G \longrightarrow 0 \quad H \longrightarrow -\alpha \text{ (a constant) as } I \longrightarrow \infty \qquad 5.7.7$$

Using these boundary conditions two sets of infinite series were found for F, G and H. At large values of I the first set was:

$$F = A e^{-\alpha I} - \frac{A^2+B^2}{2\alpha^2} . e^{-2\alpha I} + \frac{A(A^2+B^2)}{4\alpha^4} . e^{-3\alpha I} + \ldots.$$

$$G = B\, e^{-\alpha I} - \frac{B(A^2+B^2)}{12\,\alpha^4}\cdot e^{-3\alpha I} + \ldots\ldots$$

$$H = -\alpha + \frac{2A}{\alpha}\, e^{-\alpha I} - \frac{A^2+B^2}{2\,\alpha^3}\cdot e^{-2\alpha I} + \frac{A(A^2+B^2)}{6\,\alpha^5}\cdot e^{-3\alpha I}$$

At very small values of I the second set was found to be :

$$F = aI - \frac{I^2}{2} - \frac{1}{3}\, b\, I^3 + \ldots\ldots$$

$$G = 1 + b\, I + \frac{1}{3}\, a\, I^3 + \ldots\ldots$$

$$H = -a\, I^2 + \frac{1}{3}\, I^3 + \ldots\ldots$$

The constants A, B, a, b, and α were chosen such that both the values of F, G and H and their derivatives (F', G' and H') remained continuous when these two series were matched. When these results were integrated numerically the constants were found to be :

$a = 0.51023$ $\quad b = -0.616$ $\quad \alpha = 0.88447$

$A = 0.934$ $\quad B = 1.208$

Before adopting this approach to the solution of the thin film case the question must be asked, are these assumptions applicable to this case? Of these assumptions the most dubious is the one where the axial velocity component is regarded as independent of radial position (equation 5.7.5). This most clearly is not true when the radial distances are small, however, at moderate values of radial distance this assumption should not invalidate this approach.

At the surface of a flat disc the boundary condition is the same as the one described by von Karmon. That is :

$$F = 0 \quad G = 1 \quad H = 0 \quad \text{at } I = 0 \qquad 5.7.6.$$

At the liquid/air interface the boundary conditions will be :

$$F' = 0 \quad G' = 0 \quad H = -\alpha \quad \text{at } I = I_{max} \qquad 5.7.8$$

The solution for F, G and H near the surface of the disc is therefore as before. Their solutions at the liquid/air will come from the solution at the interface.

$$\text{At the interface } F'' \approx F^2 - G^2$$

$$\text{and } G'' \approx 2FG$$

If we introduce a complex function Ψ these equations may be solved.

$$\Psi = F + iG$$

$$\text{therefore } \Psi'' \approx \Psi^2$$

the solution of this being :

$$I \approx C \pm \left[\Psi - \frac{\Psi^4}{24D} + \frac{\Psi^7}{168D^2} - \frac{\Psi^{10}}{4320D^3} + \ldots \right]$$

This solution is in a highly undesirable form, that is a series in Ψ rather than I. Due to this the numerical method becomes involved. However one route that might be used to obtain a series solution in terms of I is to assume a power series of the form :

$$\Psi = a_0 I^c + a_1 I^{c+1} + a_2 I^{c+2} + a_3 I^{c+3} + ;\ldots..$$

Using regression techniques it should be possible to curve fit the above series to the previous series. Unfortunately only a small range of I values may be used as the first series is only the solution at the liquid/air interface. This may not in fact be a serious drawback as the laminar boundary layer should extend over a significant proportion of the film thickness, thus the proportion affected by the solution at the liquid/air

As the boundary layer can exist over a substantial proportion of the film the method adopted by Oyama and Endou (106) can be used.

If a modified form of Taylors (107) argument is applied, the Navier Stokes equation in spherical co-ordinates may be written as follows:

$$v_r \frac{\delta v_r}{\delta r} + \frac{v_\theta}{r}\frac{\delta v_r}{\delta \theta} - \frac{v_\phi^2}{r} = \frac{\nu}{r^2}\frac{\delta^2 v_r}{\delta \theta^2} \qquad 5.7.9$$

$$v_r \frac{\delta v_\phi}{\delta r} + \frac{v_\theta}{r}\frac{\delta v_\phi}{\delta \theta} + \frac{v_\phi v_r}{r} = \frac{\nu}{r^2}\frac{\delta^2 v_\phi}{\delta \theta^2} \qquad 5.7.10$$

whilst the continuity equation in the approximate form is:

$$\frac{\delta V_r}{\delta r} + \frac{2V_r}{r} + \frac{1}{r}\frac{\delta V_\theta}{\delta \theta} = 0 \qquad 5.7.11$$

by defining

$$\begin{aligned} V_r &= r \sin\alpha f(\theta) \\ V_\theta &= \sin\alpha g(\theta) \\ V_\phi &= r \sin\alpha h(\theta) \end{aligned} \qquad 5.7.12$$

the above equations become:

$$r \sin\alpha (f^2 - h^2) = \frac{\nu}{r} f'' - \sin\alpha g f' \qquad 5.7.13$$

$$2r \sin\alpha fh + \sin\alpha g h' = \frac{\nu}{r} h'' \qquad 5.7.14$$

$$3 \sin\alpha f + \frac{\sin\alpha}{r} g' = 0 \qquad 5.7.15$$

By changing the co-ordinate system we can define the angular co-ordinate θ in terms of the dimensionless film thickness. (I).

Hence if:

$$(\theta - \alpha) = \frac{1}{r}\left(\frac{\nu}{w}\right)^{\frac{1}{2}} I \qquad 5.7.16$$

where α is the half cup angle; and if

$$\begin{aligned} f &= wF(I) \\ g &= (\nu w)^{\frac{1}{2}} G(I) \\ h &= wH(I) \end{aligned} \qquad 5.7.17$$

then the equations become:

$$\sin\alpha (F^2 - H^2) = F'' - \sin\alpha GF' \qquad 5.7.18$$

$$2 \sin\alpha FH + \sin\alpha GH' = H'' \qquad 5.7.19$$

$$3F + G' = 0 \qquad 5.7.20$$

where F, G and H are functions of I.

For thin film flow it is assumed the film is completely within the boundary layer. Hence the boundary layer equation must define the flow within the film. The boundary-layer momentum integrals are:

$$\sin\alpha\{\int F^2\,dI - \int H^2\,dI\} + \sin\alpha\int GF'\,dI = \left[F'\right]_0^{I_{max}} \quad 5.7.21$$

$$2\sin\alpha\int FH\,dI + \sin\alpha\int GH'\,dI = \left[H'\right]_0^{I_{max}} \quad 5.7.22$$

Now $$\int GF'\,dI = \left[GF\right]_0^{I_{max}} - \int G'F\,dI \quad 5.7.23$$

from continuity: $$= \left[GF\right]_0^{I_{max}} + 3\int F^2\,dI \quad 5.7.24$$

similarly $$\int GH'\,dI = \left[GH\right]_0^{I_{max}} + 3\int FH\,dI \quad 5.7.25$$

These identities may be simplified knowing the boundary conditions,

at	$I = 0$	$F = 0$	$G = 0$	$H = 1.$
	$I = I_{max}$	$F = F_{I_{max}}$	$G \sim 0$	$H = H_{I_{max}}$
		$F' = 0$	$G' = k$	$H' = 0$

Hence the boundary layer momentum integrals become:

$$\sin\alpha\{4\int F^2\,dI - \int H^2\,dI\} = \left[F'\right]_0^{I_{max}} \quad 5.7.26$$

$$\sin\alpha\ 5\int FH\,dI = \left[H'\right]_0^{I_{max}} \quad 5.7.27$$

If it is assumed that the function F and H have the form:

$$F = aI + bI^2 \quad 5.7.28$$

$$H = 1. + AI + BI^2 \quad 5.7.29$$

then it is possible to solve for a, b, A and B using the boundary conditions and the boundary-layer momentum integral equations. These values have been found to be:

$$a = -2bI_{max}$$

$$A = -2BI_{max}$$

$$B = \frac{10\sin\alpha\, I^2_{max}\ b}{3(\frac{8}{3}\sin\alpha\, I^4_{max}\ b - 2)}$$

whilst b is found from the equation:

$$\sin\alpha\left\{\frac{32}{15}b^2 I^4_{max} - 1. - \frac{4B}{3}I^2_{max} + \frac{8}{15}B^2\ I^4_{max}\right\} = 2b$$

Hence when $I_{max} \ll 1.$

$$b = -\tfrac{1}{2}\sin\alpha$$

and therefore: $$V_r = \frac{w^2 r}{\nu} \sin\alpha \, (\delta_{max}\delta - \tfrac{1}{2}\delta^2)$$

where δ is the film thickness for small angles

$$\delta = r(\theta - \alpha) \doteq r d\theta$$

i.e. $$I = \delta\left(\frac{w}{\nu}\right)^{\frac{1}{2}}$$

The form of this equation is similar to the Nusselt model.

Deviations from the Nusselt model will therefore occur once I_{max}, the dimensionless film thickness, can no longer be considered to be very small.

Now the volumetric flowrate is given by:-

$$Q = 2\pi r \sin\alpha \int_{max} \bar{v}_r$$

$$= -\frac{4\pi r^2}{3} w^2 \sin^2\alpha \, \delta^3_{max} \quad b$$

rearranging, this becomes:

$$\frac{3}{4}\left(N_{RE}\right) = \left(N^*_T\right)^3 \left(-\frac{2b}{\sin}\right) \qquad 5.7.30$$

where the Reynolds number (N_{RE}) and the modified Nusselt parameter (N^*_T) are similar to those used previously except that the body force term is not included in N^*_T this time (see eqns. 3.1.1. and 3.2.1.).

As the coefficient 'b' in eqn. 5.7.30 is a function of I_{max} only, the dimensionless film thickness and modified Nusselt parameter may be considered independant of I_{max}, hence a Nusselt type relationship will hold if I_{max} and thus b remain constant. This will result in a family of curves of N_{RE} against N^*_T

APPENDIX 5-1

The first condition that has to be met for axisymmetrical flow is defined by equation 5.1.1.

$$\text{i.e.} \quad \frac{\partial \underline{V}}{\partial \phi} = 0 \qquad 5.1.1$$

where $\underline{V} = \underline{i}_1 V_1 + \underline{i}_2 V_2 + \underline{i}_3 V_3$

Thus equation 5.1.1 may be written as

$$\frac{\partial}{\partial \phi} (\underline{i}_1 V_1 + \underline{i}_2 V_2 + \underline{i}_3 V_3) = 0$$

In spherical coordinates the metrical coefficients are:

$$h_r = 1. \qquad h_\theta = \frac{1.}{r} \qquad h_\phi = \frac{1.}{r \sin \theta}$$

The differentials of the unit vectors are as follows :

$$\frac{\partial \underline{i}_1}{\partial \phi} = \underline{i}_1 \, h_1 \frac{\partial}{\partial q_1} \frac{1}{h_3} \; ; \; \frac{\partial \underline{i}_2}{\partial \phi} = \underline{i}_3 \, h_2 \frac{\partial}{\partial q_2} \left(\frac{1}{h_3}\right)$$

$$\frac{\partial \underline{i}_3}{\partial \phi} = -\underline{i}_1 \, h_1 \frac{\partial}{\partial q_1} \left(\frac{1}{h_3}\right) - \underline{i}_2 \, h_2 \frac{\partial}{\partial q_2} \left(\frac{1}{h_3}\right)$$

Hence the products that arise from equation 5.1.1 will be:

$$\frac{\partial \underline{V}}{\partial \phi} = \underline{i}_1 \left(\frac{\partial V_1}{\partial \phi} - V_3 \, h_1 \frac{\partial}{\partial q_1} \left(\frac{1}{h_3}\right)\right) + \underline{i}_2 \left(\frac{\partial V_2}{\partial \phi} - V_3 \, h_2 \frac{\partial}{\partial q_2} \left(\frac{1}{h_3}\right)\right) + \underline{i}_3 \left(\frac{\partial V_3}{\partial \phi} + V_1 h_1 \frac{\partial}{\partial q_1}\left(\frac{1}{h_3}\right) + V_2 h_2 \frac{\partial}{\partial q_2} \left(\frac{1}{h_3}\right)\right)$$

In terms of the spherical coordinate system this will be:

$$\frac{\partial \underline{V}}{\partial \phi} = \underline{i}_1 \left(\frac{\partial V_r}{\partial \phi} - V_\phi \sin \theta\right) + \underline{i}_2 \left(\frac{\partial V_\theta}{\partial \phi} - V_\phi \cos \theta\right) + \underline{i}_3 \left(\frac{\partial V_\phi}{\partial \phi} + V_r \sin\theta + U_\theta \cos \theta\right)$$

By considering the symmetry of the flow and assuming that we are observing the flow with respect to the cup then the coefficients of the unit vectors $\underline{i}_1$ and $\underline{i}_2$ will be zero. The coefficient of the unit vector $\underline{i}_3$ cannot be zero except in the unreal case when there is no flow of liquid.

APPENDIX 5-2

For the case of a liquid flowing film-wise on a rotating conical disc we can consider the stream function to be a function of the velocities in the r and θ directions

i.e. $\Psi = \Psi\ (r, \theta)$

This means that the velocity in the azimuthal direction does not directly influence the stream function. Thus we can say :

$$h_3\ \underline{i}_3 \times \nabla \Psi = -\underline{i}_1 h_2 h_3 \frac{\partial \Psi}{\partial \theta} + \underline{i}_2 h_1 h_3 \frac{\partial \Psi}{\partial r} + \underline{i}_3 .0$$

Hence if we are to define the velocity vector in terms of the stream function we must include a term to take account of the azimuthal velocity.

$$\underline{V} = \underline{i}_1 V_r + \underline{i}_2 V_\theta + \underline{i}_3 V_\phi$$

$$= \underline{i}_1 h_2 h_3 \frac{\partial \Psi}{\partial \theta} + \underline{i}_2 h_1 h_3 \frac{\partial \Psi}{\partial r} + \underline{i}_3 V_\phi$$

$$= h_3\ \underline{i}_3 \times \nabla \Psi + \underline{i}_3 V_\phi$$

If this is to prove satisfactory it must satisfy the continuity equation

ie $\nabla . \underline{V} = 0$

$$= h_1 h_2 h_3 \left[\frac{\partial}{\partial r}\left(\frac{V_r}{h_2 h_3}\right) + \frac{\partial}{\partial \theta}\left(\frac{V_\theta}{h_1 h_3}\right) + \frac{\partial}{\partial \phi}\left(\frac{V_\phi}{h_1 h_2}\right) \right]$$

$$= h_1 h_2 h_3 \left[-\frac{\partial}{\partial r}\left(\frac{h_2 h_3}{h_2 h_3} \frac{\partial \Psi}{\partial \theta}\right) + \frac{\partial}{\partial \theta}\left(\frac{h_1 h_3}{h_1 h_3} \frac{\partial \Psi}{\partial r}\right) + \frac{\partial}{\partial \phi}\left(\frac{V_\phi}{h_1 h_2}\right) \right]$$

Hence it can be seen that continuity is observed.

APPENDIX 5-3

Derivation of equation 5.3.9

$$\underline{V}\nabla\underline{V} - \nu\nabla^2\underline{V} = \underline{g}$$

or
$$\frac{1}{2}\nabla \underline{V}^2 - \underline{V}x\nabla x\underline{V} + \nu\nabla x\nabla x\underline{V} = \underline{g}$$

$$-w^2 r \sin^2\theta - \frac{1}{r^2\sin\theta}\frac{\partial}{\partial\theta}\left(\sin\theta\frac{\partial V_r}{\partial\theta}\right) = -g\cos\theta$$

$$\sin\theta\frac{\partial}{\partial\theta}\left(\sin\theta\frac{\partial V_r}{\partial\theta}\right) = g\cos\theta\sin^2\theta - w^2 r\sin^4\theta$$

let $t = \cos\theta$

$$\frac{\partial t}{\partial\theta} = -\sin\theta$$

$$\therefore + \frac{\partial}{\partial t}\left(\sin^2\theta\frac{\partial V_r}{\partial t}\right) = gt - w^2 r(1-t^2)$$

$$\text{i e } \frac{\partial}{\partial t}\left((1-t^2)\frac{\partial V_r}{\partial t}\right) = gt - w^2 r(1-t^2)$$

$$\text{i e } (1-t^2)\frac{\partial^2 V_r}{\partial t^2} - 2t\frac{\partial V_r}{\partial t} = gt - w^2 r(1-t^2)$$

Solution of the complementary function

Assume solution of the form

$$V_r = t^c\ (a_o + a_1 t + a_2 t^2 + a_3 t^3 + \ldots + a_n t^n)$$

$$\frac{\partial V_r}{\partial t} = a_o c t^{c-1} + a_1(c+1)t^c + a_2(c+2)t^{c+1} + \ldots + a_n(c+n)t^{c+n-1}$$

$$\frac{\partial^2 V_r}{\partial t^2} = a_o c(c-1)t^{c-2} + a_1(c+1)c\,t^{c-1} + a_2(c+2)(c+1)t^c + \ldots$$

When these are substituted back into the complementary function we will have an equation of the form :

$$A_o t^{c-2} + A_1 t^{c-1} + A_2 t^c + A_3 t^{c+1} + \ldots = 0$$

To solve, the coefficients (A's) are equated to zero

(c-2) coeff $\quad a_o\, c(c-1) = 0 \quad \therefore\ c = 0$ or 1

(c-1) coeff $\quad a_1\,(c+1)\,c = 0 \quad \therefore\ a_1 = 0$

c coeff $a_2 = \frac{c}{(c+2)} a_o$

$a_5 = a_3 = a_1 = 0$ etc i e odd coeffs = 0

(c+2) coeff $a_4 = \frac{c}{(c+4)} a_o$

More generally $a_n = \frac{c}{(c+n)} a_o$ when n is even.

Solution of indicial equation is:

$$V_r = a_o(1+t+\tfrac{1}{3} t^3 + \tfrac{1}{5} t^5 + \tfrac{1}{7} t^7 + \ldots\ldots+)$$

Full solution:

$$\text{Let } R = (gt - w^2 r\ (1-t^2))\ \frac{r^2}{\nu}$$

$$\text{Let } V_r = A + B\ (t + \tfrac{1}{3} t^3 + \tfrac{1}{5} t^5 + \tfrac{1}{7} t^7 + \ldots\ldots\ )$$

where A and B are functions of t.

$$\text{if } \frac{\delta V_r}{\delta t} = B\ (1 + t^2 + t^4 + t^6 + \ldots\ldots)$$

$$\text{then } A' + B'\ (t + \tfrac{1}{3} t^3 + \tfrac{1}{5} t^5 + \tfrac{1}{7} t^7 + \ldots.) = 0$$

$$\frac{\delta^2 V_r}{\delta t^2} = B'(1+t^2+t^4+t^6+ \ldots) + B\ (2t+4t^3+6t^5+8t^7+ \ldots.)$$

Substituting back into original equation gives us

hence $$B = \left[\frac{gt^2}{2} - w^2 r(t-\frac{t^3}{3}) \right] \frac{r^2}{\nu} + b$$

$$B' = R$$

$$\text{Now } A = \int A' \, dt$$

$$= -\int R \left(t + \frac{1}{3} t^3 + \frac{1}{5} t^5 + \frac{1}{7} t^7 + \ldots.\right) dt$$

$$= -\frac{gr^2}{\nu}\left[\frac{t^3}{3} + \frac{1}{15} t^5 + \frac{1}{35} t^7 + \frac{1}{63} t^9 + \ldots.\right]$$

$$+ \frac{w^2 r^3}{\nu}\left[\frac{t^2}{2} - \frac{1}{6} t^4 - \frac{1}{45} t^6 - \frac{1}{140} t^8 - \frac{1}{315} t^{10} - \ldots.\right]$$

Hence full solution in the range $-1 < t < 1$ where $t = \cos \theta$

$$V_r = a - \frac{w^2 r^3}{\nu}\left[\frac{t^2}{2} + \frac{t^4}{6} + \frac{t^6}{9} + \frac{t^8}{12} + \frac{t^{10}}{15} + \ldots.\right]$$

$$- \frac{gr^2}{\nu}\left[\frac{t^3}{6} + \frac{t^5}{10} + \frac{t^7}{14} + \frac{t^9}{18} + \ldots\ldots\ldots\right]$$

$$- b\left[t + \frac{t^3}{3} + \frac{t^5}{5} + \frac{t^7}{7} + \frac{t^9}{9} + \ldots\ldots\right]$$

The values of a and b, the two constants of integration, may be found once the boundary conditions are determined.

Boundary conditions (see Figure 5.1)

when $\theta = \alpha$ $t = \cos \alpha = T$ (say)

then $V_r = 0$

When $\theta = \theta_{min}$ $t = \cos \theta_{min} = P$ (say)

then $\frac{\partial V_r}{\partial t} = 0$

$$\text{hence } b = \frac{-w^2 r^3 [P + \frac{2}{3} P^3 + \frac{2}{3} P^5 + \frac{2}{3} P^7 + ..] - \frac{1}{2} gr^2 [P^2 + P^4 + P^6 + P^8 + ..]}{\nu [1 + P^2 + P^4 + P^6 + P^8 + ..]}$$

$$\text{Hence} \quad a = b\left[T + \frac{T^3}{3} + \frac{T^5}{5} + \frac{T^7}{7} + \ldots\right] + \frac{gr^2}{\nu}\left[\frac{T^3}{6} + \frac{T^5}{10} + \frac{T^7}{14} + \frac{T^9}{18} + \ldots\right]$$

$$+ \frac{w^2 r^3}{\nu}\left[\frac{T^2}{2} + \frac{T^4}{6} + \frac{T^6}{9} + \frac{T^8}{12} + \frac{T^{10}}{15} + \ldots\right]$$

This solution can be tested by taking the case where $\alpha = 90^\circ$

i e the flat disc case.

for this case $a = 0$ as $T = \cos 90^\circ$

for thin films $b \triangleq -\frac{w^2 r^3 P}{\nu}$ as terms P^2 and greater $\longrightarrow 0$

Hence

$$V_r = \frac{w^2 r^3}{\nu}\left[Pt - \frac{t^2}{2}\right]$$

$$= \frac{w^2 r}{\nu}\left[\delta_{max}.\delta - \frac{\delta^2}{2}\right]$$

This is of an identical form to equation 5.3.8.

CHAPTER SIX

DISCUSSIONS AND CONCLUSIONS OF THE EXPERIMENTAL WORK

6.1. The Averaged Film Thickness Results

6.2. The Continuous Film Thickness Results

6.3. The Drop Size Distribution Results

6.4. Suggestions for Further Work

6.1. The Averaged Film Thickness Results

Before an attempt was made to record the instantaneous film thickness results it was felt that the light extinction technique should be thoroughly tested by obtaining the time and position averaged film thicknesses and comparing these with the results of other authors. To obtain these results the signal from the silicon light cell was fed into a data logging unit. This unit accepted the signal and integrated it over $^{1}/_{50}$th sec. Thus the value recorded by the digital voltmeter, which formed part of the data logger, represented the average value over $^{1}/_{50}$th sec, during which time the disc travelled a finite distance. The system was slightly more complex as the liquid was also moving in two orthogonal directions with respect to the cup. A distribution of averaged film thickness results was obtained as the film thicknesses recorded were found to be a function of the orientation and position of the waves as the disc traversed the probe area. Time averaging of an individual reading was inevitable, however, due to the relatively short period over which the signal was integrated the time averaging effect was not found to be predominant.

These results, Tables 1-8 inclusive, have been plotted in the way described by Espig and Hoyle[3], that is the Modified Nusselt Parameter against Reynolds number, see Graph 1. This plot compares favourably with the graphs obtained by Beardall[18] for film flow of liquids down the external surface of a rotating "male" cone. Throughout the whole of this work the liquid under test was mains water which contained a nigrosine dye; no other liquids were used as it was felt that this liquid exhibited the desired properties for the continuous film thickness experiments.

These same results have been plotted in accordance with Bruin's Theory, see Graph 2, Tables 1-8. In contrast with the work of Nikolaev where the presented experimental work followed the theoretically predicted curve closely, this work contains considerable scatter. It might be concluded that this work suffers from large experimental errors, however it is equally possible that the obtained results cannot be compared directly as they do not represent the same physical phenomenon. The difference being that Nikolaev's data supposedly represents smooth film flow on an infinite cone with no wave formations present whereas the data presented in this investigation would certainly represent the wavy film flow conditions on a finite cup.

The results obtained using the optical technique were biased in several ways. When waves were present on the cup the signal recorded by the data logging unit was the average value corresponding to the area under the signal/time curve. This average was taken as the linear average of the signal whereas the average corresponding to the logarithm of the signal should have been taken due to the exponential relationship defined by the Lambert-Beer Law. At least fifty of these so-called average signal values were taken from the data logging unit. The arithmetic average of these readings was then found and transformed into a film thickness. As in the case of the integrated signal recorded by the data logging unit a more precise average film thickness value would have been obtained if each of the fifty or so readings was transformed into a film thickness before the mean was found. However, errors involved in averaging the signals from the data logger before finding the film thicknesses have been found to be insignificant, that is they are less than 1%.

When helical waves were present on the cup, see Photograph 5, the volumetric flowrate through these waves became important. With reference to the photographs it can be seen that the large ligament has been formed as a direct result of the helical wave on the cup. On either side of this wave there appear to be regions of relatively smooth film flow. Without detailed information regarding the volumetric flowrate through such waves their effect on the relatively smooth flow regions cannot be predicted. If, however, these waves are regarded as areas operating at some known step change in volumetric flowrate and hence thickness, their effect can be easily quantified. A simple calculation shows that this error is relatively small.

The amount of scatter in the experimental results shown in Graph 1 and consequently Graph 2 is of interest. It is possible that these average film thickness results contain a high degree of inaccuracy inherent in the method used for their determination. This should not be the case as this technique is capable of high accuracy although the light extinction technique is normally used in precision instruments such as spectrophotometers. Furthermore the control test, that of base-line stability proved excellent, the base-line drift was in the order of $\frac{1}{2}\%$ or less. This indicates that the recorded scatter was not solely a function of experimental error.

A number of explanations can be put forward to account for this scatter. The first and most obvious of these is the modified Nusselt theory is only applicable for smooth unidirectional flow on an infinite conical cup. Wave distributions would violate the initial assumptions on which this theory is based. If, however, the standard

deviations of these distributions were found to be relatively small there remains the possibility that the presence of these waves would not violate the theoretical assumptions to such an extent that the general theory should be discarded. The second point that needs to be emphasised is the modified Nusselt theory is only applicable to an infinite system, one in which the liquid continues to 'thin' with increasing radius. No account is made in this theory of the liquid "capacitance" at the torus. Intuitively one may argue that for modest volumetric flowrates per unit length of periphery the effect of the torus will be to retard the incoming liquid. The overall effect being a thickening of the film in the vicinity of the torus. Whether this thickening could be traced back from the periphery of the cup to the weir that distributes the liquid onto the cup is highly debatable. Certainly it is a possibility. Some justification for this proposed thickening exists. If Fig 2.3 is examined it can be seen that for small distances from the lip of the cup the magnitude of the surface meridional velocity component is extremely small. Indeed if these values are extrapolated to the lip itself the estimated surface meridional velocity would be zero. Obviously this is unlikely as the system was operated at constant volumetric flowrate. The most plausible explanation of this result is the method of estimating the surface velocity was not sufficiently accurate to detect these low velocities. None the less in the vicinity of the lip the surface meridional velocity has been found to be much lower than the theoretical value at the prevailing operating conditions. These experiments were conducted in the transient direct-drop/ligament régime, for the sheet régime the same conditions of hold-up would not apply presumably.

Considering the environment in which the film thicknesses were measured, that is one containing a large number of airborne droplets, there must have been a real risk of droplets of the dyed liquid impinging on the light cell and artificially affecting the results obtained. Little could be done about this possibility as by necessity the air gap between the moving film and the light cell had to be maintained so as not to affect the film flow itself. Observation of the light cell showed little if any contamination. As a result it was concluded that this risk of droplet impaction on to the light cell surface although real, could be eliminated by careful inspection of the probe surface after each experimental run.

6.2. The Continuous Film Thickness Results

After being satisfied that the optical technique accurately recorded the time and position averaged film thicknesses it was then necessary to determine whether the same apparatus could be used to monitor continuous film thicknesses. It soon became evident that the 24 watt light bulb was inadequate as an image of the filament was produced. This image was approximately 4 mm long and 1 mm wide and so it was relatively large compared with the waves which it was supposed to scan. A laser was chosen as the replacement light source, see Photograph 2, this laser produced a parallel light beam of approximately 1 mm diameter. Under the no liquid flow condition the output of the light cell, using the laser as the light source, was found to be extremely stable.

An option was available on how to record the signal from the light cell. It was decided to store this signal using the facilities of an ultra-violet oscillograph as this enabled a rapid qualitative assessment of the results to be made. To test the accuracy of the output as stored on the U.V. recorder some idea of the attenuation of the galvanometers was necessary. To this end a small strip of black adhesive tape was stuck on the underside of the conical section of one of the perspex discs such that it interrupted the light beam as it passed by each revolution. The output on the U.V. recorder was then compared with the width of the signal expected from a knowledge of the relative sizes of the strip and the effective diameter of the cup. It was found that the attenuation was insignificant, however, it was noted that the strip of adhesive tape gave an excellent indication of the speed of rotation of the disc and so it was retained for this purpose. Some preliminary work using the U.V. recorder indicated the presence of small waves immediately preceding the main waves. These waves had previously been noted when a photographic study of the wave formations had been undertaken. The detection of these waves was therefore considered to be further qualitative proof that attenuation was not a serious problem.

The continuous film thickness results have been plotted and found to fit the log-normal probability distribution law[100]. These results can be seen in Graphs 3-7 whilst the data is shown in Table 9. As the instantaneous film thickness results closely fit the log-normal probability distribution law it follows that there must be negligible periodicity in the region where these results were obtained. This is compatible with the results of Telles and Dukler[101] and Hewitt et al[102]. Telles and Dukler found that for all but the smallest Reynolds numbers

the film is random in nature whilst the photographs of Hewitt et al showed that no two waves are alike in the region furthest from the entrance of an inclined plane. Although these authors conducted their experiments on inclined planes their results would appear to be applicable to the spinning cup case. Indeed at the distributor of the spinning cup periodic waves were observed under stroboscopic lighting at small flowrates thus providing additional confirmation that there is a similarity between a spinning disc and an inclined plane. A further test was made to ensure that there was no periodic wave motion over a large proportion of the disc. The signal from the silicon light cell was fed after amplification into a F.M. tape recorder. Sufficient data was collected in order that a Fourier analysis could be made. This was done automatically using aHewlett Packard Fourier Analyser. As there were no dominant peaks it was concluded that the waves were in fact randomly distributed.

From Graphs 3-7 it is possible to determine the arithmetic mean and standard deviations of these continuous film thickness distributions. The mean values can be used to determine the modified Nusselt parameter, the result of which can be seen in Graph 8. The results shown in this graph are consistent with those obtained using the 24 watt light bulb, that is the time and position averaged film thickness results. Consequently, it was felt that these continuous film thickness results were accurate, within the limits of experimental error.

The second parameter which together with the mean value completely characterises the distribution is the standard deviation. The standard deviation for a log normal probability distribution is expressed as the

logarithm of the ratio of the film thicknesses at either the 50% and 16% or the 84% and 50% probabilities respectively. When this ratio is plotted against the modified film thickness parameter

, the resulting , plot yields a straight line relationship, see Graph 9. Qualitatively it can be seen from this graph that for a given speed of rotation the ratio defined above decreases with increasing liquid throughput. Thus the film becomes more smooth as this group increases. As only one liquid was used during this investigation the effect of viscosity was not established. Intuitively one would imagine that an increase in viscosity would decrease the amount of waviness on the cup. However this effect needs to be investigated more fully.

6.3. The Drop Size Distribution Results

The drop size distribution results which were measured using the charged wire drop sizer can be seen in Graphs 11-25, Tables 11-25. These results fit the log-normal probability distribution law quite closely, except at the extreme ends of the distributions. Possibly there is a case for using the Upper Limit Distribution[103] so that the coarse end of the distribution could be defined more closely. However for most purposes the log-normal probability distribution law adequately defines the spray using two values only, the arithmetic mean and the standard deviation. If the Upper Limit distribution law was used three values would have to be defined to completely characterise the spray. In addition, to the arithmetic mean and the standard deviation, the maximum drop size would also be required.

At low flowrates or high speeds of rotation the spray distribution becomes bimodal (c.f. the Direct Drop Régime). In fact the transition from direct drop to ligament formation as predicted by Figure 3.5 is not clearly defined, rather this transition seems to be diffuse. All the distributions presented in this work should correspond to the ligament régime of atomization, however photographic evidence indicates that direct-drop formation occurs concurrently with ligament formation - Photograph 4.

The transition from a bimodal distribution to a continuous distribution has been plotted in Graph 26. All the values in this graph were obtained using the 14.8 cm cup at 9.6 r.p.s. It can be seen that the ratio of the means (that is the satellite to main drops) increases with increasing volumetric flowrate until the distribution becomes continuous. At no time does the arithmetic mean of the main drops approach a constant value. This raises an interesting point. The operating equations 3.5-1-4 predict the drop size at low volumetric flowrates when the mode of atomization is supposedly in the Direct Drop régime. No mention of the volumetric flowrate is given. This unwittingly implies that so long as the flowrates are small its effect on the atomization is also small. However, most clearly this is not always the case (see Graph 27). Indeed this graph indicates the arithmetic mean drop size decreases with increasing volumetric flowrate. This observation qualitatively substantiates the theoretical work outlined in Appendix 6-1. Of course, for a spinning cup atomizer operating in the Direct Drop régime the number of atomization sites on the torus is not constant, nor is the single droplet formation a steady-state process.

This being so the volumetric flowrate into the stem of the embroyonic droplets becomes indeterminant analytically. If this equation could be applied to ligament formation the volumetric flowrate term could then be equated to the overall volumetric flowrate and the spacing between the ligaments. Unfortunately this equation is only applicable to single drop formation, see Figure 6.1.

The charged wire drop sizer was calibrated using one of these four operating equations. Obviously as the volumetric flowrate has been shown to affect the arithmetic mean drop size at otherwise constant operating conditions then the credibility of using the cup in the Direct Drop regime for primary calibration must be questioned. Quantitative measurements taken from a high speed cine film (of which Photograph 3 is an example) indicate that the operating equation was accurate within $\pm$ 10%. This however may have been entirely fortuitous. None the less the results describe the transitions adequately even if there is some doubt as to the precise numerical value of these measurements.

6.4. Conclusions

Neither the modified Nusselt theory nor the Nikolaev/Bruin theories totally describe the smooth film flow of a liquid on a rotating cup except when the dimensionless film thickness parameter (I_{max} or $\delta^+ = \delta_{max}\left(\frac{w}{v}\right)^{\frac{1}{2}}$) is extremely small. This infers that deviations from the Nusselt, and similar models, occur when the dimensionless thickness parameter can no longer be considered small. This has been verified experimentally using the model described in Section 5.7, namely the three dimensional solution of a modified form of the Navier Stokes equation. It can be seen that the experimental data presented in Graph 1 lies between the operating band used during these investigations. This indicates that the three dimensional solution more nearly represents the fluid motion on a spinning cup, even

though in practice the results were obtained when wavy flow was present.

The continuous film thickness distributions were found to fit the log normal probability law quite closely. This, coupled with the fact that no dominant peaks were found when a Fourier analysis was made of the film thickness distribution leads to the conclusion that there is no periodic tendency when the film thickness is investigated at some distance from the liquid distributor.

The standard deviations of the continuous film thickness distribution decrease with increase in modified Nusselt film thickness parameter. The conclusion reached from this evidence is that as this thickness parameter increases the film will become smoother until eventually the standard deviation approaches zero. This appears to occur in the regime where there is transition from ligament to sheet formation.

The drop size distribution results were also found to fit the log normal probability law when the distribution was continuous. Bimodal distributions were also found and it would seem from the scant evidence available that the continuous distribution was only obtained once the mode of atomisation was entirely that of ligament formation.

The standard deviations obtained from the drop size distribution data indicate that as the volumetric flowrate of the liquid to be atomized increases under otherwise constant conditions, the standard deviation of the size distribution also increases even though the d_{50} drop size remains essentially constant. Consequently as the standard deviation of the drop size distribution increases whilst the standard deviation of the film thickness distribution decreases it must be concluded that there is no direct correlation between the impaction of the waves into the liquid torus and the spread in the drop size distribution.

6.5 Suggestions for Further Work

1. The influence of viscosity on the amount of waviness on the liquid film surface should be investigated.
2. The apparent periodicity of the surface waves, observed visually using stroboscopic lighting, in the region of the weir distributor should be examined to see if indeed these waves are periodic.
3. An attempt should be made to find the steady state solution of the equations of motion. The most promising approaches would seem to be that of solving the equations as outlined in Chapter 5 (Sections 5, 6, 7). Hopefully small perturbations might then be introduced into these solutions in order that a periodic solution might be found.
4. Using correlation techniques the waviness in the vicinity of the lip of the cup should be monitored along with the signal from the pulse height analyser, that is the signal due to the spray, thereby determining whether there is any direct correlation between these two events.
5. The approach, as outlined in Appendix 6-1, should be considered more deeply as this might well explain what is happening in the direct drop regime.
6. The transition from the bimodal to the continuous distribution should be quantified by observing this occurence at other speeds of rotation and also by using different discs.

Appendix 6-1

For single droplet formation, that is where there is no jet formation, the mechanism of drop formation may be considered using the following simple model. Consider the forces acting on the liquid torus. These may be listed as follows:

1. force due to the addition of mass into the droplet
2. force due to the excess pressure
3. force due to surface tension
4. centrifugal force due to the cup's rotation.

Applying Newton's second law of motion (see Fig 6-1) the rate of change of momentum may be equated as follows:

$$\frac{d(mv)}{dt} = v_0\frac{dm}{dt} + \frac{mdv}{dt} - \frac{\pi d_1^2}{4}(p_i - p) - \pi d_2 \gamma$$

It has been shown[104, 105] that:

$$\frac{d(mv)}{dt} - v_0\frac{dm}{dt} = -4q^2\rho_L\left[1 - \frac{1}{12}\frac{d_2^2}{d_1^2}\right]$$

and $$\frac{mdv}{dt} = \frac{\pi d_1^3}{6}\rho_L \omega^2 R$$

Hence the diameter of the resultant droplet may be found from

$$d_1^3 = \frac{1}{\pi^2 d_2^2 \rho_L \omega^2 R}\left\{\pi^2 d_2^2 \gamma + \pi^2 d_2^2 \frac{\gamma}{d_1} - 4q^2\rho_L\left[1 - \frac{1}{12}\frac{d_2^2}{d_1^2}\right]\right\}$$

where q = volumetric flowrate into each undetached droplet

d_1 = diameter of the droplet

d_2 = diameter of the stem

v_o = velocity of the incoming mass into the undetached droplet

p_i = internal pressure of droplet

p = external pressure of continuous phase.

For the case where the volumetric flowrate term is extremely small and the γ/d_1 term is large compared with γ, then the operating equation proves to be similar to equations 3.5 1-4 namely:

$$d_1 = \frac{1}{2\pi n}\sqrt{\frac{\gamma}{\rho_L R}}$$

FIG. 6.1.

ENLARGED SCHEMATIC VIEW OF A DROPLET IN THE DETACHMENT STAGE OF GROWTH.

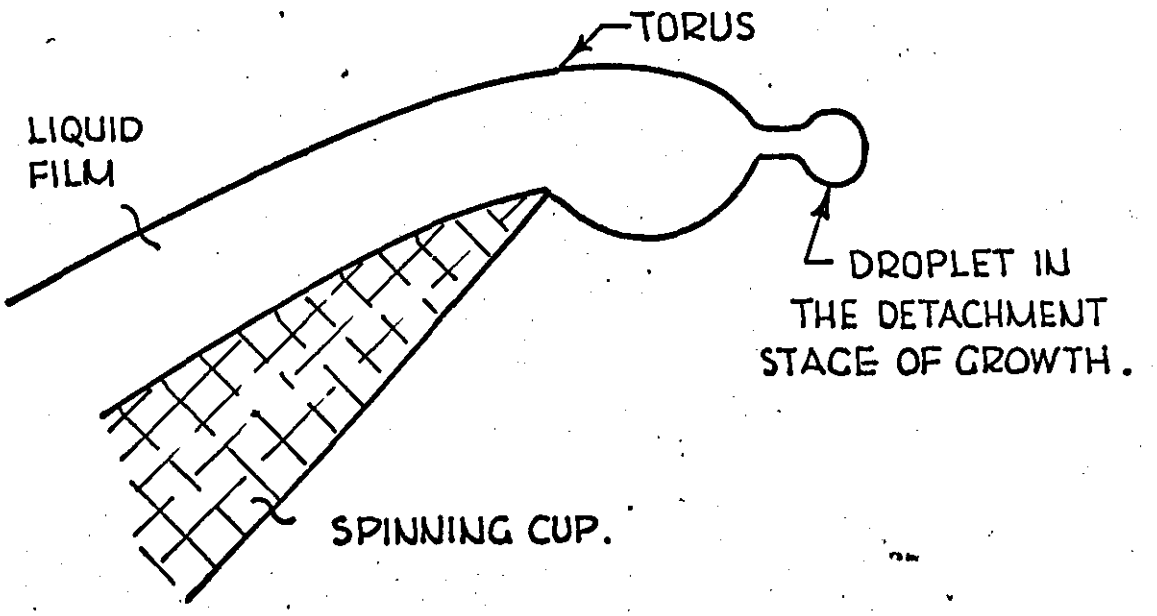

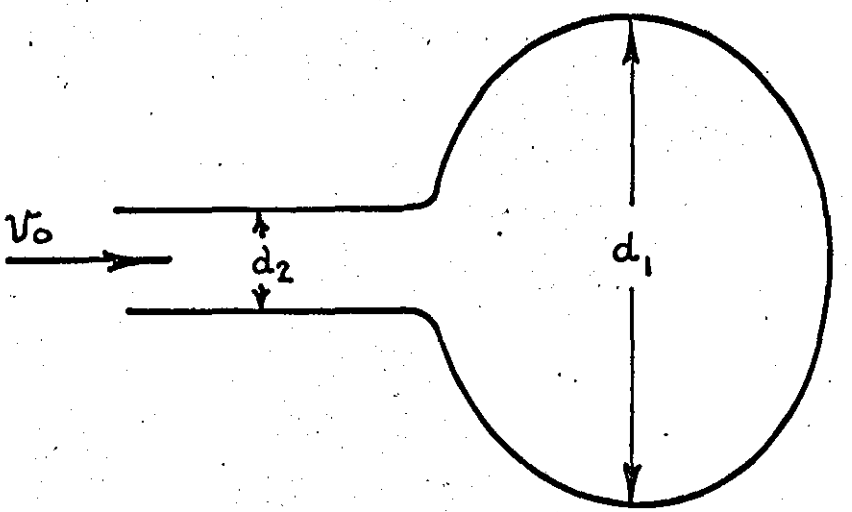

NOMENCLATURE

Symbol		Units	Eqn.
a	area of capacitor	m^2	2.1.1.
a	extent of liquid from the lip of the cup	cm	3.6.4.
a	a constant		3.5.12.
a	a constant		5.3.9.
A	a constant		5.7.7.
b	the reservoir depth		
b	a constant		3.5.12.
b	a constant		5.3.9.
B	a constant		5.7.7.
C	a constant		3.5.12.
C	the capacitance of a parallel plate capacitor	farads	2.1.1.
C	constant (subscript 1,2,3,4,5)		3.2.2-3
d	a constant		3.5.12.
d	droplet diameter	cm.	3.5.1.
D	the spinning disc diameter	cm.	3.1.1.
D	the hydraulic diameter	cm.	3.1.10.
f	the dimensionless velocity (subscript ℓ, $\emptyset$, δ)		3.2.2-3-6
f(θ)	a function of θ		5.5.1.
F	a function of f(θ)		5.5.3.
F	a function of θ		5.7.1.

Symbol		Units	Eqn.
g	gravitational force constant	$cm.sec^{-2}$	
G	a function of θ		5.7.1.
h	metrical coefficient (subscripts 1,2,3 and r, θ, ϕ)		5.1.3.
H	a function of θ		5.7.1.
i	unit vector (subscripts 1,2,3 and r,θ,ϕ)		5.1.2.
I	Bessel Function (subscripts 1 and 0)		
I	the dimensionless film thickness		5.7.5.
k	wave number		3.6.13.
K	a constant		3.5.12.
l	the length from the apex of the cone to any point on the cone		3.2.6.
L	the dimensionless length from the apex of the cone to any point on the cone		3.2.6.
m	the mass of a droplet		Appendix 6-1
n	the rotational speed	sec^{-1}	3.5.1.
N_T^*	the modified Nusselt film thickness parameter		

Symbol		Units	Eqn.
p	pressure	dynes/cm^2	3.1.1.
p	dimensionless pressure		3.2.14.
q	the Rosin Rammler distribution constant		3.5.8.
q	growth rate		3.7.1.
q	invariant co-ordinate (subscript 1,2,3)		5.2.6.
Q	volumetric flowrate	cc/sec.	3.1.10.
r	radial co-ordinate		5.2.8.
r	the radius from the centreline of the cone to any point normal to that centreline		3.2.6.
r	the radius of a droplet (subscript d)		3.5.15
R	the radius of a spinning disc	cm.	3.5.13.
R	the dimensionless radius		3.2.3.
R	the Rosin Rammler distribution variable		3.5.8.
t	the distance between the plates of a parallel plate capacitor	m	2.1.1.
t	time	sec.	3.1.1.
t	a variable equivalent to cos. θ		5.3.9.
T	the mass flowrate per unit length of periphery	gm/(cm-sec)	3.5.6.
T	surface tension	dynes/cm^2	3.7.3.
u	velocity	cm/sec	3.1.3.
U	dimensionless velocity		3.2.11.

Symbol		Units	Eqn.
v	velocity	cm/sec	3.1.1.
V	dimensionless velocity		3.2.12
w	angular velocity	radians/ sec	3.2.6.
W	dimensionless velocity		3.2.13.
W	angular velocity	radians/ sec.	3.2.1.
x	the displacement due to the inclination of a parallel plate capacitor	m	2.1.3
y	the thickness of a water layer between the plates of a capacitor	m	2.1.4.
y	rectangular co-ordinate		3.1.3.
z	rectangular co-ordinate		3.1.3.
z	the number of ligaments from a spinning disc.		3.6.1.

Symbol		Units	Eqn.
α	the half cup angle	radians	3.2.3.
α	a constant		5.7.7.
β	the dimensionless film thickness		3.2.2.
γ	surface tension	dynes/cm^2	3.6.4.
δ	the film thickness	cm	3.1.6.
ϵ	amplitude of a disturbance		3.7.1.
ζ	the disturbance function at the free surface of the liquid torus		3.6.10.
θ	angle that inclined plane subtends with the horizontal	radians	3.1.3.
θ	spherical co-ordinate		
λ	wavelength, Rayleigh instability theory		3.7.1.
μ	viscosity		
ν	kinematic viscosity	cm^2/sec	3.1.1.
ρ	density	gm/cc	3.1.1.
σ	surface tension	dynes/cm^2	3.3.3.
ϕ	surface deformation function		3.1.15.
ϕ	azimuthal co-ordinate		
ϕ	the scalar in the potential flow equation		5.6.1.
ψ	stream function		5.2.4.
Ω	gravitational force scalar		

REFERENCES

1. Hinze, J.O. and Milborn, H. J. Applied Mech., 17, 145 (1950)
2. Mukhutdinov, R.Kh., Cand. Dissertation (Kazan, 1958)
3. Espig, H. and Hoyle, R., J. Fluid Mech., 22, 4, 671, (1965)
4. Kapitsa, P.L., J. Exp. Theor. Phys. U.S.S.R., 1, (1948)
5. Kapitsa, P.L., and Kapitsa, S.P., Zh. Eksp. Teor. Fiz., 19, 105, (1949)
6. Nusselt, W., V.D.I. 60, 549, 569, (1916)
7. Happle, J., and Brenner, H. Low Reynolds Number Hydrodynamics, Prentice-Hall (1966)
8. Hopf, L., Ann.Physik 32, 777, (1910)
9. Benjamin, T.B., J. Fluid Mech. 2, 554, (1957)
10. Yih, C.S. Proc. 2nd U.S. Natl. Congr. Applied Mech. (1954), 623, American Society of Mechanical Engineers, New York (1955)
11. Levich, V.G., "Physico-Chemical Hydrodynamics" Prentice-Hall, Englewood Cliffs, New Jersey (1962)
12. Rushton, E., M.Sc. Thesis, Univ. Manchester (1968)
13. Rushton, E., and Davis, G.A., A.I.Ch.E. Journal, 17, 3, 670,(1971)
14. Byatt-Smith, J.G.B., A.I.Ch.E. Journal, 17, 3, 557, (1971)
15. Portalski, S., and Clegg, A.J., Chem.Eng.Sci. 26, 773, (1971)
16. Clegg, A.J., Ph.D. Thesis, Surrey University, (1969)
17. Espig, Hans, Ph.D. Thesis, University of London (1964)
18. Beardall, L.R., Ph.D. Thesis, Loughborough University (1968)
19. Emslie, A.G., Bonner, F.T. and Peck, L.G., J.App. Physics 29, 5, 858, (1958)
20. Nikolaev, V.S., Vachagin, K.D. and Baryshev, Yu N., Int.Chem. Eng., 7, 4, 595, (1967)
21. Bruin, S., Chem.Eng.Sci., 24, 1647, (1969)
22. Hege, H., Chemie-Ing. Techn 36, 1, 52, (1964)
23. Voinov, A.K., and Khapilova, N.S. P.M.T.F. Zh. Prikl. Mekhan Tekh. Fiz. 2, 107, (1967)

24. Jaymond, M., Chem. Eng. Sci., 14, 126, (1961)

25. Kirkbride, C.G. Trans. Am. Inst. Chem. Engrs. 30, 170, (1937)

26. Jeffreys, H., Phil. Mag. 49, 793, (1925)

27. Hanratty, T.J. and Engen, J.M. A.I.Ch.E.J. 3, 299, (1957)

28. Reinus, E., Trans. Roy. Inst. Technol. Stokholm, 179, (1961)

29. Binnie, A.M., J.Fluid Mech. 5, 561, (1959)

30. Bird, R.B., Stewart, W.E. and Lightfoot, E.N. "Transport Phenomena" Wiley, New York, (1960)

31. Glasstone, S. "Textbook of Physical Chemistry" 2nd Edn. 481, Macmillan (1947)

32. Dukler, A.E., and Bergelin, O.P., Chem.Eng.Progr. 48, 557, (1952)

33. Hewitt, G.F., King, R.D. and Lovegrove, P.C. At.Energy.Res.Est. Harwell, A.E.R.E.-R 3921, (1962)

34. Portalski, S. "The mechanism of flow in wetted wall columns" Ph.D. Thesis, Univ. London, (1960).

35. Hewitt, G.F., and Lovegrove, P.C. At.Energy.Res.Est. Harwell A.E.R.E.-R. 3953, (1962)

36. Jackson, M.L., A.I.Ch.E.J., 1, 231, (1955)

37. Fraser, R.P., Dombrowski, N., and Routley, J.H. Chem.Eng.Sci. 18, 315, (1963)

38. Philips, O.M., J.Fluid Mech. 7, 340, (1960)

39. Boshoff, W.H., Proc. Inst. Mech. Engrs. A. 166, 443, (1952)

40. Walton, W.H. and Prewett, W.C., Proc. Phys. Soc., 62, 341, (1949)

41. Pattison, J.R. and Aldridge, J.D. Engineer, 203, 514, (1957)

42. Bär, P., Doctorate Dissertation, Technical College, Karlsruhe, Germany (1935)

43. Maraszew, A., Engineering, 166, 316, (1948)

44. Fraser, R.P., Dombrowski, N, and Routley, J.H., Chem.Eng.Sci. 18, 339, (1963).

45. Triebnigg, H., "Der Einblase und Einspritzvorgang bei Diesel Maschinen" J.Springer, Wien, Germany (1925)

46. Ryley, D.J., Br. J. Appl. Phys. 10, 180, (1959)

47. Rosin, P.O., and Rammler, E. J. Inst. Fuel, 7, 29, (1933-4)

48. Friedman, S.J., Gluckert, F.A., Marshall, W.R., Chem. Eng. Prog. 48, 181, (1952)

49. May, K.R., J.Sci. Instrum., 22, 187 (1945)

50. Baryshev, Yu.N., Vachagin, K.D., and Nikolaev, V.S., Int. Chem. Eng. 9, 4, 579, (1969)

51. Dunsky, V.F., Nikitin, N.V., and Tonkacheeva, N.F., Inzh-Fiz. Zh., 20, 5, (1951)

52. Reusova, L.A., and Lykov, M.V., Inzh-Fiz. Zh., 19, 5, 920, (1970)

53. Straus, R., Ph.D. dissertation, London Univ. (1950)

54. Dunskii, V., and Nikitin, N.V., Inzh;Fiz. Zh., No.9, 54, (1965)

55. Hidy, G.M., and Brock, J.R., The Dynamics of Aerocolloidal Systems, Pergammon Press, (1970)

56. Fraser, R.P., Dombrowski, N., Routley, J.H. Chem. Engng. Sci. 18, 323, (1963)

57. Eisenklam, P. Chem. Eng. Sci. 19, 693, (1964)

58. Taylor, G.I., Proc. Roy. Soc. 201A, 192, (1950)

59. Ohnesorge, W., Z. angew. Math. U. Mech., 16, 355, (1936)

60. Haenlein, A., Forsch. Gebiete Ingenieurw., Forschungsheft, 2, 139, (1931)

61. Marshall, W.R., Jnr. Chem. Eng. Prog. Nomograph (1954)

62. Rayleigh, Lord The Theory of Sound, Vol.II (2nd Ed.) New York:Dover (1945)

63. Plateau, "Statiques des Liquides" (1873)

64. Chandrasakhar, S., Hydrodynamic and Hydromagnetic Stability. Oxford:Clarendon Press (1961)

65. Yuen, M.C., J. Fluid Mech., 33, 151, (1968)

66. Goedde, E.F. and Yuen, M.C. J. Fluid Mech., 40, 3, 495, (1970)

67. Donnelly, R.J. and Glaberson, W., Proc. Roy. Soc. Lond. A.290, 547-556, (1966)

68. Rutland, D.F., and Jameson, G.J., Chem. Eng. Sci., 25, 1689 and 1301, (1970)

69. Rutland, D.F., and Jameson, G.J., J. Fluid. Mech., 46, 2, 267 (1971)

70. Parkin, S. Private communication

71. Wells, F. Amer. J. Hyg., 20, 611, (1934)

72. Fraser, R.P., and Eisenklam, P. Trans. Inst. Chem. Eng., 34, 301, (1956)

73. Tate, R.W., and Marshall, W.R. Jnr. Chem. Eng. Prog. 49, 169, 226, (1953)

74. Darnell, W.H. "Centrifugal Atomisation" Ph.D. Thesis, Univ. of Wisconsin (1953)

75. Tarat, E.Ya., and Fialkov, Yu.G. Int. Chem. Eng. 10, 4, 604, (1970)

76. Dombrowski, N., and Hooper, P.C. Chem. Eng. Sci. 17, 291, (1962)

77. Fraser, R.P., Eisenklam, P., Dombrowski, N., and Hasson, D. A.I.Ch.E.J. 8, 672, (1962)

78. York, J.L., and Stubbs, H.E., T.A.S.M.E., 1157-1162, (1952)

79. Kim, K.Y., and Marshall, W.R. Jnr. A.I.Ch.E.J., 17, 3, 575, (1971)

80. Hasson, D., and Mizrahi, J. T.I.Ch.E. 39, 415, (1961)

81. Turner, G.M., and Moulton, R.W., Chem. Eng. Prog. 49, 185, (1953)

82. Joyce, J.R., J.Inst. Fuel, 22, 150, (1949)

83. Nelson, P.A., "Drop-Size Distribution from Centrifugal Spray Nozzle" Ph.D. Thesis, North-Western University, (1958)

84. Longwell, J.P., "Fuel Oil Atomisation" D.Sc. Thesis. Mass. Inst. Tech., (1943)

85. McIrvine, J.D., "Atomisation of Viscous Liquid with Swirl Pressure Nozzles" Ph.D. Thesis, Univ. of Wisconsin (1957).

86. Gretzinger, J., Marshall, W.R. Jnr. A.I.Ch.E.J. 7, 312, (1961)

87. Giffen, E., and Muraszuer, A. M.I.R.A. Report No.4, "The Measurement of Atomisation in Fuel Sprays" (1948)

88. Dorman, R.G., Brit. J. Appl. Phys., 3, 189, (1952)

89. Radcliffe, A. Proc. Inst. Mech. Engrs., 169, 93, (1955)

90. Sigma Drop Size Analyser, Sigma Electronics Ltd., Surrey, England

91. Sauter, T. Forsch. Gebiete. Ingenieurw, 279, 278, (1926)

92. Gardiner, J.A., Inst. Practice, 18, 353, (1964)

93. Ryley, D.J., and Wood, M.R., J. Sci. Instrum., 40, 303, (1963)

94. Steen, W.M. and Chatterjee, A., J. Phys. E:Scientific Instruments, 3, 1020, (1970)

95. Hawkins and Jordan, J.A.C.S., 52, 1751, (1930)

96. Whitaker, D.F., "Introduction to Fluid Mechanics", Prentice-Hall, (1970)

97. Bland, D.R., Solutions of Laplace's Equation, Routledge and Kegan Paul (1961)

98. Karman, T., Z. angew, Math. i. Mech. 1, 244 (1921)

99. Cochran, Proc. Cambridge. Phil. Soc. 30, 365, (1934)

100. Herdan, Small Particles Statistics, 2nd Ed., Butterworths, (1960)

101. Telles, A.S., and Dukler, A.E., Ind. Eng. Chem. Fund., 9, 3, 412, (1970)

102. Hewitt, G.F., Lacey, P.M.C. and Nichols, B., Proc. Symposium on Two-Phase Flow, 2, Exeter, England, (1965)

103. Mugele, R.A., and Evans, H.D., Ind. Eng. Chem. 43, 6, 1317, (1951)

104. Hayes, W.B., Hardy, B.W., and Holland, C.D., A.I.Ch.E.J. 5, 319, (1959)

105. Kumar, R., Kuloor, N.R., Advances in Chemical Engineering 8, 305, Academic Press (1970)

106. Oyama, Y., and Endou, K. Chem. Eng. (Tokyo) 17, 256-260, (1953)

107. Taylor, G.I., Quart. Journ. Mech. and Applied Math., III, 2 (1950).

LIST OF FIGURES

LIST OF PHOTOGRAPHS

EXPERIMENTAL RESULTS

LIST OF TABLES

LIST OF GRAPHS

TABLE 1

D = 11.9 cm. α = 1.073 rads ν = 1.04 cP ρ = 1.0 gm/cc

REYNOLD'S NUMBER	SPEED OF ROTATION R.P.S.	FILM THICKNESS CM.	MODIFIED NUSSELT PARAMETER	BRUIN'S THICKNESS PARAMETER	BRUIN'S INTEGRAL PARAMETER
155	6.9	.0107	4.74	.704	.322
	8.1	.0098	4.83	.70	.3
	8.9	.0092	4.84	.675	.276
	9.9	.0082	4.66	.645	.267
	11.0	.0078	4.77	.645	.248
	12.1	.0072	4.67	.629	.237
212	6.9	.0149	6.60	.98	.44
	8.1	.0129	6.40	.92	.41
	8.9	.0120	6.35	.91	.38
	9.9	.0111	6.32	.88	.37
	11.0	.0104	6.35	.86	.34
	12.1	.0095	6.20	.83	.32
397	6.9	.0167	7.40	1.1	.825
	8.1	.0144	7.15	1.03	.77
	8.9	.0131	6.94	.99	.71
	9.9	.0123	7.00	.97	.68
	11.0	.0113	6.90	.94	.64
	12.1	.0105	6.85	.91	.61

TABLE 2

D = 11.0 cm. α = 1.1 rads ν = 1.01 cP ρ = 1.0 gm/cc

REYNOLD'S NUMBER	SPEED OF ROTATION R.P.S.	FILM THICKNESS CM.	MODIFIED NUSSELT PARAMETER	BRUIN'S THICKNESS PARAMETER	BRUIN'S INTEGRAL PARAMETER
268	6.9	.0134	5.92	.878	1.17
	8.1	.0119	5.87	.845	1.07
	8.9	.0111	5.82	.822	1.01
	9.9	.0099	5.59	.774	.95
	11.0	.0090	5.45	.741	.90
	12.1	.0086	5.59	.746	.86
312	6.9	.0154	6.79	1.01	1.36
	8.1	.0136	6.70	.97	1.24
	8.9	.0127	6.70	.95	1.18
	9.9	.0117	6.63	.92	1.11
	11.0	.0108	6.55	.89	1.05
	12.1	.0100	6.50	.87	1.00
325	6.9	.0154	6.80	1.01	1.41
	8.1	.0139	6.83	.98	1.3
	8.9	.0131	6.90	.95	1.22
	9.9	.0115	6.51	.90	1.15
	11.0	.0108	6.55	.89	1.09
	12.1	.0100	6.45	.86	1.04

TABLE 3

D = 11.0 cm. α = 1.1 rads ν = 1.01 cP ρ = 1.0 gm/cc

REYNOLD'S NUMBER	SPEED OF ROTATION R.P.S.	FILM THICKNESS CM.	MODIFIED NUSSELT PARAMETER	BRUIN'S THICKNESS PARAMETER	BRUIN'S INTEGRAL PARAMETER
363	6.9	.0173	7.65	1.13	1.57
	8.1	.0152	7.50	1.08	1.44
	8.9	.0141	7.41	1.05	1.37
	9.9	.0128	7.21	1.00	1.29
	11.0	.0117	7.12	.97	1.22
	12.1	.0108	7.01	.94	1.16
439	6.9	.0183	8.10	1.20	1.91
	8.1	.0166	8.17	1.18	1.74
	8.9	.0151	7.96	1.12	1.66
	9.9	.0141	7.98	1.11	1.34
	11.0	.0128	7.76	1.06	1.28
	12.1	.0119	7.69	1.03	1.40

TABLE 4

D = 10.0 cm. α = 1.1 rads ν = 1.01 cP ρ = 1.0 gm/cc

REYNOLD'S NUMBER	SPEED OF ROTATION R.P.S.	FILM THICKNESS CM.	MODIFIED NUSSELT PARAMETER	BRUIN'S THICKNESS PARAMETER	BRUIN'S INTEGRAL PARAMETER
325	6.9	.0174	7.4	1.14	1.01
	8.1	.0155	7.36	1.10	0.92
	8.9	.0143	7.25	1.06	0.87
	9.9	.0129	7.04	1.01	0.82
	11.0	.0121	7.09	1.00	0.78
	12.1	.0112	7.00	0.97	0.74
388	6.9	.0192	8.15	1.26	1.25
	8.1	.0174	8.26	1.23	1.14
	8.9	.0163	8.25	1.21	1.08
	9.9	.0152	8.29	1.19	1.02
	11.0	.0139	8.15	1.15	0.96
	12.1	.0130	8.13	1.13	0.91
514	6.9	.0220	9.35	1.44	1.66
	8.1	.0200	9.5	1.42	1.51
	8.9	.0190	9.61	1.41	1.43
	9.9	.0177	9.65	1.39	1.34
	11.0	.0167	9.78	1.38	1.27
	12.1	.0157	9.8	1.37	1.21

TABLE 5

D = 10.0 cm α = 1.1 rads ν = 1.04 cP ρ = 1.0 gm/cc

REYNOLD'S NUMBER	SPEED OF ROTATION R.P.S.	FILM THICKNESS CM.	MODIFIED NUSSELT PARAMETER	BRUIN'S THICKNESS PARAMETER	BRUIN'S INTEGRAL PARAMETER
143	7.8	.0113	5.22	0.73	0.47
	8.6	.0103	5.09	0.72	0.42
	9.6	.0096	5.12	0.70	0.40
	10.5	.0090	5.09	0.69	0.38
	11.4	.0085	5.10	0.69	0.36
	12.1	.0079	5.18	0.68	0.34
184	7.8	.0115	5.31	0.74	0.60
	8.6	.0102	5.03	0.71	0.55
	9.6	.0095	5.08	0.70	0.52
	10.5	.0090	5.09	0.70	0.49
	11.4	.0084	5.03	0.69	0.46
	12.1	.0078	5.09	0.67	0.44
285	7.8	.0126	5.85	0.81	0.94
	8.6	.0114	5.63	0.80	0.85
	9.6	.0108	5.76	0.79	0.80
	10.5	.0098	5.54	0.76	0.76
	11.4	.0092	5.52	0.75	0.72
	12.1	.0086	5.61	0.74	0.68

TABLE 6

D = 10.0 cm α = 1.1 rads ν = 1.03 cP ρ = 1.0 gm/cc

REYNOLD'S NUMBER	SPEED OF ROTATION R.P.S.	FILM THICKNESS CM.	MODIFIED NUSSELT PARAMETER	BRUIN'S THICKNESS PARAMETER	BRUIN'S INTEGRAL PARAMETER
138	7.8	.0100	4.21	.69	.42
	8.6	.0092	4.32	.67	.39
	9.6	.0087	4.37	.66	.37
	10.5	.0080	4.32	.64	.35
	11.4	.0075	4.35	.62	.34
	12.1	.0069	4.28	.61	.32
227	7.8	.0124	5.21	.86	.69
	8.6	.0114	5.36	.83	.65
	9.6	.0105	5.28	.80	.61
	10.5	.0098	5.29	.78	.58
	11.4	.0092	5.34	.77	.55
	12.1	.0085	5.27	.75	.52
288	7.8	.0137	5.75	.95	.87
	8.6	.0125	5.88	.91	.82
	9.6	.0115	5.78	.88	.77
	10.5	.0105	5.68	.84	.74
	11.4	.0099	5.75	.83	.71
	12.1	.0091	5.64	.81	.66
308	7.8	.0139	5.85	.96	.93
	8.6	.0127	5.96	.92	.88
	9.6	.0123	6.19	.94	.83
	10.5	.0112	6.05	.90	.79
	11.4	.0104	6.04	.87	.76
	12.1	.0099	6.14	.87	.71

TABLE 7

D = 14.0 cm. α = 1.1 rads ν = 1.05 cP ρ = 1.0 gm/cc

REYNOLD'S NUMBER	SPEED OF ROTATION R.P.S.	FILM THICKNESS CM.	MODIFIED NUSSELT PARAMETER	BRUIN'S THICKNESS PARAMETER	BRUIN'S INTEGRAL PARAMETER
65	7.8	.0079	4.02	.54	.14
	8.6	.0076	4.10	.54	.13
	9.6	.0073	4.28	.55	.13
	10.5	.0070	4.23	.55	.12
	11.4	.0068	4.44	.56	.12
	12.1	.0063	4.38	.55	.11
77	7.8	.0077	3.92	.53	.17
	8.6	.0073	3.97	.52	.16
	9.6	.0073	4.28	.55	.15
	10.5	.0066	4.00	.52	.14
	11.4	.0062	4.09	.51	.14
	12.1	.0061	4.24	.54	.13
103	7.8	.0091	4.63	.62	.22
	8.6	.0081	4.40	.58	.21
	9.6	.0077	4.51	.58	.20
	10.5	.0071	4.30	.56	.19
	11.4	.0066	4.35	.55	.18
	12.1	.0062	4.27	.54	.17
159	7.8	.0100	5.09	.68	.34
	8.6	.0091	4.95	.65	.33
	9.6	.0085	4.93	.67	.31
	10.5	.0079	4.78	.63	.29
	11.4	.0074	4.87	.63	.28
	12.1	.0071	4.93	.62	.26

TABLE 8

D = 140 cm. α = 1.1 rads ν = 1.05 cP ρ = 1.0 gm/cc

REYNOLD'S NUMBER	SPEED OF ROTATION R.P.S.	FILM THICKNESS CM.	MODIFIED NUSSELT PARAMETER	BRUIN'S THICKNESS PARAMETER	BRUIN'S INTEGRAL PARAMETER
173	7.8	.0103	5.21	.70	.37
	8.6	.0096	5.22	.69	.36
	9.6	.0088	5.16	.66	.34
	10.5	.0083	5.03	.66	.32
	11.4	.0076	5.01	.63	.31
	12.1	.0073	5.07	.64	.29
256	7.8	.0128	6.52	.88	.55
	8.6	.0120	6.53	.86	.53
	9.6	.0113	6.61	.86	.49
	10.5	.0105	6.35	.83	.47
	11.4	.0098	6.46	.81	.45
	12.1	.0093	6.45	.82	.42
292	7.8	.0133	6.75	.91	.61
	8.6	.0123	6.70	.88	.58
	9.6	.0114	6.68	.87	.54
	10.5	.0106	6.41	.84	.52
	11.4	.0097	6.39	.80	.50
	12.1	.0089	6.18	.78	.47

TABLE 9

D = 8.2 cm. α = 1.1 rads ν = 0.996 cP ρ = 1.0 gm/cc

	7.8 R.P.S.		9.1 R.P.S.		12.4 R.P.S.		7.8 R.P.S.		11.5 R.P.S.	
	FILM THICKNESS	CUMULATIVE %	FILM THICKNESS	CUMULATIVE %	FILM THICKNESS	CUMULATIVE %	FILM THICKNESS	CUMULATIVE %	FILM THICKNESS	CUMULATIVE %
	.0272	1.57	.0280	.327	.0166	6.6	.0166	5.45	.0109	9.5
	.0266	2.74	.0276	.65	.0162	14.8	.0161	8.05	.0104	14.2
	.0258	5.3	.0271	1.96	.0157	28.4	.0155	14.6	.0098	21.0
	.0252	12.4	.0261	3.59	.0149	48.8	.0149	25.7	.0093	31.6
	.0241	21.4	.0253	9.8	.0140	66.2	.0144	37.9	.0087	46.7
	.0238	34.1	.0244	16.7	.0134	84.4	.0137	50.4	.0082	61.0
	.0234	55.1	.0234	28.1	.0125	94.2	.0133	61.6	.0076	76.5
	.0222	72.3	.0225	44.7			.0128	71.7		
	.0220	83.7	.0217	65.4			.0123	79.5		
	.0212	93.8	.0209	80.0			.0118	85.7		
	.0207	99.1	.0200	90.8						
	.0200	99.5	.0192	94.1						
REYNOLD'S NUMBER	899		898		890		375		200	

TABLE 10

D = 8.2 cm. α = 1.1 rads ν = 0.996 cP ρ = 1.0 gm/cc.

ARITHMETIC MEAN FILM THICKNESS	STARDARD DEVIATION	MODIFIED NUSSELT PARAMETER	REYNOLD'S NUMBER
.0086	0.0736	5.1	200
.0136	0.0531	5.91	375
.0148	0.0414	8.9	890
.0222	0.0374	10.75	898
.0240	0.0253	10.42	899

TABLE 11 (Graph 11)

FLOWRATE = 1010 gm/min.
SPEED OF ROTATION = 8.6 R.P.S.
DISC DIAMETER = 5.82 inch dia.
SURFACE TENSION = 67.4 dynes/cm.

DROP SIZE μm	CUMULATIVE FRACTION BY NUMBER
640	.0027
740	.1044
840	.3036
920	.4528
990	.5613
1040	.6498
1110	.7246
1150	.7912
1205	.8456
1240	.8844
1300	.9099
1340	.9299
1380	.9449
1420	.9574
1450	.9669

Mean Drop Diameter = 950 μm

$\frac{d_{50}}{d_{16}}$ (main) = 1.25

TABLE 12 (Graph 12)

FLOWRATE = 1140 gm/min.
SPEED OF ROTATION = 9.6 R.P.S.
DISC DIAMETER = 5.82 inch dia.
SURFACE TENSION = 67.4 dynes/cm.

DROP SIZE μm	CUMULATIVE FRACTION BY NUMBER
640	.0062
740	.1498
840	.3604
920	.5147
990	.6337
1040	.7288
1110	.7991
1150	.8491
1205	.8832
1240	.9079
1300	.9254
1340	.9408
1380	.9529
1420	.9628
1450	.9715

Mean Drop Diameter = 920 μm

$\frac{d_{50}}{d_{16}}$ (main) = 1.27

TABLE 13 (Graph 13)

FLOWRATE = 1190 gm/min.
SPEED OF ROTATION = 10.5 R.P.S.
DISC DIAMETER = 5.82 inch dia.
SURFACE TENSION = 67.4 dynes/cm.

DROP SIZE µm	CUMULATIVE FRACTION BY NUMBER
640	.0112
740	.1777
840	.4070
920	.5709
990	.6910
1040	.7710
1110	.8260
1150	.8661
1205	.895
1240	.917
1300	.934
1340	.9486
1380	.9590
1420	.9677
1450	.9747

Mean Drop Diameter = 880 µm

$\frac{d_{50}}{d_{16}}$ (main) = 1.31

TABLE 14 (Graph 14)

FLOWRATE = 440 gm/min
SPEED OF ROTATION = 7.8 R.P.S.
DISC DIAMETER = 5.8ℓinch dia.
SURFACE TENSION = 63.7 dynes/cm.

DROP SIZE µm	CUMULATIVE FRACTION BY NUMBER
635	.052
740	.218
840	.325
910	.382
990	.418
1040	.445
1100	.483
1140	.550
1200	.651
1240	.763
1300	.864
1320	.928

Mean Drop Diameter = 1180 µm

$\frac{d_{50}}{d_{16}}$ (main) = 1.09

Satellite Drop Diameter = 800 µm

$\frac{d_{50}\ \text{(satellite)}}{d_{50}\ \text{(main)}}$ = .68

TABLE 15 (Graph 15)

FLOW RATE = 513 gm/min.
SPEED OF ROTATION = 7.8 R.P.S.
DISC DIAMETER = 5.8½ inch dia.
SURFACE TENSION = 63.7 dynes/cm.

DROP SIZE μm	CUMULATIVE FRACTION BY NUMBER
740	.043
840	.194
910	.318
990	.407
1040	.474
1100	.525
1140	.572
1200	.620
1240	.674
1300	.730
1320	.795
1380	.849
1430	.887

Mean Drop Diameter = 1190 μm

$\frac{d_{50}}{d_{16}}$ (main) = 1.18

Satellite Drop Diameter = 940 μm

$\frac{d_{50}\ \text{(satellite)}}{d_{50}\ \text{(main)}}$ = .79

TABLE 16 (Graph 16)

FLOW RATE = 390 gm/min.
SPEED OF ROTATION = 9.6 R.P.S.
DISC DIAMETER = 5.8½ inch dia.
SURFACE TENSION = 63.7 dynes/cm.

DROP SIZE μm	CUMULATIVE FRACTION BY NUMBER
635	.0005
740	.066
840	.238
910	.337
990	.405
1040	.512
1100	.686
1140	.845
1200	.932

Mean Drop Diameter = 1040 μm

$\frac{d_{50}}{d_{16}}$ (main) = 1.1

Satellite Drop Diameter = 840 μm

$\frac{d_{50}\ \text{(satellite)}}{d_{50}\ \text{(main)}}$ = 0.81

TABLE 17 (Graph 17)

FLOW RATE = 520 gm/min.
SPEED OF ROTATION = 9.6 R.P.S.
DISC DIAMETER = 5.8½inch dia.
SURFACE TENSION = 63.7 dynes/cm.

DROP SIZE μm	CUMULATIVE FRACTION BY NUMBER
635	.012
740	.134
840	.310
910	.435
990	.542
1040	.651
1100	.755
1140	.833
1200	.880

Mean Drop Diameter = 1010 μm

$\frac{d_{50}}{d_{16}}$ (main) = 1.15

Satellite Drop Diameter = 840 μm

$\frac{d_{50}\ \text{(satellite)}}{d_{50}\ \text{(main)}}$ = 0.83

TABLE 18 (Graph 18)

FLOWRATE = 640 gm/min.
SPEED OF ROTATION = 9.6 R.P.S.
DISC DIAMETER ≐ 5.8½inch dia.
SURFACE TENSION = 63.7 dynes/cm.

DROP SIZE μm	CUMULATIVE FRACTION BY NUMBER
635	.001
740	.052
840	.252
910	.409
990	.521
1040	.641
1100	.765
1140	.861
1200	.922

Mean Drop Diameter = 1000 μm

$\frac{d_{50}}{d_{16}}$ (main) = 1.12

Satellite Drop Diameter = 860 μm

$\frac{d_{50}\ \text{(satellite)}}{d_{50}\ \text{(main)}}$ = 0.86

TABLE 19 (Graph 19)

FLOWRATE = 890 gm/min.
SPEED OF ROTATION = 9.6 R.P.S.
DISC DIAMETER = 5.8½ inch dia.
SURFACE TENSION = 63.7 dynes/cm.

DROP SIZE μm	CUMULATIVE FRACTION BY NUMBER
740	.070
840	.278
910	.439
990	.556
1040	.662
1100	.753
1140	.833
1200	.888
1240	.921

Mean Drop Diameter = 980 μm

$\frac{d_{50}}{d_{16}}$ (main) = 1.18

Satellite Drop Diameter = 910 μm

$\frac{d_{50}\ \text{(satellite)}}{d_{50}\ \text{(main)}}$ = 0.93

TABLE 20 (Graph 20)

FLOWRATE = 1240 gm/min.
SPEED OF ROTATION = 9.6 R.P.S.
DISC DIAMETER ≐ 5.8½ inch dia.
SURFACE TENSION = 63.7 dynes/cm.

DROP SIZE μm	CUMULATIVE FRACTION BY NUMBER
740	.089
840	.298
910	.462
990	.582
1040	.676
1100	.751
1140	.810
1200	.852
1240	.883

Mean Drop Diameter = 950 μm

$\frac{d_{50}}{d_{16}}$ (main) = 1.23

TABLE 21 (Graph 21)

FLOWRATE = 1350 gm/min.
SPEED OF ROTATION = 9.6 R.P.S.
DISC DIAMETER = 5.82 inch dia.
SURFACE TENSION = 63.7 dynes/cm.

DROP SIZE μm	CUMULATIVE FRACTION BY NUMBER
740	.098
840	.310
910	.470
990	.584
1040	.674
1100	.743
1140	.800
1200	.843
1240	.874

Mean Drop Diameter = 950 μm

$\frac{d_{50}}{d_{16}}$ (main) = 1.26

TABLE 22 (Graph 22)

FLOWRATE = 630 gm/min.
SPEED OF ROTATION = 11.4 R.P.S.
DISC DIAMETER ≐ 5.82 inch dia.
SURFACE TENSION = 63.7 dynes/cm.

DROP SIZE μm	CUMULATIVE FRACTION BY NUMBER
740	.10
840	.348
910	.553
990	.755
1040	.882

Mean Drop Diameter = 900 μm

$\frac{d_{50}}{d_{16}}$ (main) = 1.17

TABLE 23 (Graph 23)

FLOWRATE = 740 gm/min.
SPEED OF ROTATION = 11.4 R.P.S.
DISC DIAMETER = 5.8½inch dia.
SURFACE TENSION = 63.7 dynes/cm.

DROP SIZE µm	CUMULATIVE FRACTION BY NUMBER
740	.103
840	.358
910	.578
990	.769
1040	.883
1100	.936

Mean Drop Diameter = 895 µm

$\frac{d_{50}}{d_{16}}$ (main) = 1.16

TABLE 24 (Graph 24)

FLOWRATE = 1500 gm/min
SPEED OF ROTATION = 11.4 R.P.S.
DISC DIAMETER = 5.8½inch dia.
SURFACE TENSION = 63.7 dynes/cm.

DROP SIZE µm	CUMULATIVE FRACTION BY NUMBER
740	.182
840	.395
910	.545
990	.651
1040	.725
1100	.781
1140	.823

Mean Drop Diameter = 900 µm

$\frac{d_{50}}{d_{16}}$ (main) = 1.28

TABLE 25 (Graph 25)

FLOWRATE = 1800 gm/min.

SPEED OF ROTATION = 11.4 R.P.S.

DISC DIAMETER = 5.82 inch dia.

SURFACE TENSION = 63.7 dynes/cm.

DROP SIZE μm	CUMULATIVE FRACTION BY NUMBER
740	.168
840	.366
910	.512
990	.619
1040	.694
1100	.750
1140	.794

Mean Drop Diameter = 910 μm

$$\frac{d_{50}}{d_{16}} \quad \text{(main)} = 1.26$$

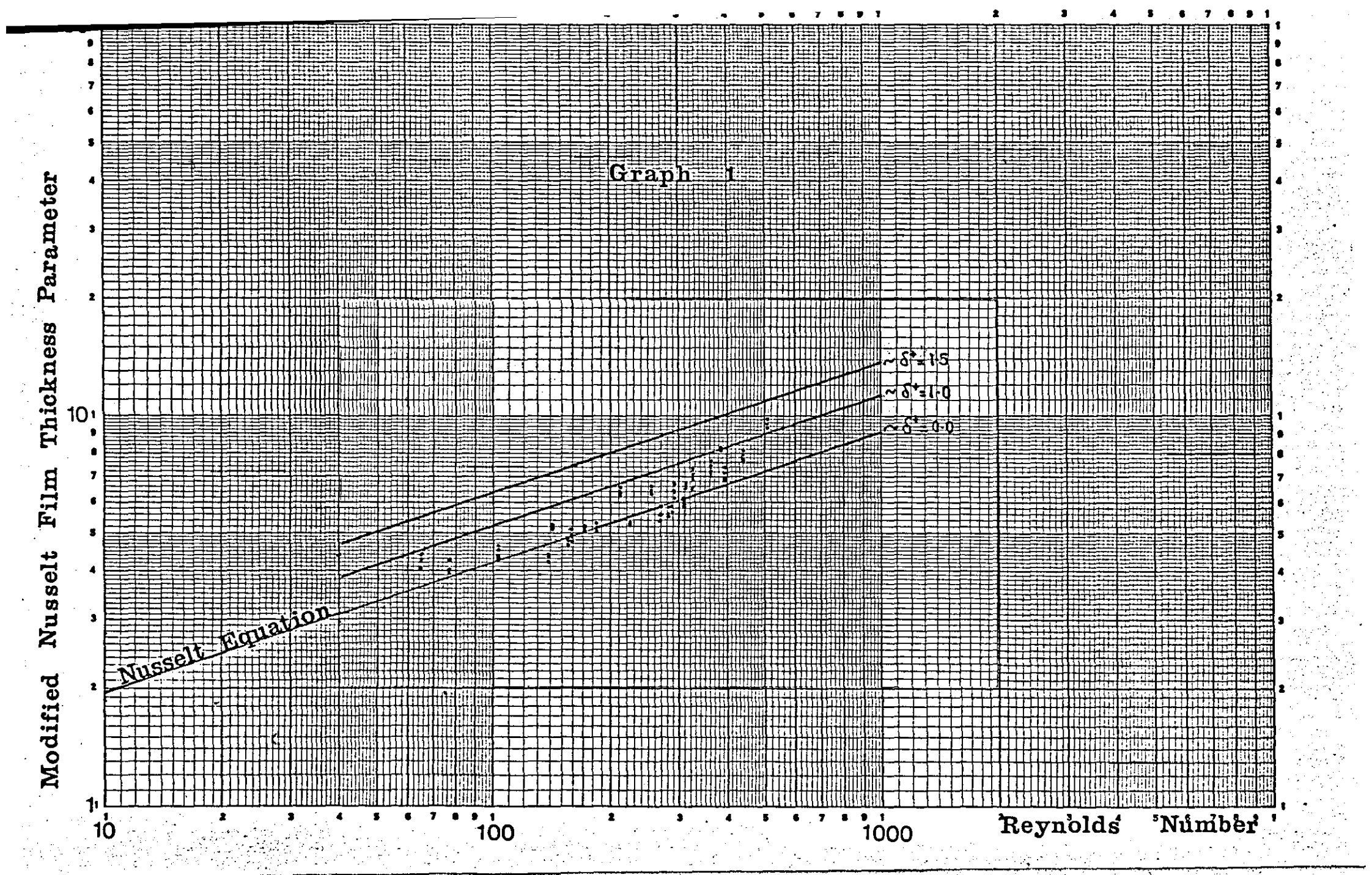
Graph 1
Modified Nusselt Film Thickness Parameter
Reynolds Number
10
100
1000
Nusselt Equation
≃ δ* = 1·5
≃ δ* = 1·0
≃ δ* = 0·0

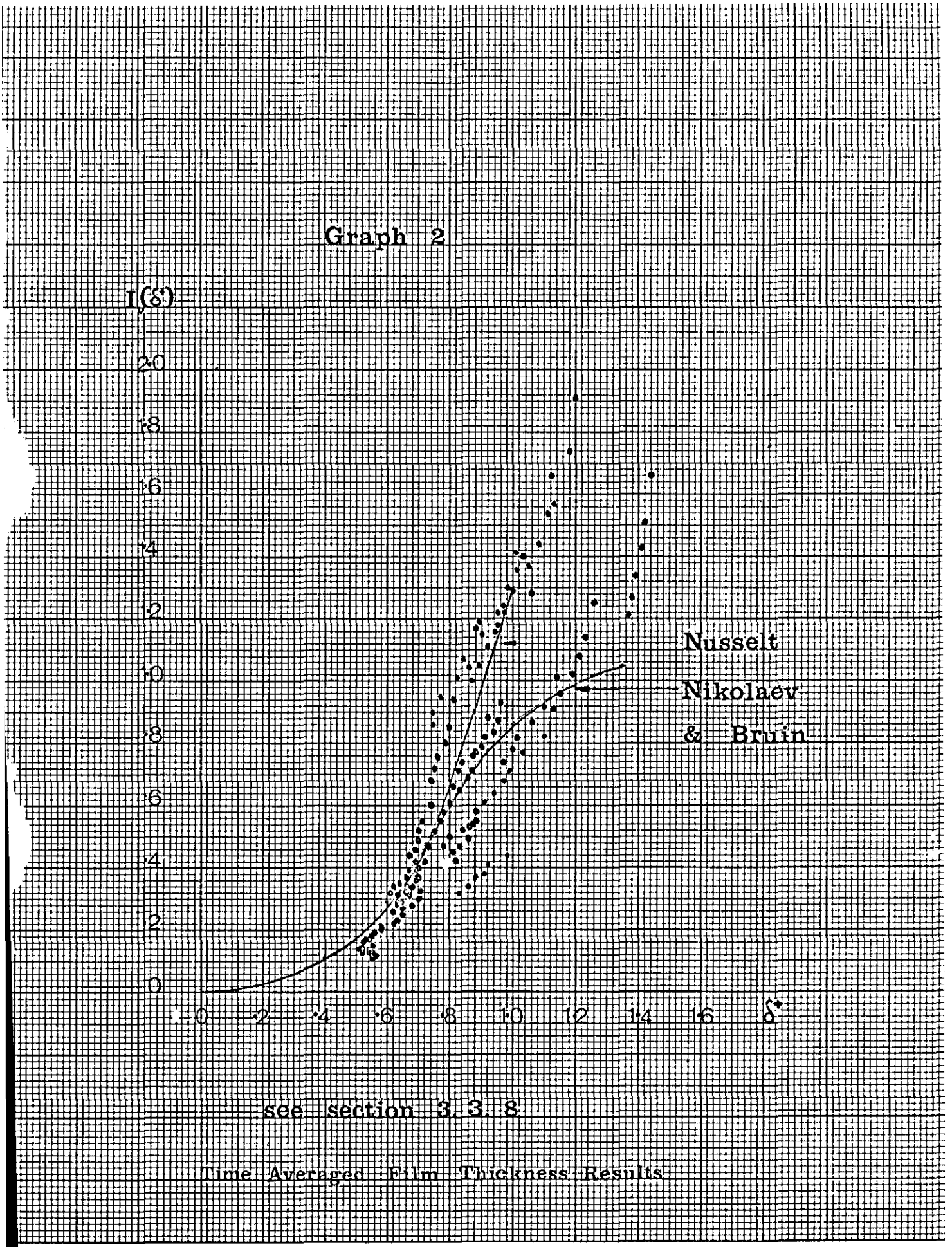
Graph 2
I(δ)
2·0
1·8
1·6
1·4
1·2
1·0
·8
·6
·4
·2
0
·0
·2
·4
·6
·8
1·0
1·2
1·4
1·6
δ+
Nusselt
Nikolaev
& Bruin
see section 3.3.8
Time Averaged Film Thickness Results

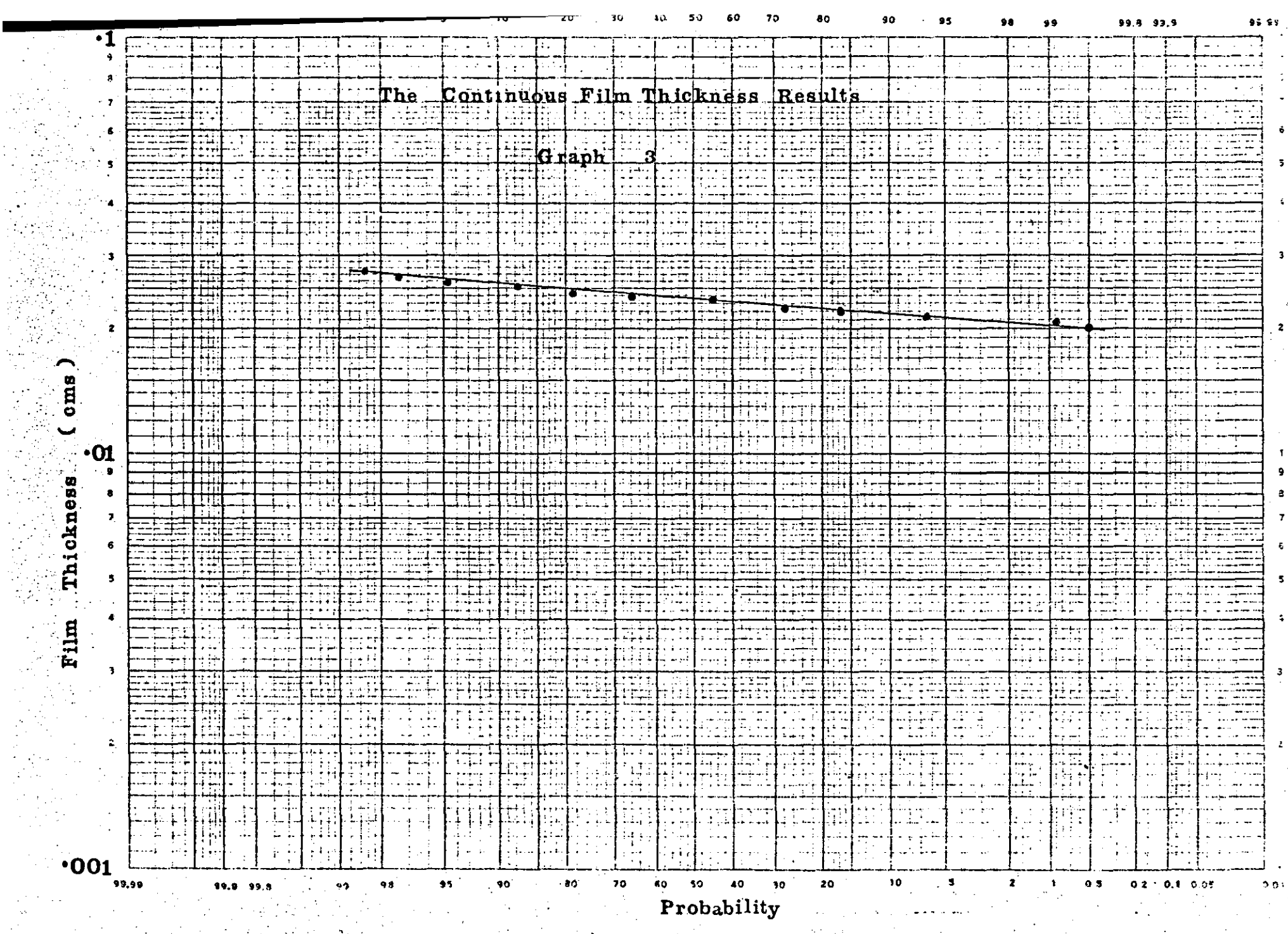
The Continuous Film Thickness Results
Graph 3
Film Thickness (cms)
•1
•01
•001
99.99
99.9
99.8
99
98
95
90
80
70
60
50
40
30
20
10
5
2
1
0.5
0.2
0.1
0.05
0.01
Probability

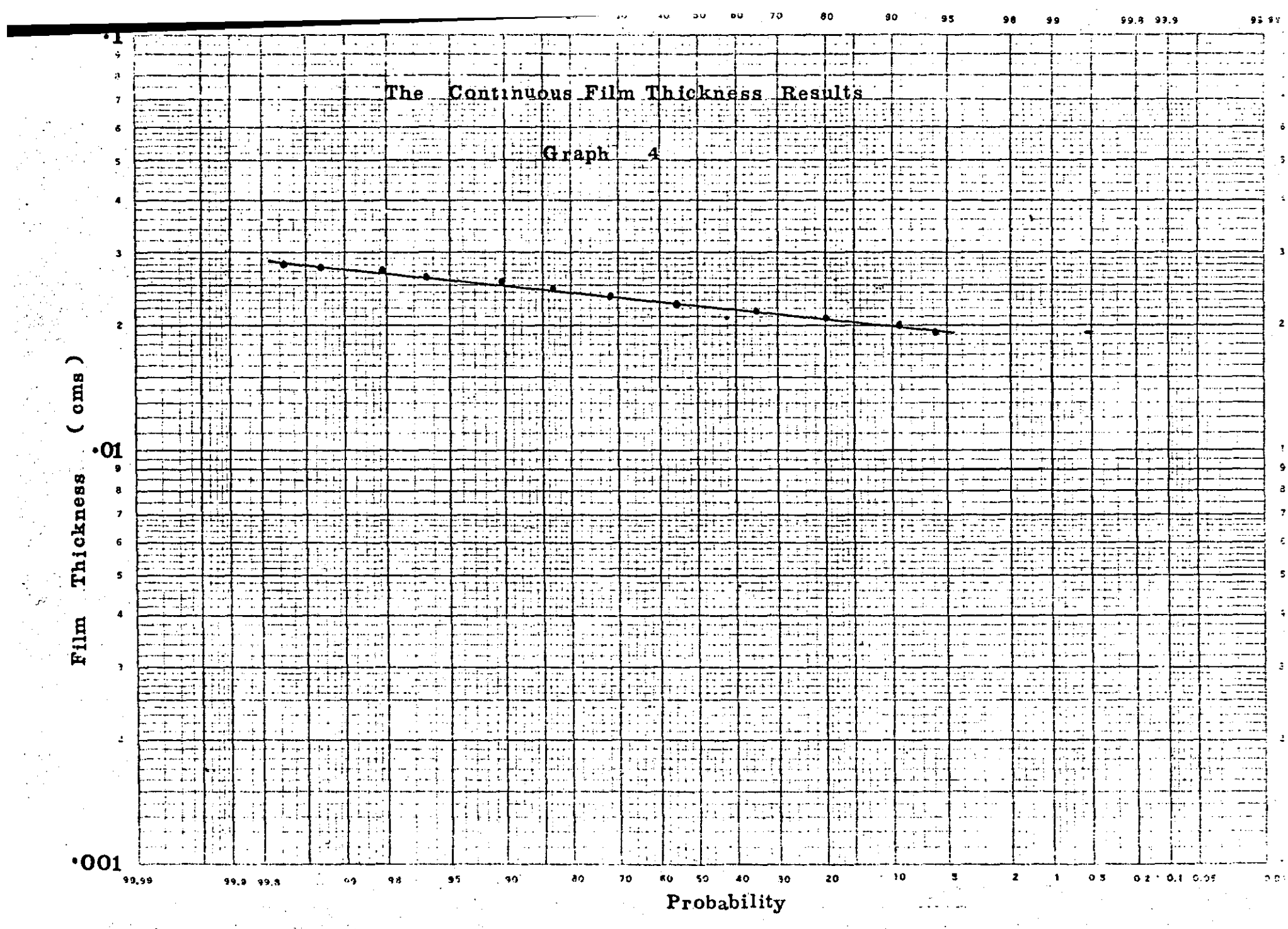
The Continuous Film Thickness Results
Graph 4
Film Thickness (cms)
·1
·01
·001
99.99 99.9 99.8 99 98 95 90 80 70 60 50 40 30 20 10 5 2 1 0.5 0.2 0.1 0.05
Probability

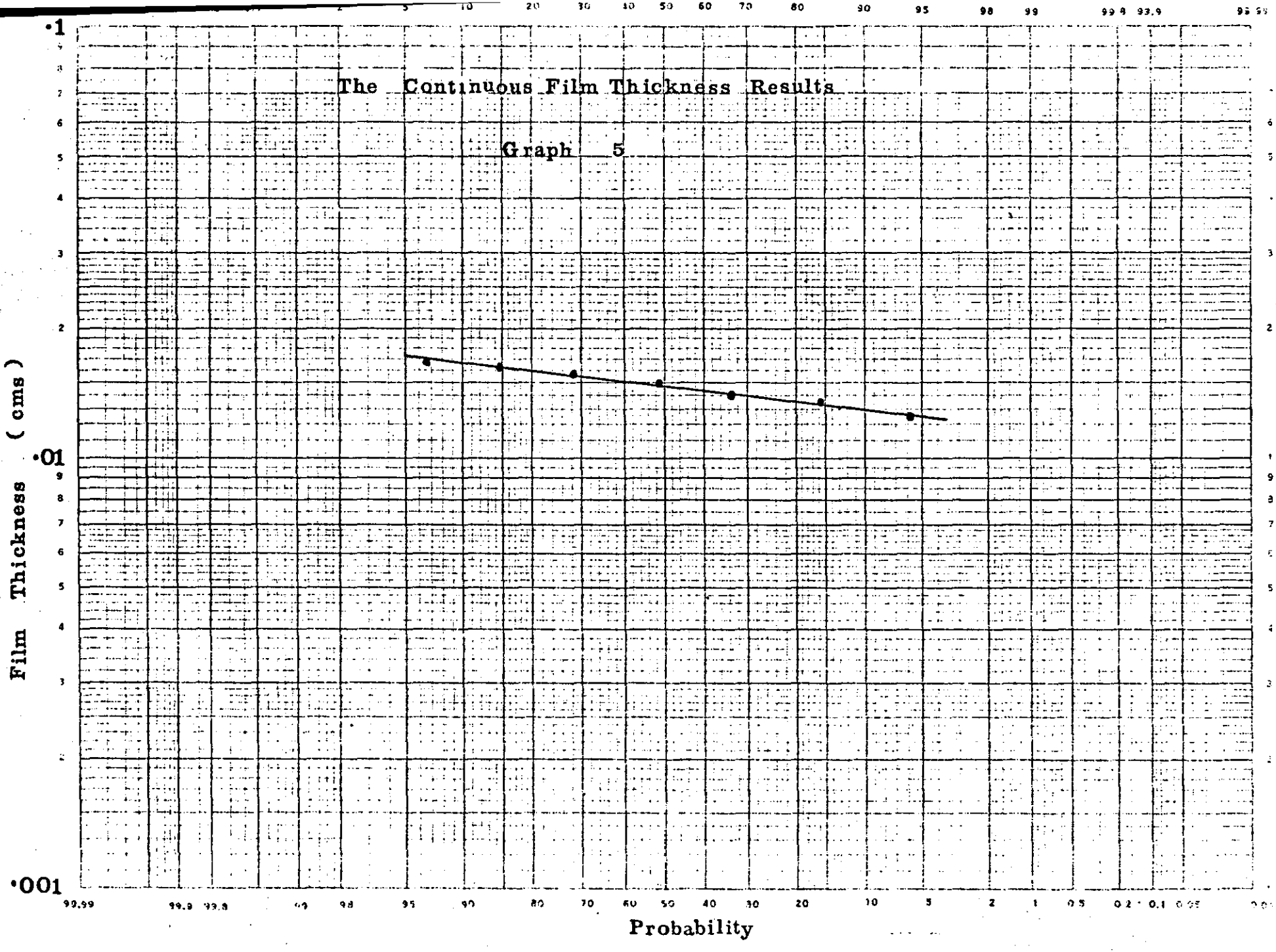
The Continuous Film Thickness Results
Graph 5
Film Thickness (cms)
·1
·01
·001
Probability

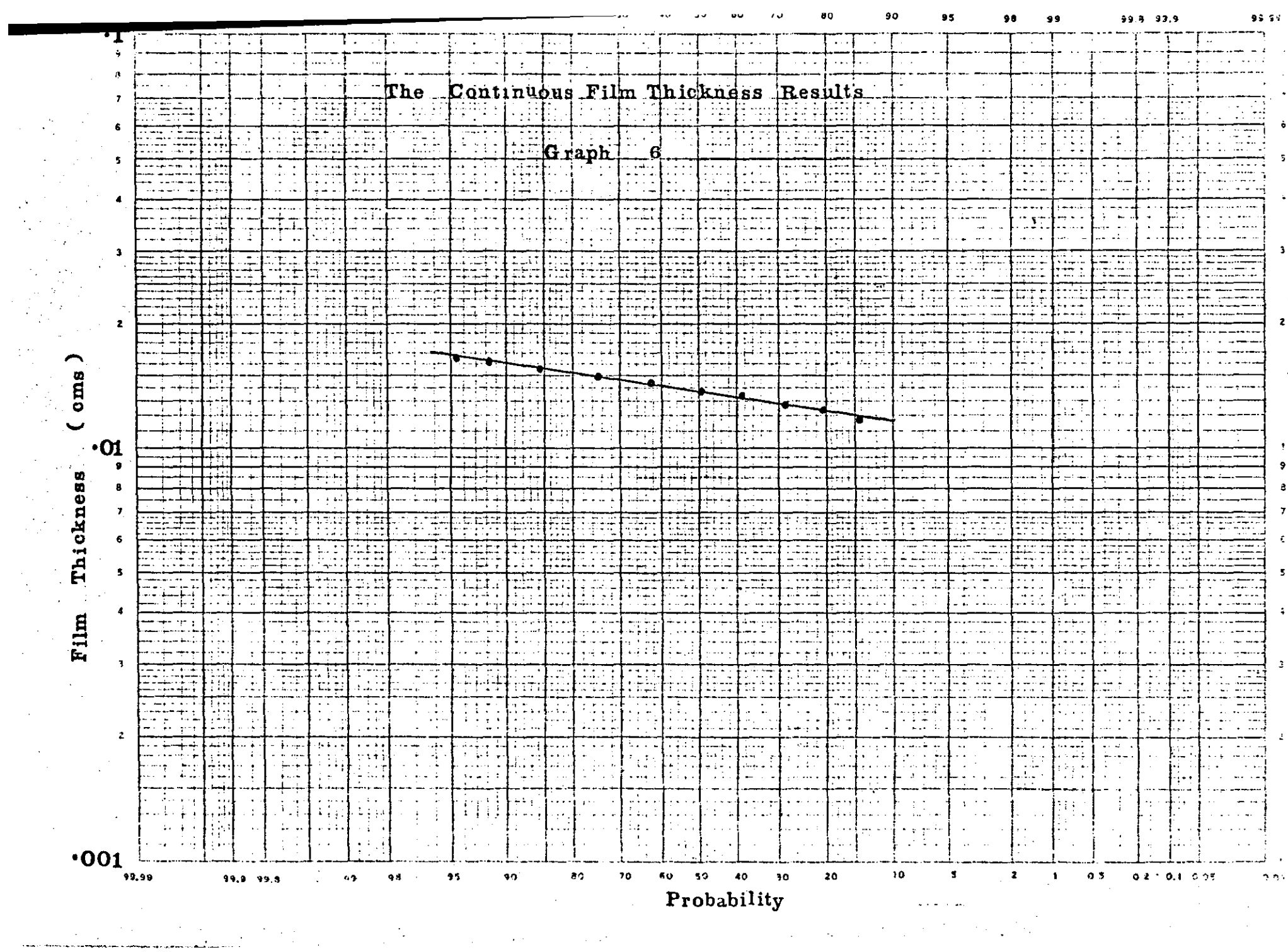
The Continuous Film Thickness Results
Graph 6
Film Thickness (ems)
·1
·01
·001
99.99
99.9
99.8
98
95
90
80
70
60
50
40
30
20
10
5
2
1
0.5
0.2
0.1
Probability

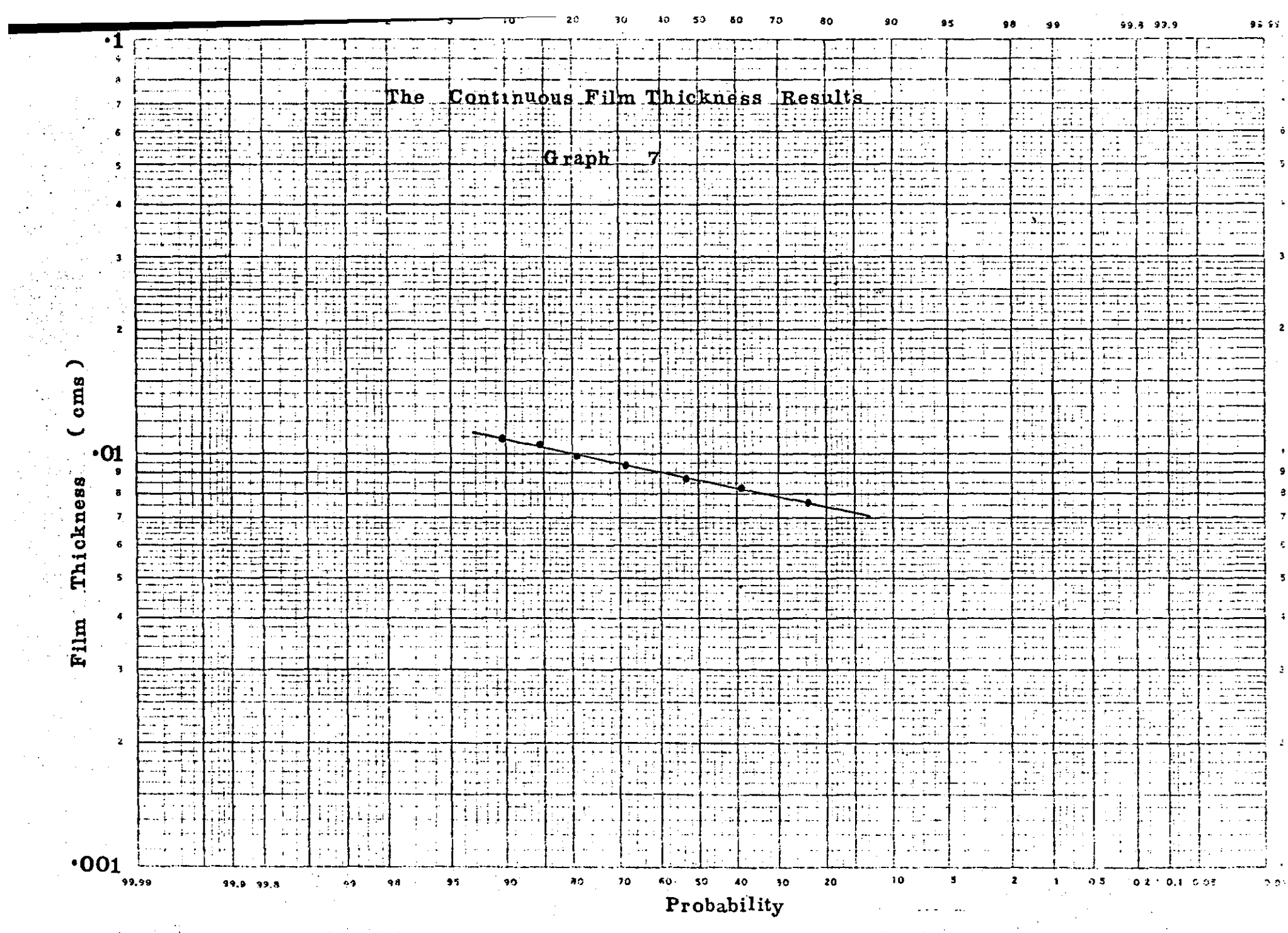
The Continuous Film Thickness Results
Graph 7
Film Thickness (cms)
•1
•01
•001
99.99 99.9 99.8 99 98 95 90 80 70 60 50 40 30 20 10 5 2 1 0.5 0.2 0.1
Probability

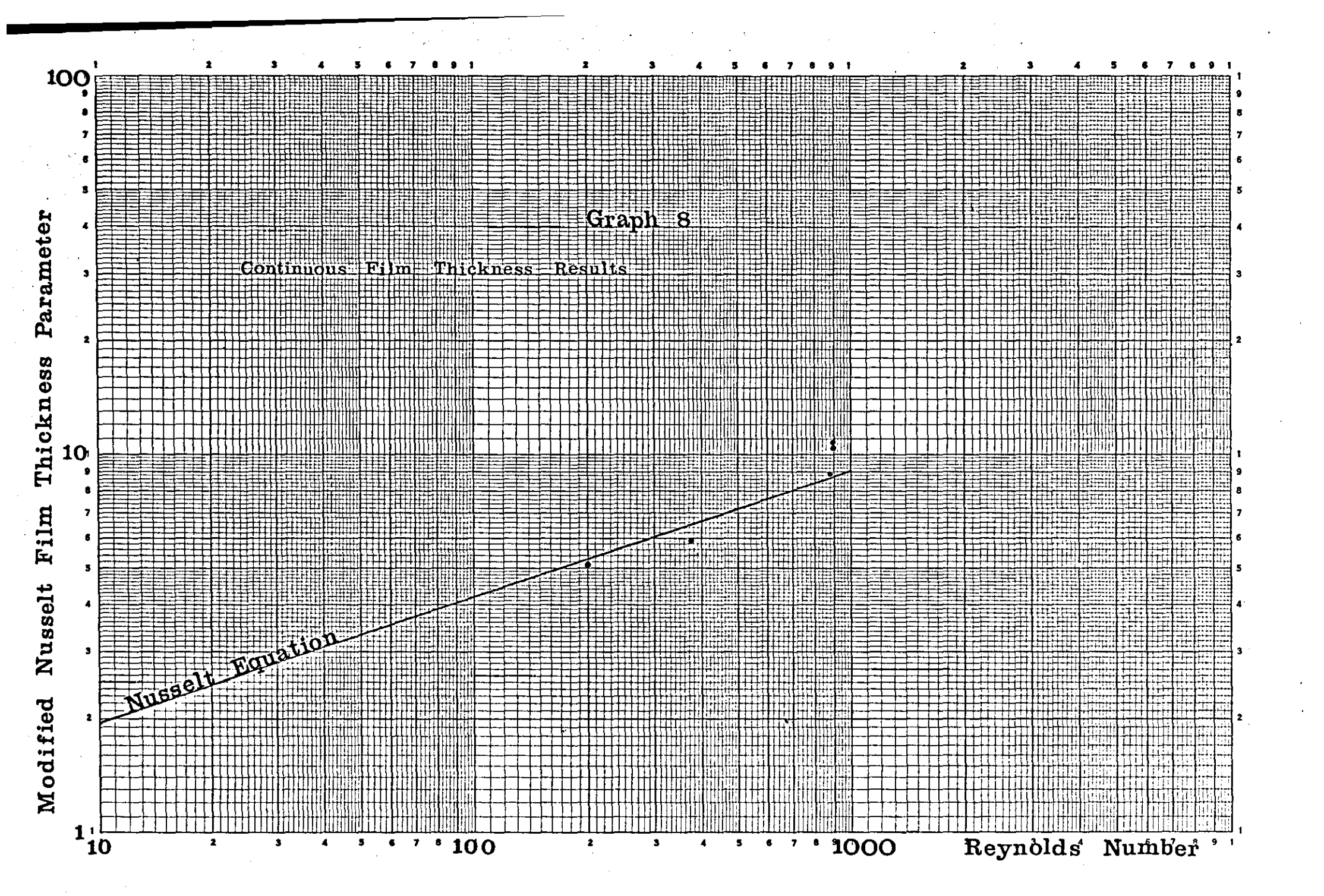
Graph 8
Continuous Film Thickness Results
Nusselt Equation
Modified Nusselt Film Thickness Parameter
Reynolds Number
100
10
1
10
100
1000

Graph 9

Standard Deviation, Continuous Film Thickness Results

·10
·09
·08
·07
·06
·05
·04
·03
·02
·01
0

·0 ·1 ·2 ·3 ·4 ·5 ·6 ·7 ·8 ·9 1·0 1·1 1·2 1·3 1·4 1·5

Logarithmic Modified Nusselt Film Thickness Parameter

$\text{Log}(N_f^*)$

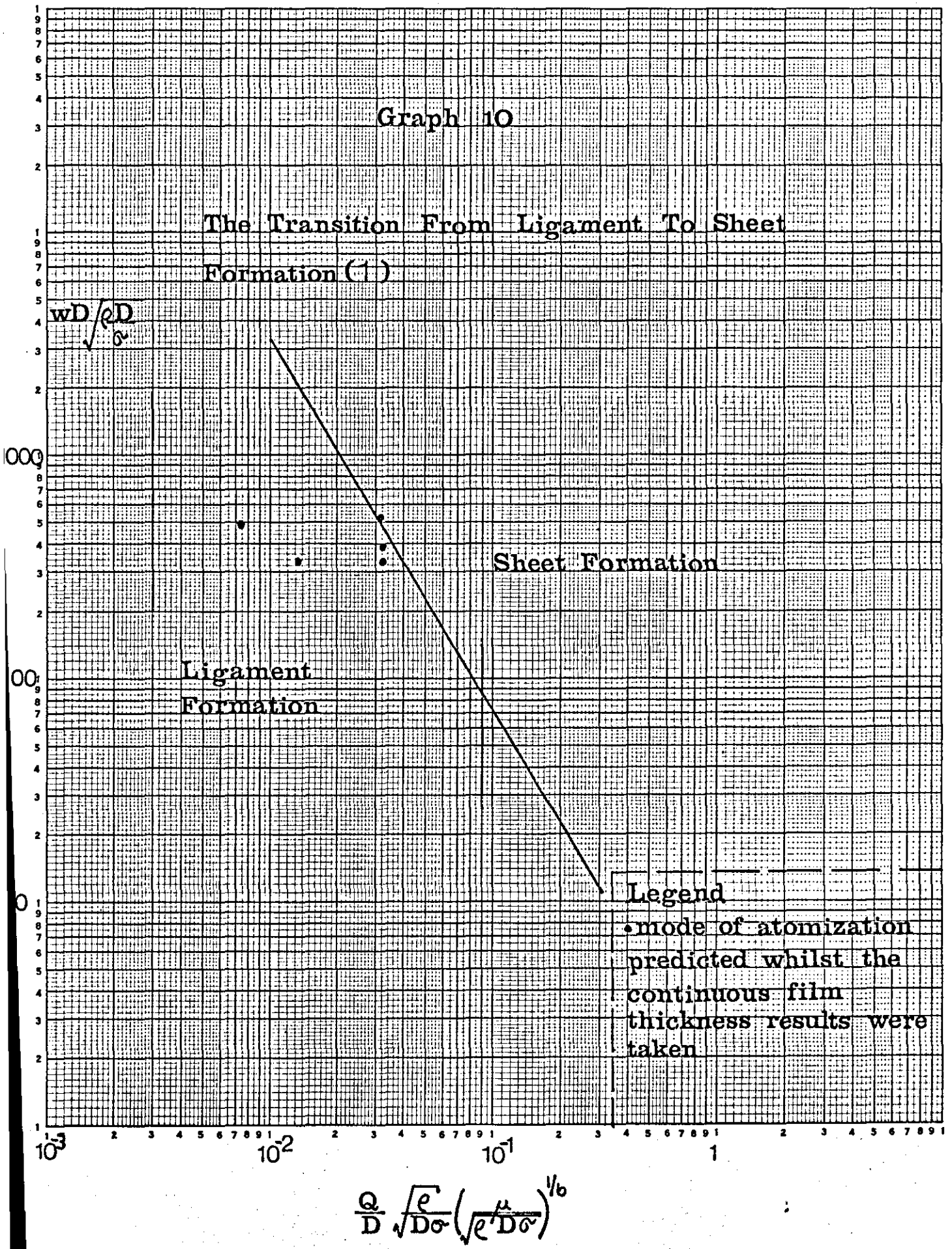
Graph 10
The Transition From Ligament To Sheet Formation (-1)
$wD\sqrt{\frac{\rho D}{\sigma}}$
Sheet Formation
Ligament Formation
Legend
•mode of atomization predicted whilst the continuous film thickness results were taken
10^{-3}
10^{-2}
10^{-1}
1
$\frac{Q}{D}\sqrt{\frac{\rho}{D\sigma}}\left(\sqrt{\rho}\frac{\mu}{D\sigma}\right)^{1/6}$

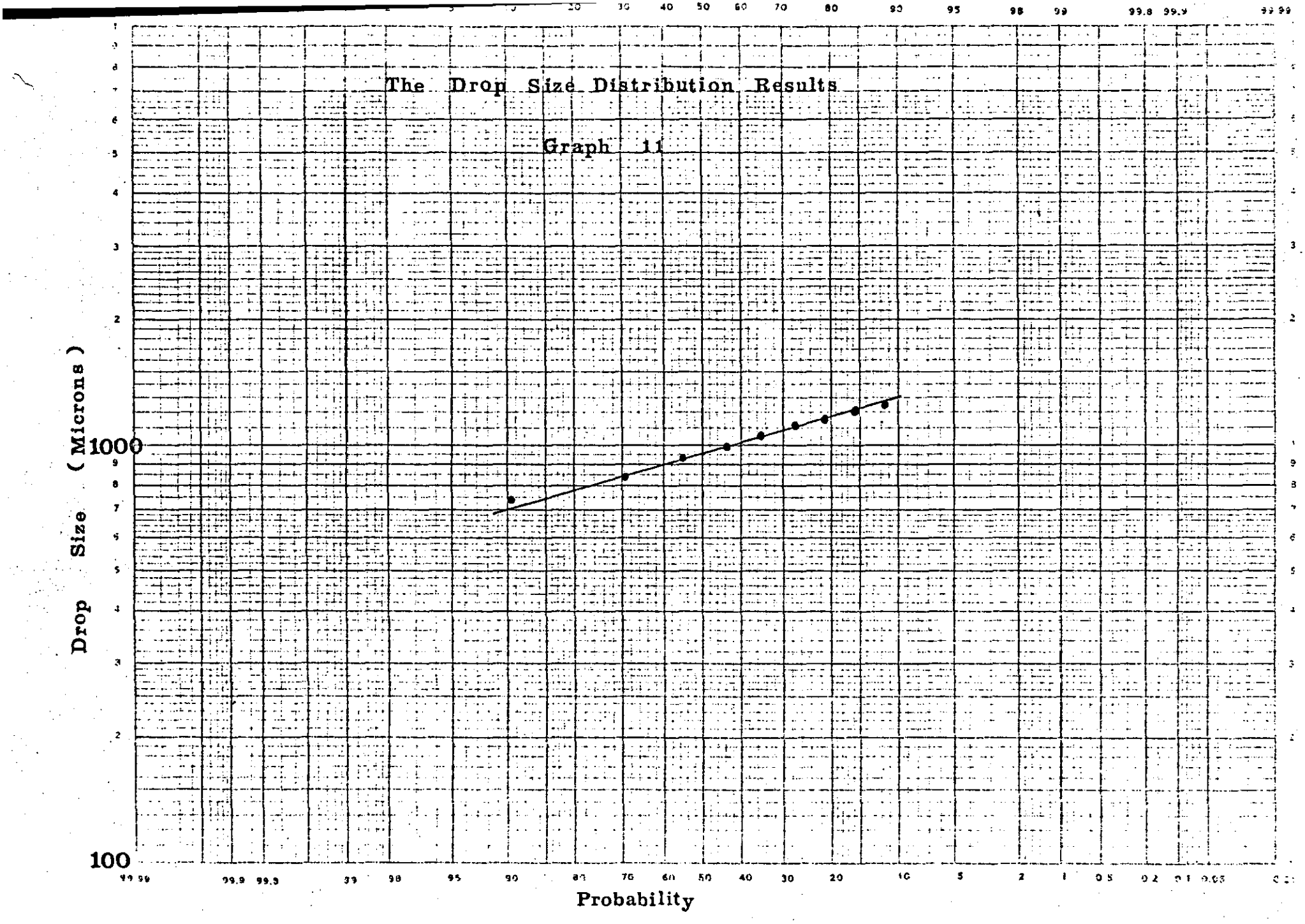
The Drop Size Distribution Results
Graph 11
Drop Size (Microns)
1000
100
Probability

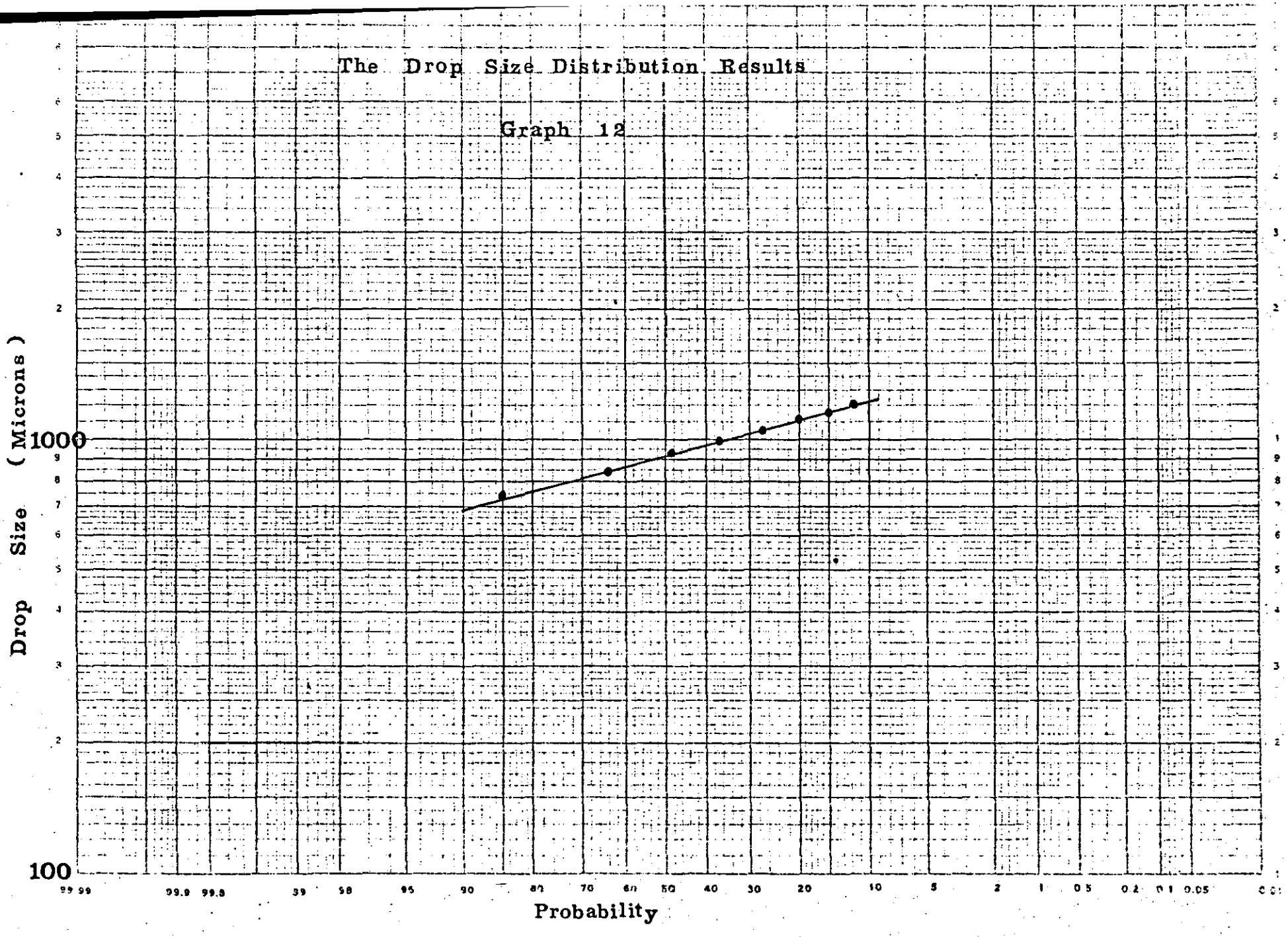
The Drop Size Distribution Results
Graph 12
Drop Size (Microns)
1000
100
99.99
99.9
99.8
99
98
95
90
80
70
60
50
40
30
20
10
5
2
1
0.5
0.2
0.1
0.05
0.01
Probability

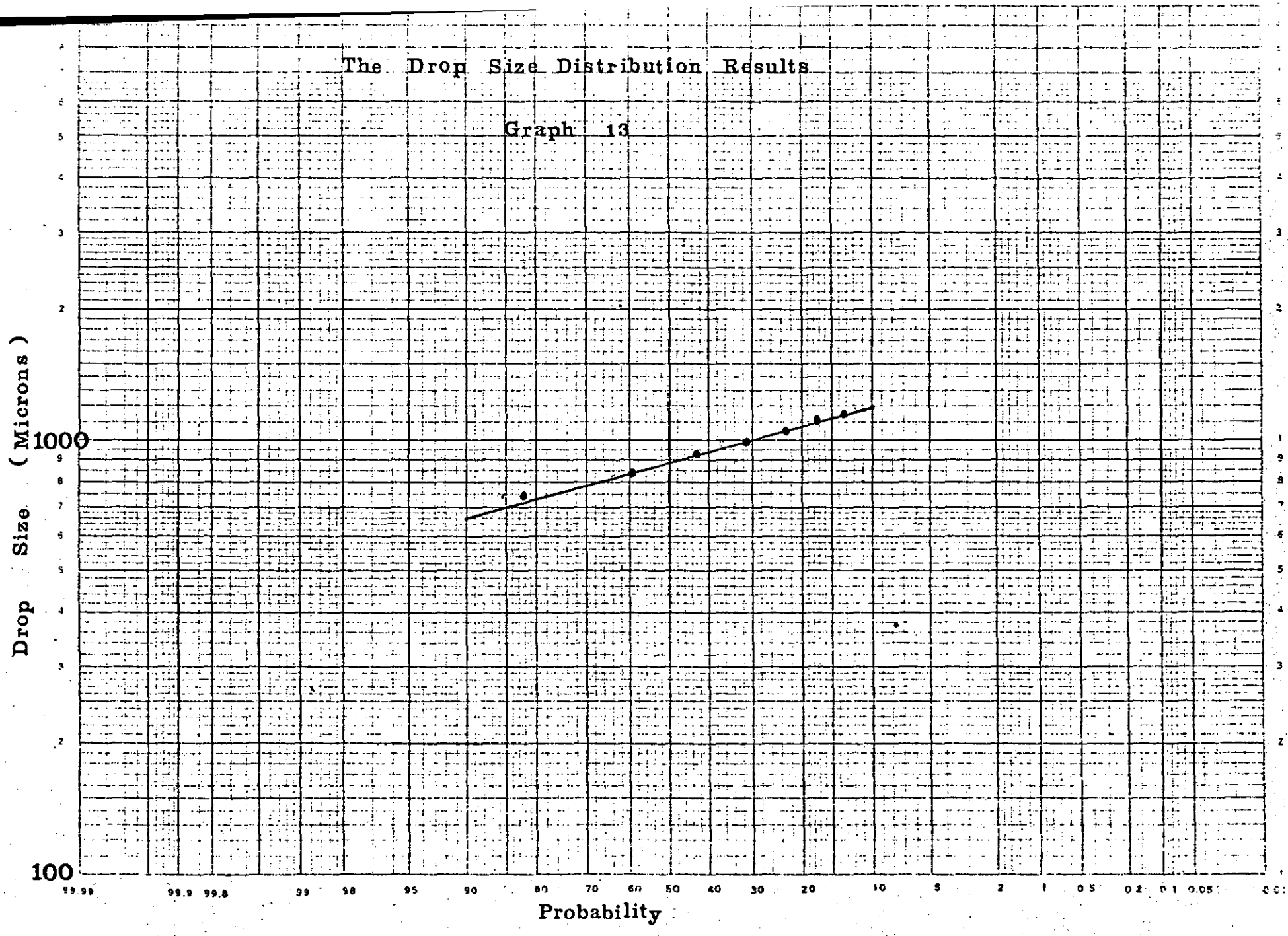
The Drop Size Distribution Results
Graph 13
Drop Size (Microns)
1000
100
99.99
99.9
99.8
99
98
95
90
80
70
60
50
40
30
20
10
5
2
1
0.5
0.2
0.1
0.05
0.0
Probability

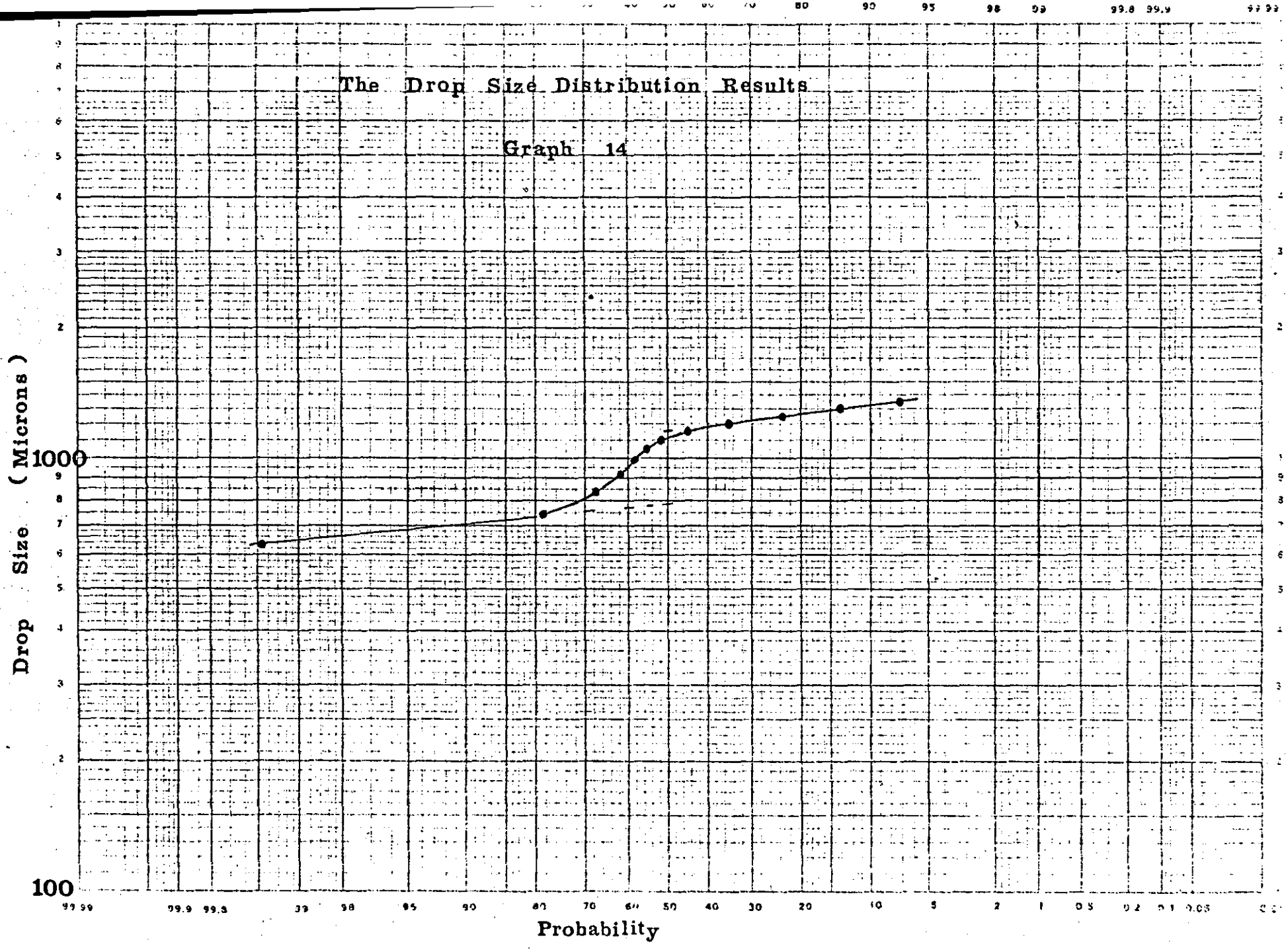
The Drop Size Distribution Results
Graph 14
Drop Size (Microns)
1000
100
99.99 99.9 99.8 99 98 95 90 80 70 60 50 40 30 20 10 5 2 1 0.5 0.2 0.1 0.05
Probability

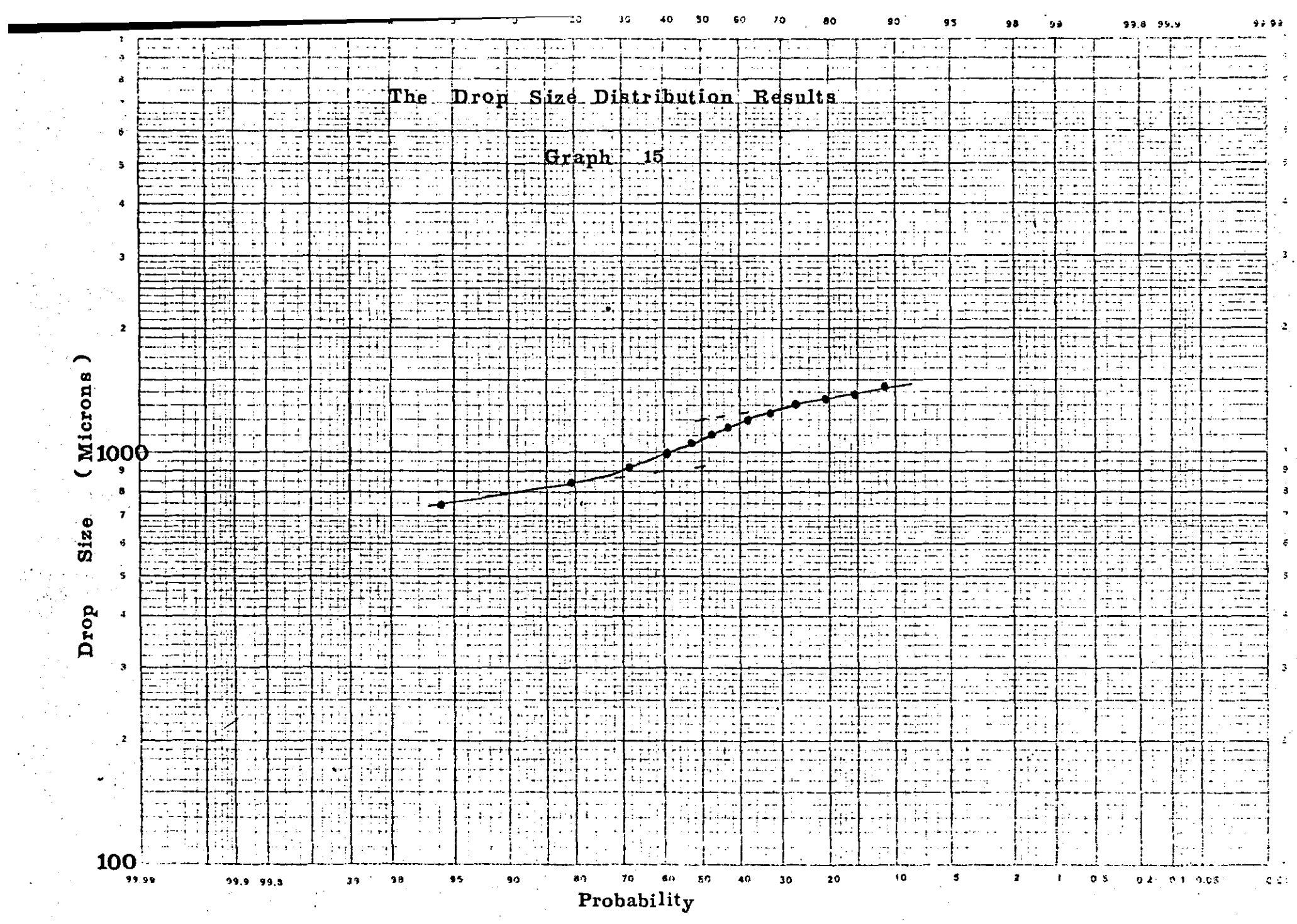
The Drop Size Distribution Results
Graph 15
Drop Size (Microns)
1000
100
Probability

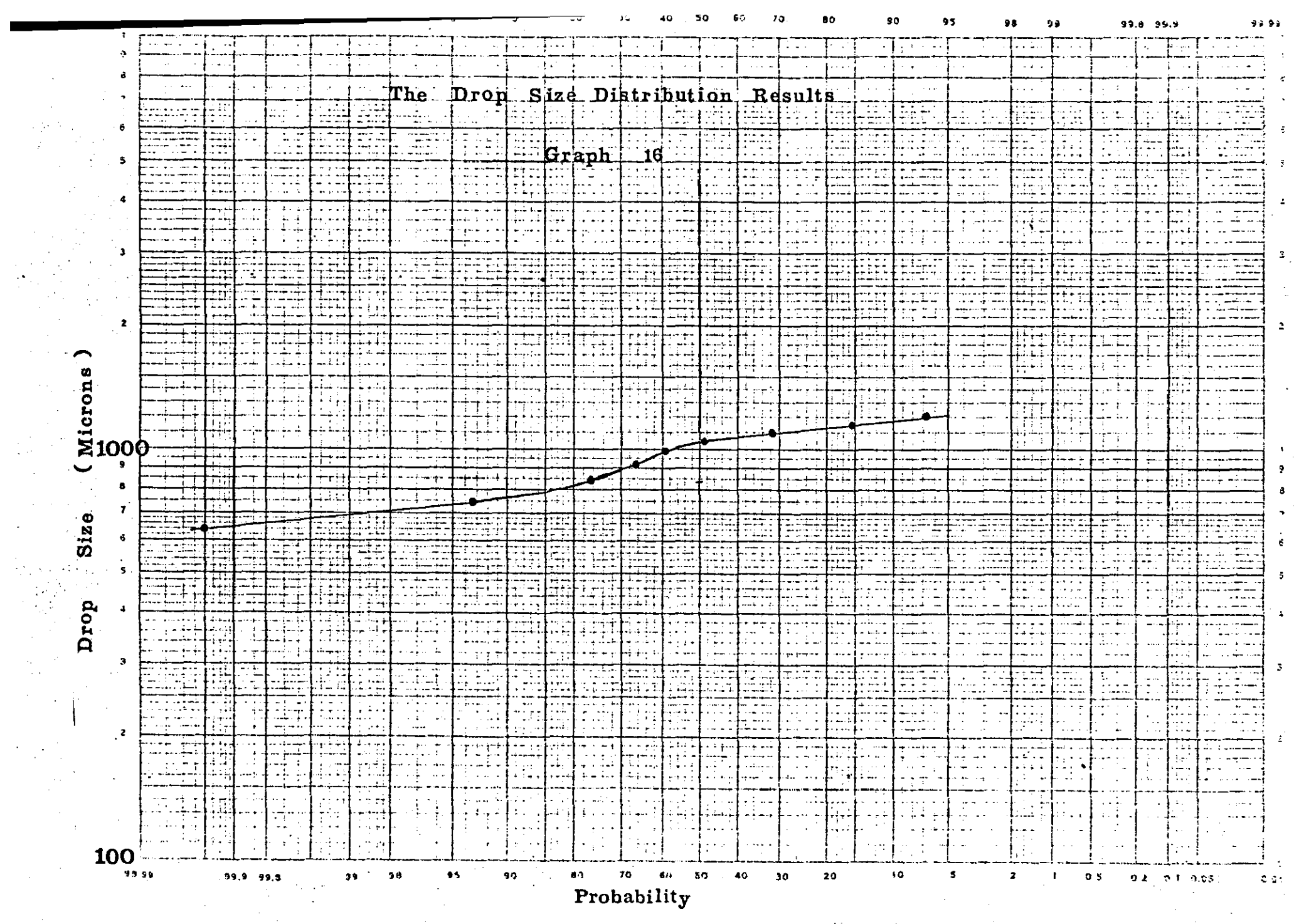
The Drop Size Distribution Results
Graph 16
Drop Size (Microns)
1000
100
Probability

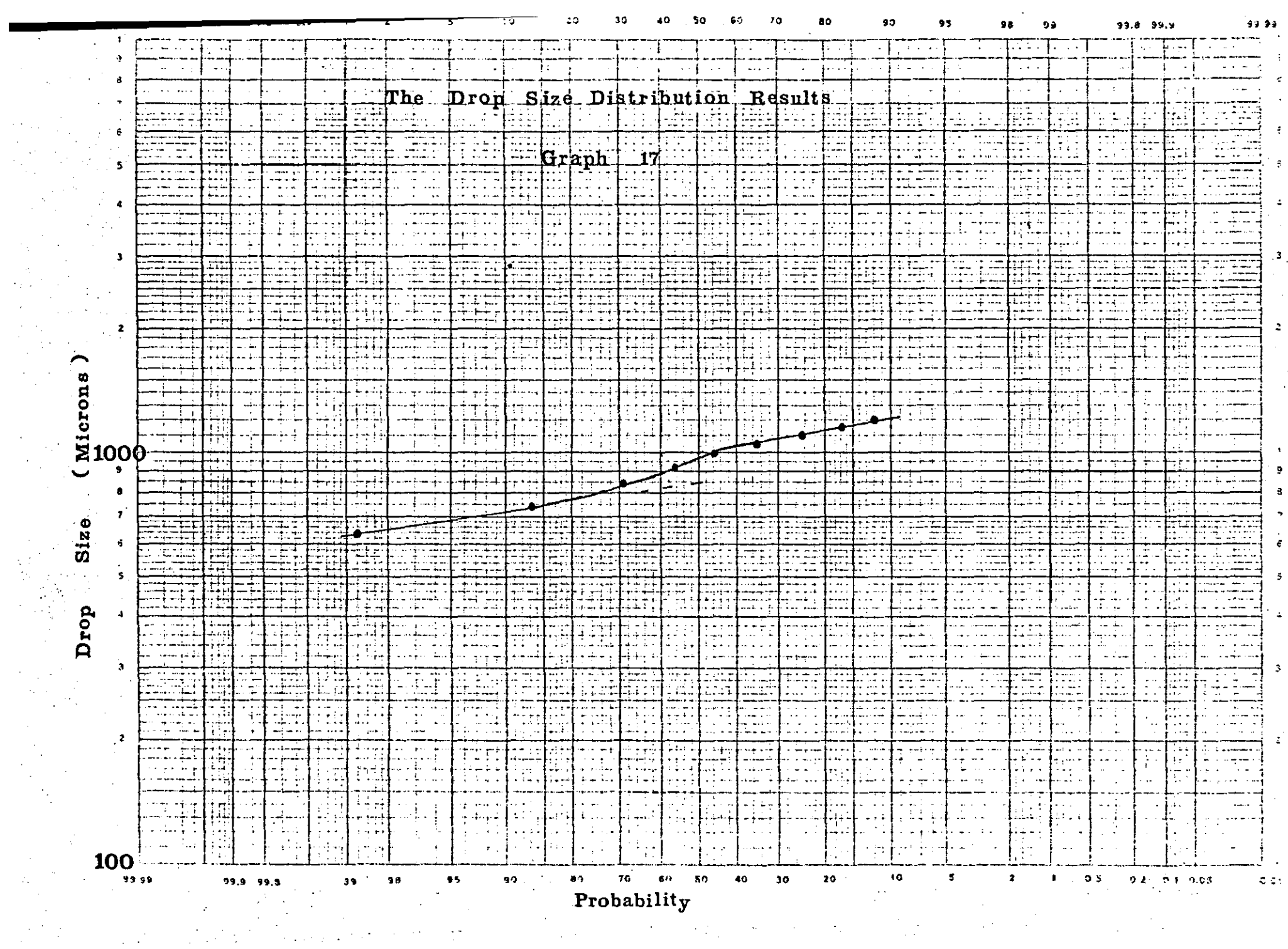
The Drop Size Distribution Results
Graph 17
Drop Size (Microns)
1000
100
Probability

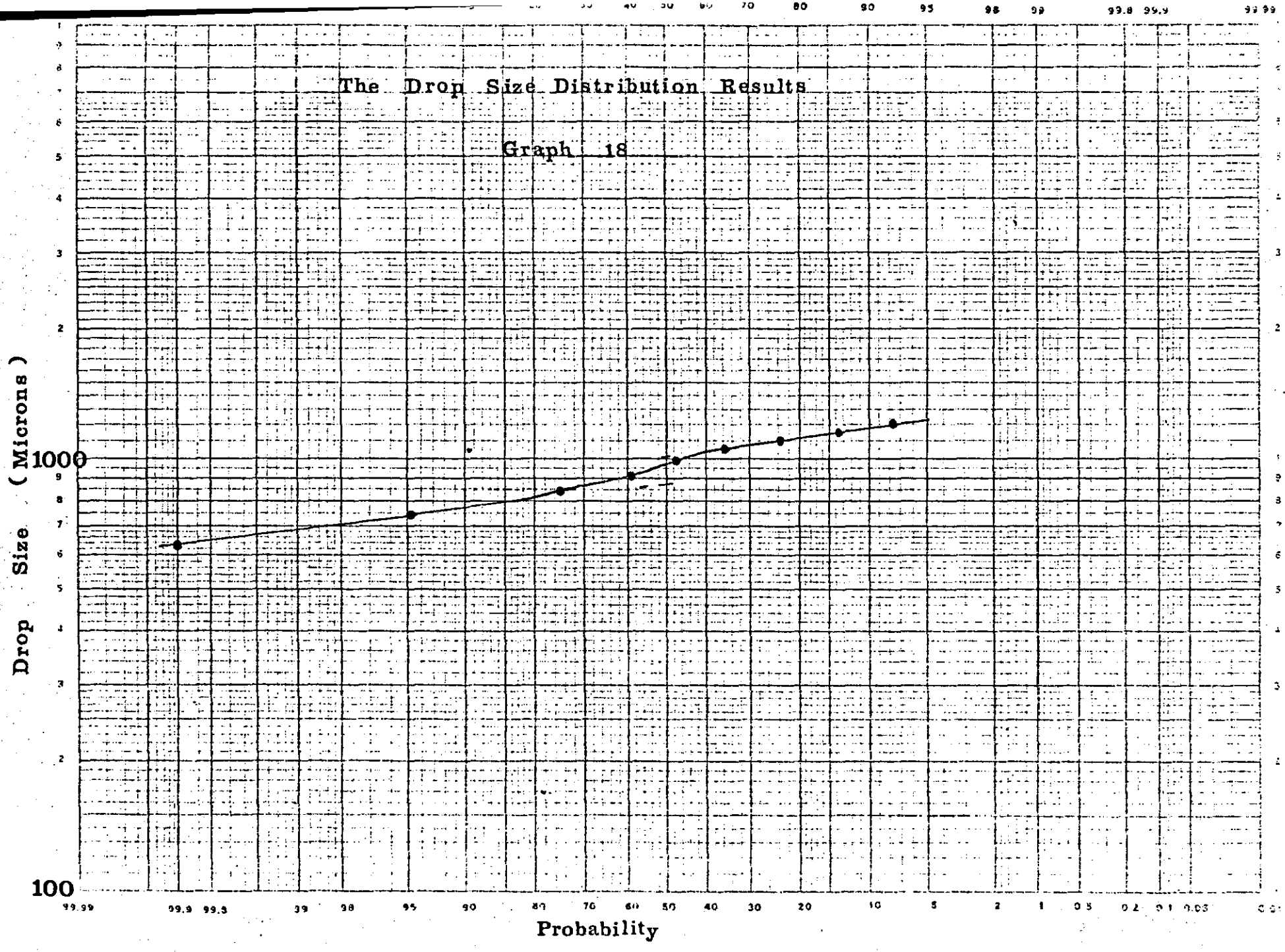
The Drop Size Distribution Results
Graph 18
Drop Size (Microns)
1000
100
99.99
99.9
99.8
99
98
95
90
80
70
60
50
40
30
20
10
5
2
1
0.5
0.2
0.1
0.05
0.01
Probability

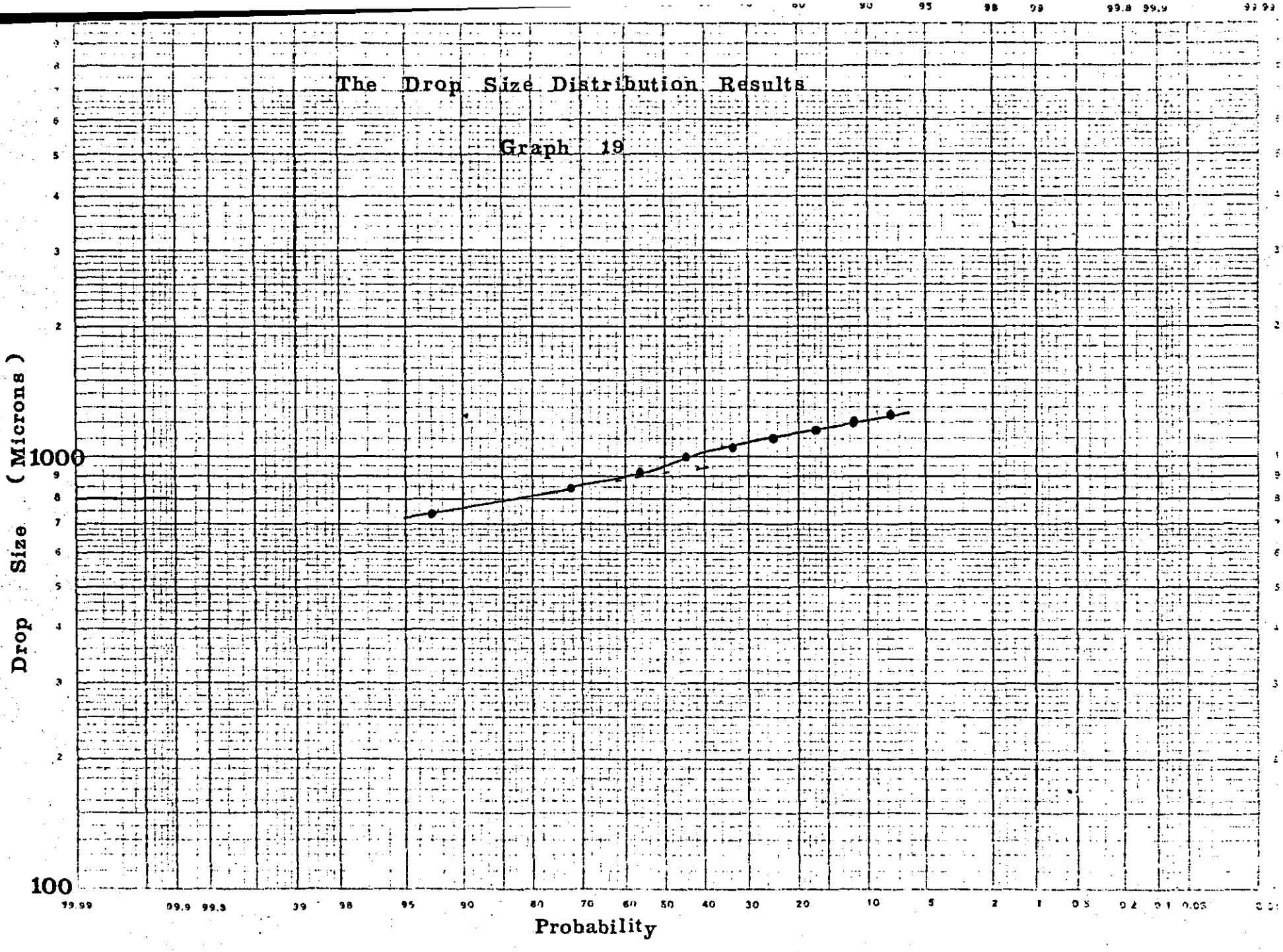
The Drop Size Distribution Results
Graph 19
Drop Size (Microns)
1000
100
99.99
99.9
99.8
99
98
95
90
80
70
60
50
40
30
20
10
5
2
1
0.5
0.2
0.1
0.05
Probability

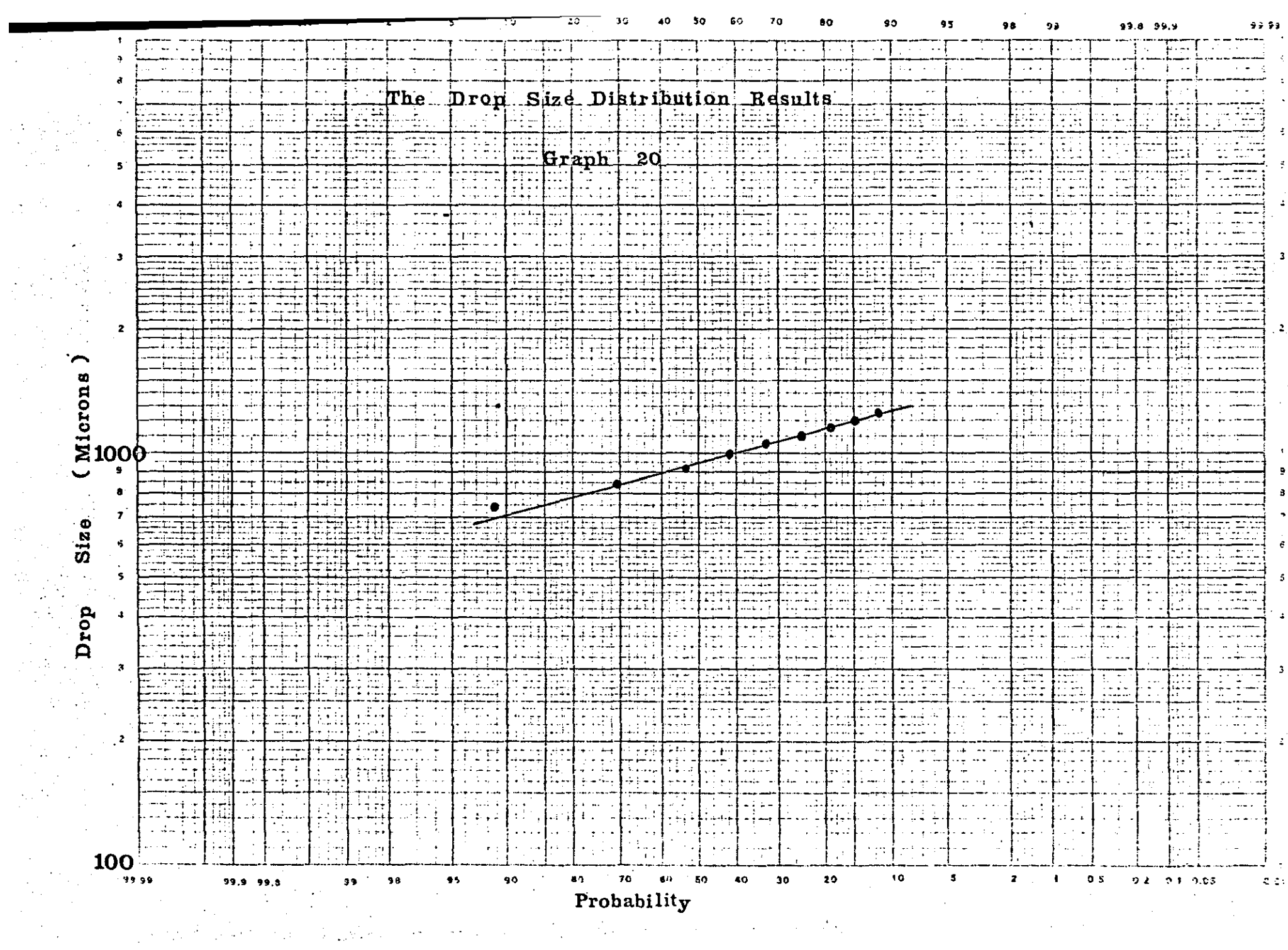
The Drop Size Distribution Results
Graph 20
Drop Size (Microns)
1000
100
99.99 99.9 99.8 99 98 95 90 80 70 60 50 40 30 20 10 5 2 1 0.5 0.2 0.1 0.05
Probability

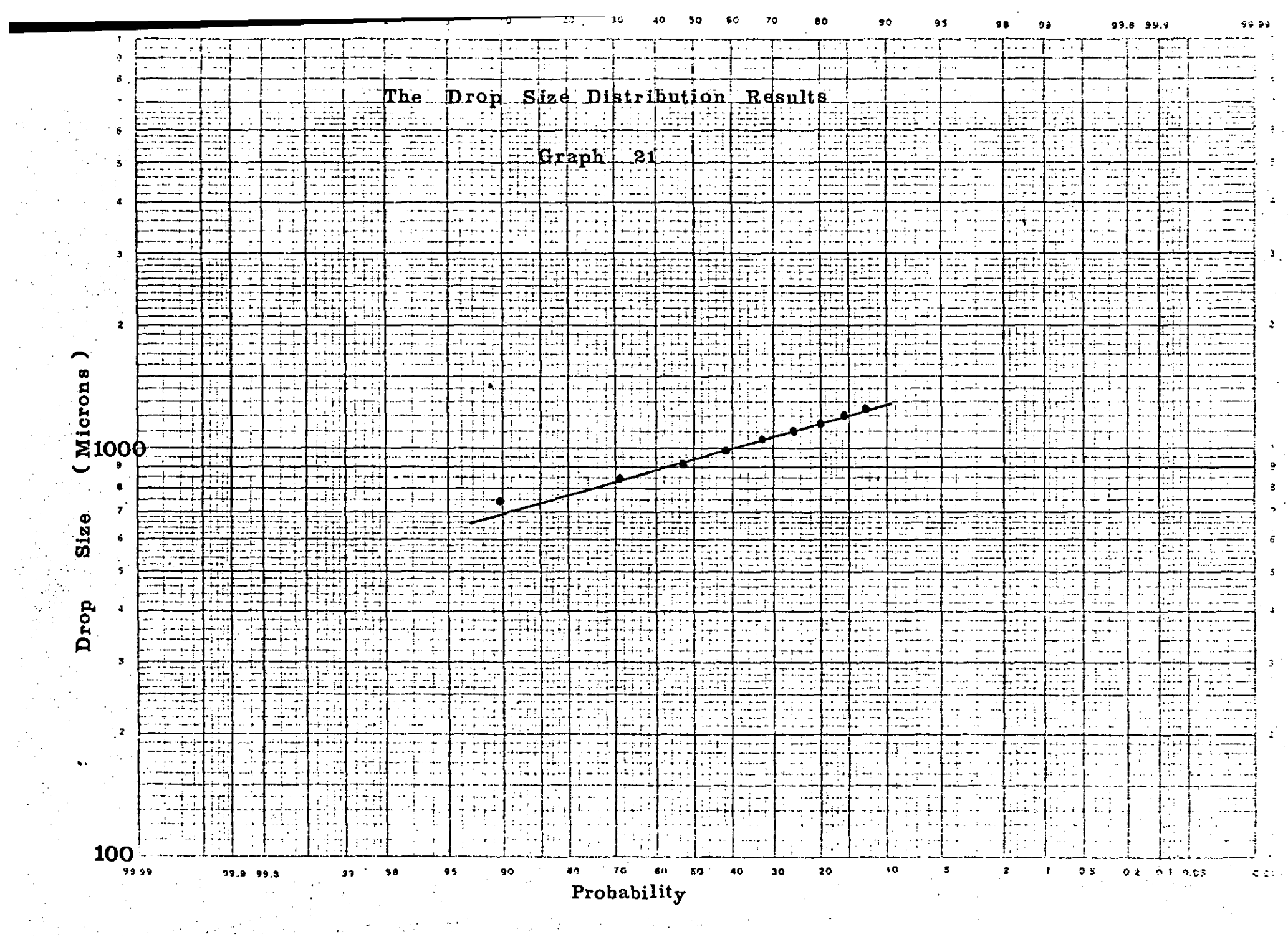
The Drop Size Distribution Results
Graph 21
Drop Size (Microns)
1000
100
Probability

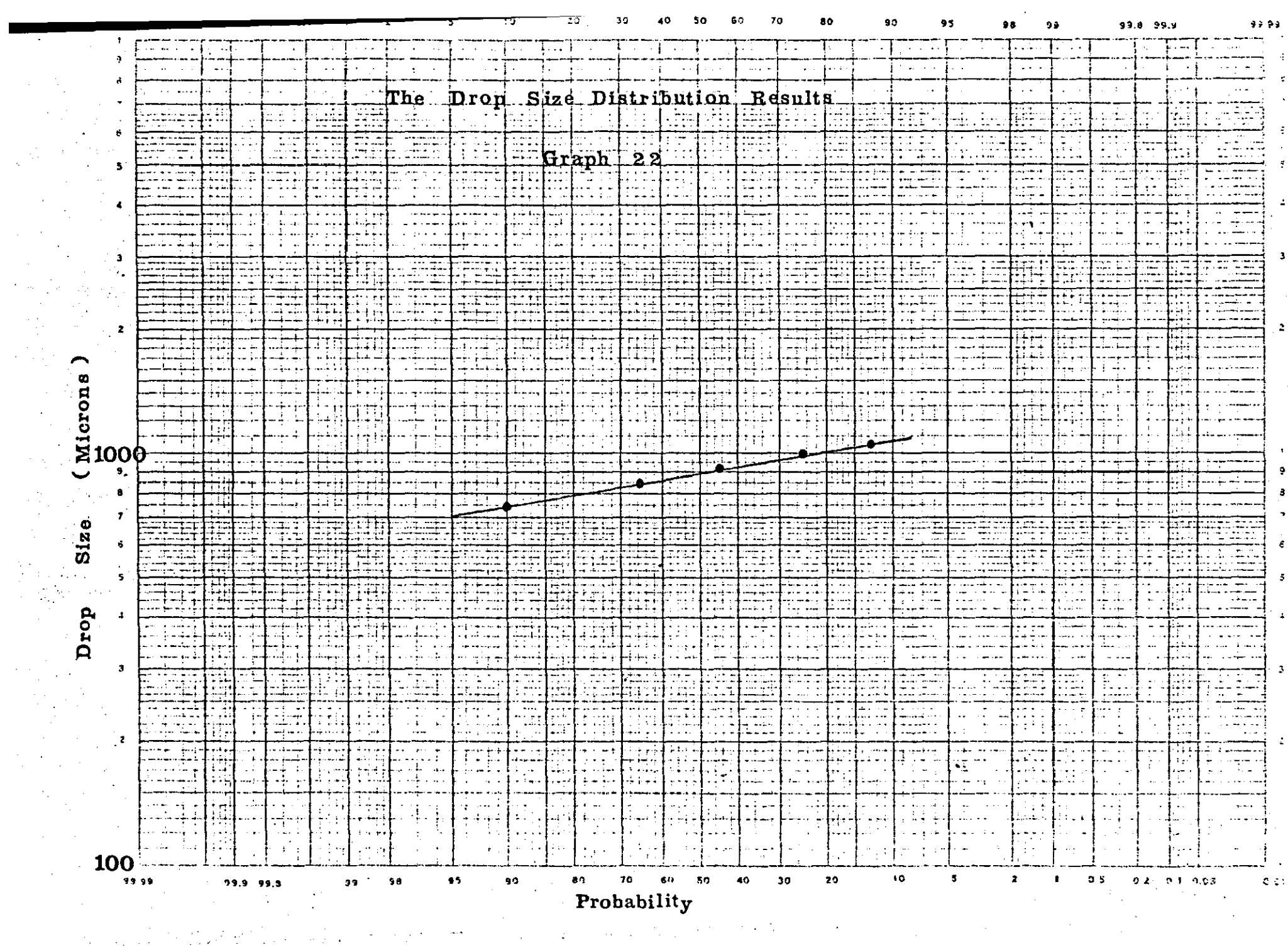
The Drop Size Distribution Results
Graph 22
Drop Size (Microns)
1000
100
99.99 99.9 99.5 99 98 95 90 80 70 60 50 40 30 20 10 5 2 1 0.5 0.2 0.1 0.05
Probability

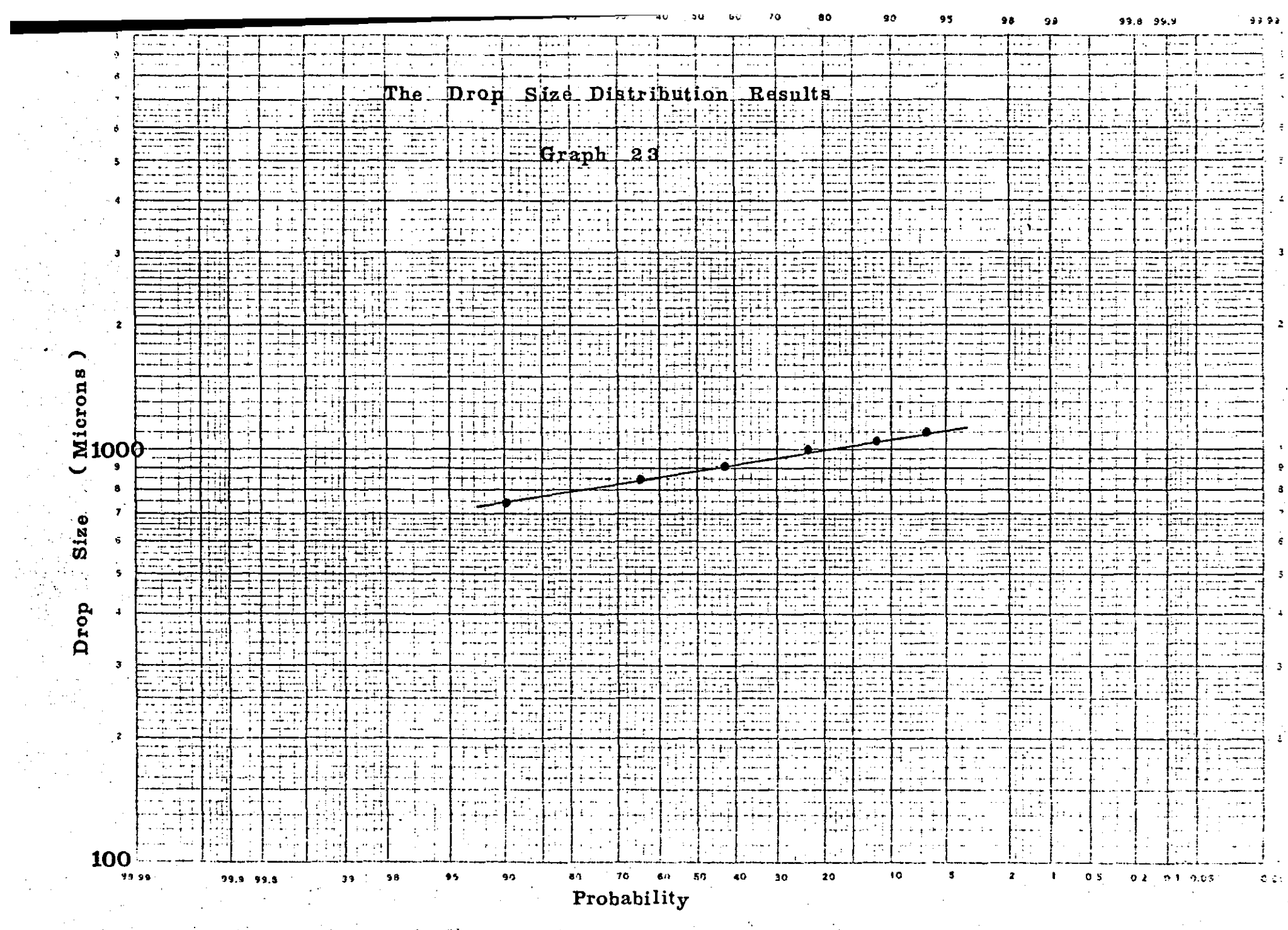
The Drop Size Distribution Results
Graph 23
Drop Size (Microns)
1000
100
99.99 99.9 99.8 99 98 95 90 80 70 60 50 40 30 20 10 5 2 1 0.5 0.2 0.1 0.05
Probability

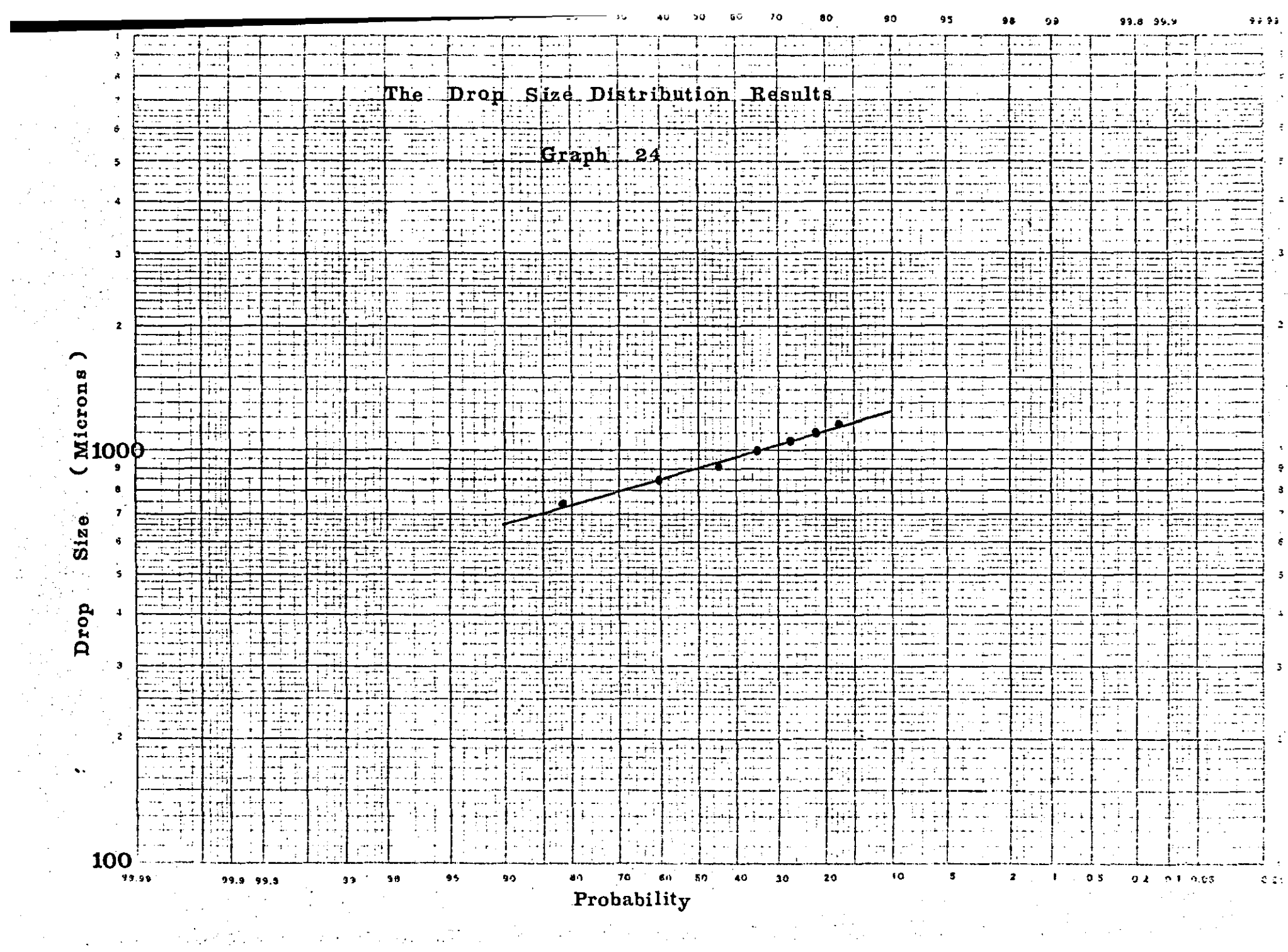
The Drop Size Distribution Results
Graph 24
Drop Size (Microns)
1000
100
Probability

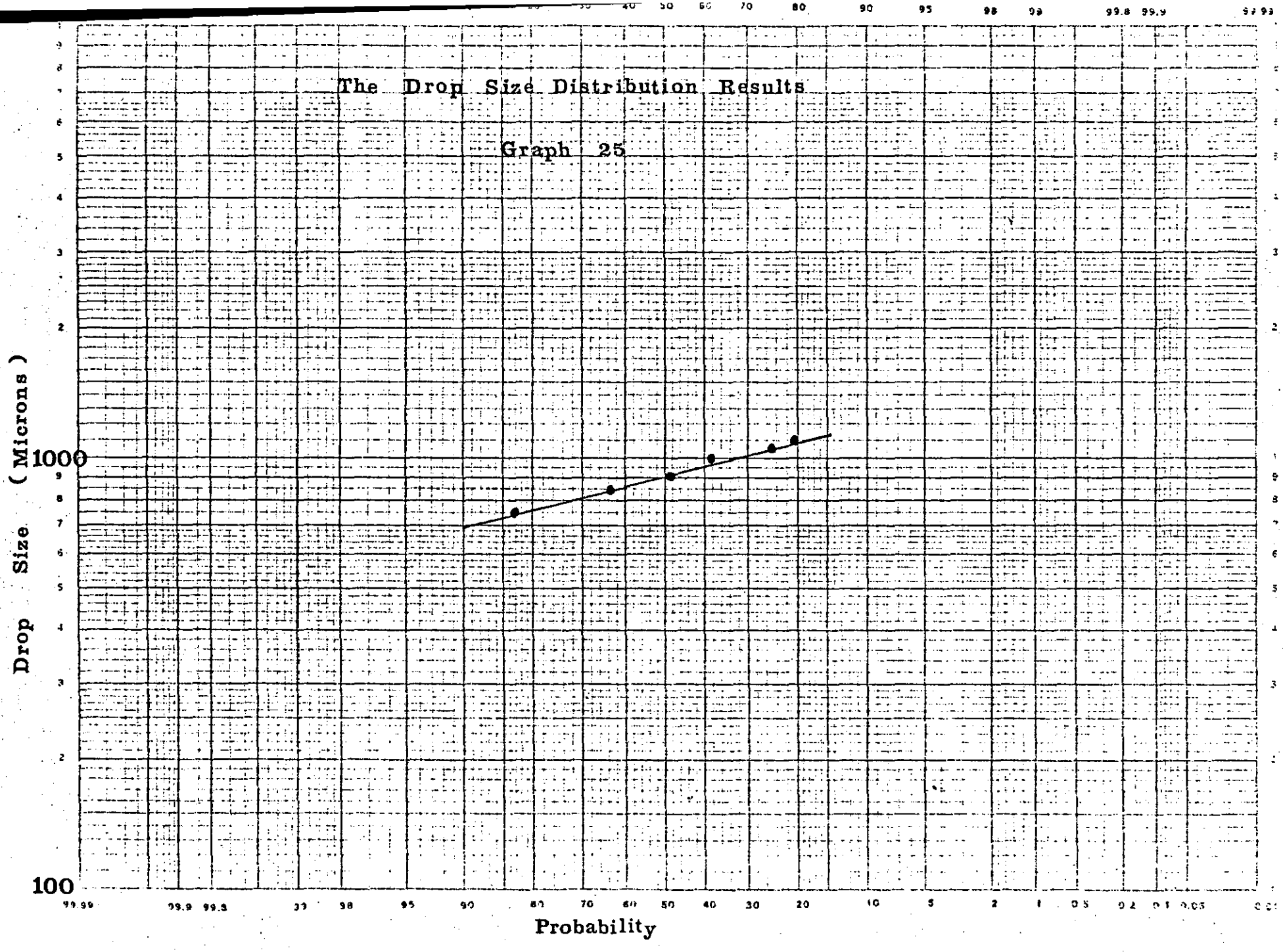
The Drop Size Distribution Results
Graph 25
Drop Size (Microns)
1000
100
99.99
99.9
99.8
99
98
95
90
80
70
60
50
40
30
20
10
5
2
1
0.5
0.2
0.1
0.05
Probability

Graph 26

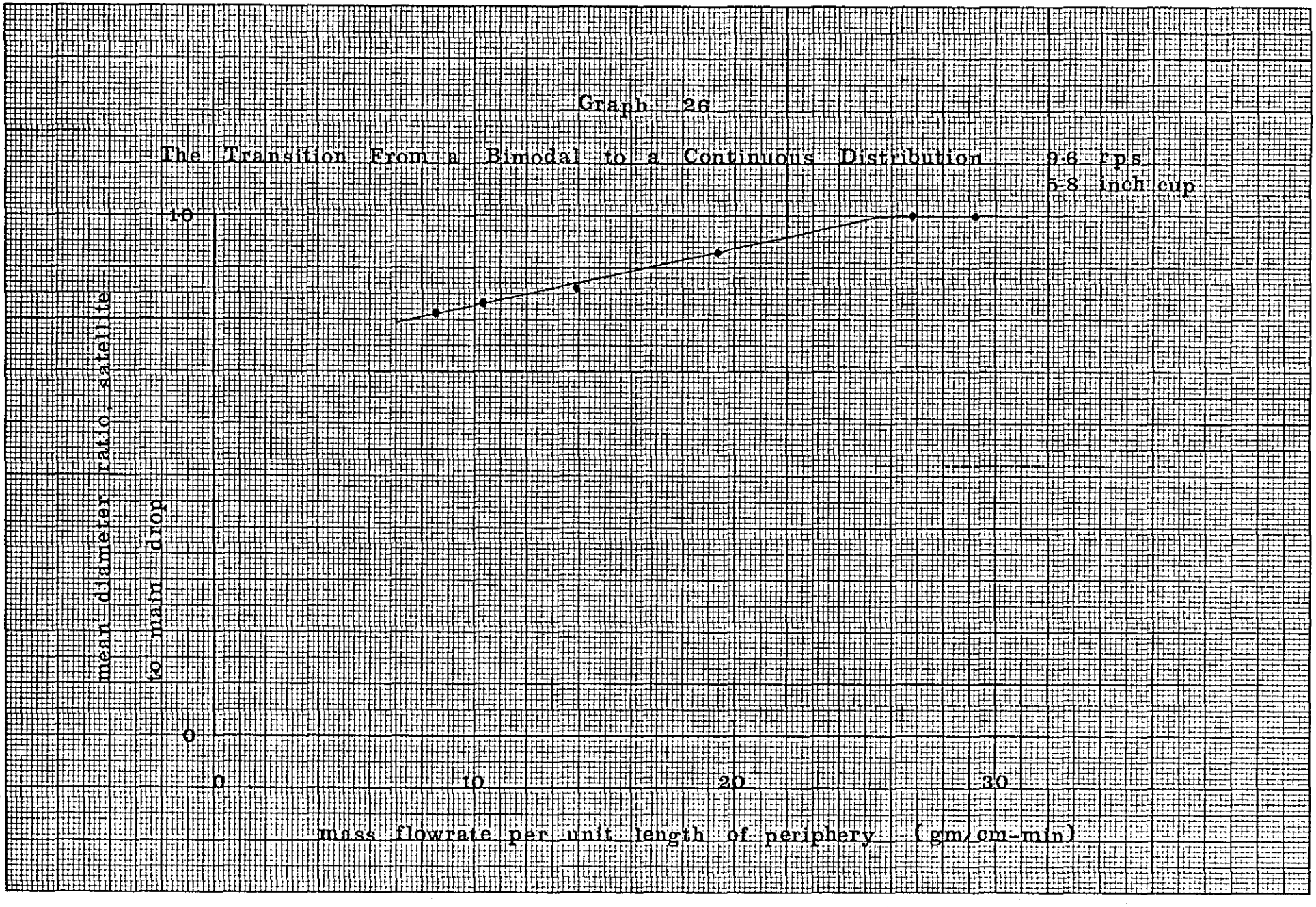
The Transition From a Bimodal to a Continuous Distribution
9.6 rps
5-8 inch cup
1.0
0
mean diameter ratio satellite to main drop
0
10
20
30
mass flowrate per unit length of periphery (gm/cm-min)

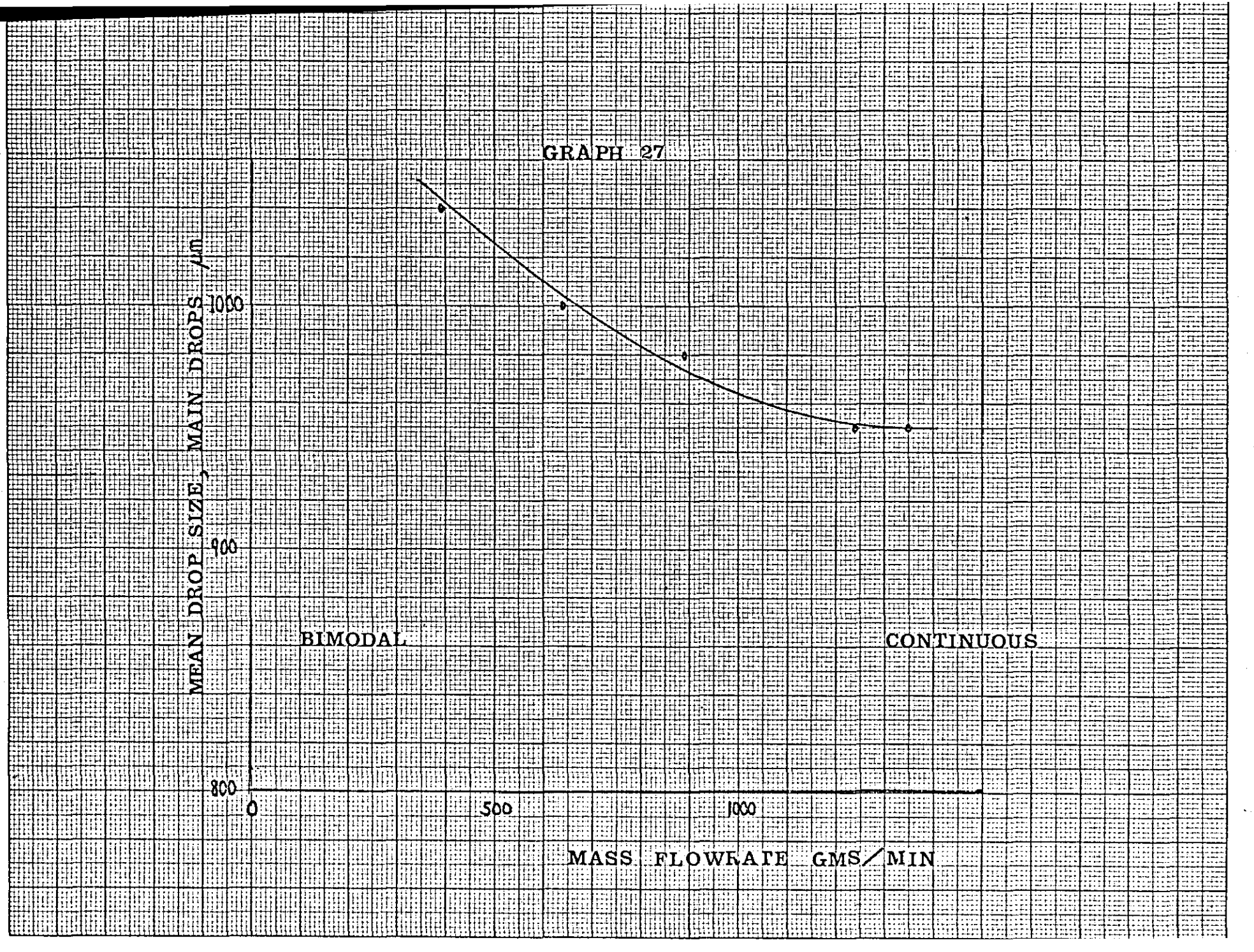
GRAPH 27
MEAN DROP SIZE, MAIN DROPS, μm
1000
900
800
BIMODAL
CONTINUOUS
0
500
1000
MASS FLOWRATE GMS/MIN

ADDENDUM

Page 8 — Paragraph 3, add "(see sections 3.1 and 3.2)" at the end of this paragraph.

Page 18 — Eqn. 3.1.10. (i.e. based on the hydraulic diameter).

Page 31 — Delete the word "experimentally" from the statement before eqn. 3.3.2.

Page 38 — Eqn. 3.5.6. add "where the Sauter mean diameter $d_{sv} = \sum nd^3 / \sum nd^2$".

Page 47 — 3. " ..... down of a liquid jet due to ....."

Page 49 — Last paragraph, first sentence, delete "Chandrasekhar (64)"

Page 54 — Paragraph 2, add sentence at end of paragraph "As this technique is sensitive to the electrostatic environment, it is necessary to calibrate this drop sizer where it is to be used".

Paragraph 3, delete "catchment area" insert "collision diameter".

Page 57 — Paragraph 1, first sentence, add " see Fig. 4.3" at the end of this sentence.

Page 62 — Paragraph 1, add "The accuracy should be within $\pm$ 5%" at end of paragraph.

Page 64 — Last paragraph, second sentence, " ..... by placing ten nominal 90 volt dry cell ..... "

Page 95 — Paragraph 1, first sentence, add asterisk (Table 1-8*) then add footnote "*Where D in these tables refers to the diameter at which these results were obtained".

Page 95 — Paragraph 2, first sentence, delete "biased in several ways" insert "potentially inaccurate in two ways".

Page 96 — Paragraph 2, third sentence, delete "although" insert "as".

Page 105 — Appendix 6-1, delete "and $\frac{mdv}{dt}$ = ..." insert "furthermore $\frac{mdv}{dt}$ = ..."

Nomenclature T (units dynes/cm); δ (units dynes/cm) and δ' (units dynes/cm).

Table 1 add "5.82 inch cup"

Tables 2-8 add "6.2 inch cup".